UNIVERSITÀ DEGLI STUDI DI MILANO
FACOLTÀ DI MEDICINA E CHIRURGIA

PhD program in Translational Medicine

XXXV cycle

Department of Biomedical Sciences for Health

Optimization of AAV9 gene therapy for Spinal Muscular Atrophy with Respiratory Distress type 1 using in vivo disease models

MED/26

Tutor: Prof.ssa Stefania Corti

Supervisor: Dr.ssa Monica Nizzardo

Degree course coordinator: Prof.ssa Chiarella Sforza

Elisa Pagliari

ID n° R12659

Academic year 2021-2022

Index

1. Abstract

Spinal Muscular Atrophy with Respiratory Distress type 1 (SMARD1) is a rare autosomal recessive motoneuron disease with infantile onset, with an estimated incidence of 1/100'000. It is caused by mutations in the *immunoglobulin mu-binding protein 2* (*IGHMBP2*) gene, which lead to a deficient amount of the encoded protein. The main clinical symptoms are distal muscular atrophy associated with diaphragmatic palsy. Nowadays no therapies are approved.

In this work, we compared the efficiency of two adeno-associated virus serotype 9 (AAV9)-*IGHMBP2* vectors, carrying different promoters, by administering them intracerebroventricularly in SMARD1 mice model (*nmd*), during the presymptomatic phase of the disease at postnatal day 1. This comparison allowed us to determine which is the best construct to be translated to the clinic. Then, with the aim to precisely define the therapeutic window, we evaluated AAV9-based treatment in already symptomatic mice at P7 by systemic subcutaneous injection.

Expression analysis at P20 on mice treated at the presymptomatic stage demonstrated a significant increase in the IGHMBP2 protein expression level compared to the control. Treatments also resulted in an extended survival time, higher body weight, and improvement in motor behaviors. Histopathological analysis showed in muscles increased innervation of the neuromuscular junctions and enlargement of fibers diameter and, in spinal cords, increased motoneurons number with reduced gliosis and astrogliosis. We also found a restoration of the IGF1 axis, altered in *nmd* mice. To support the translatability of the therapy, we confirmed the lack of a significant alteration of the major toxicity biomarkers after the treatment and the rescue of the one pathologically altered. Long-term effects were also evaluated at P200 demonstrating differences between the two constructs in maintaining the motoneurons number and mediating cardiac fibrosis amelioration.

Results of similar analysis performed on delayed treated mice cohort showed equivalent results, demonstrating that also a treatment in the symptomatic phase could partially rescue the SMARD1 phenotype.

Our presymptomatic treatment results lay the foundation for the launch of the ongoing gene therapy-mediated phase I/IIa clinical trial for IGHMBP2-related disease, a crucial step forward in the authorization of the first therapy for SMARD1 pathology, which is up to now treated only with palliative and supportive care. Good results were obtained also delaying the treatment in the early symptomatic phase, but further studies are needed to assess the therapeutic window of this extremely promising approach.

2. Introduction

2.1. Motor Neuron Diseases

The National Institute of Neurological Disorders and Stroke (NINDS) defines Motor Neuron Diseases (MNDs) as a group of rare heterogeneous progressive neurological disorders that bring to death the cells that control essential muscle activity, the so-called Motor Neurons (MNs)[1].

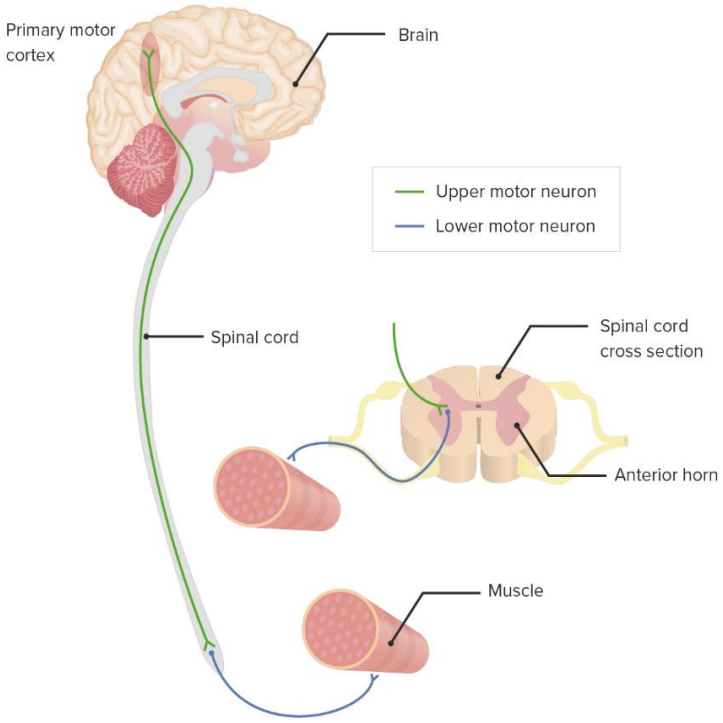

Figure 1. Corticospinal tract

MNs are fundamental for the transmission of motor signals from the motor cortex to the muscles through the two-step descending motor pathway, named corticospinal tract (*Figure 1*): the upper MNs, located in the motor cortex of the brain, communicate through glutamatergic synapsis to the lower MNs, sited in the brain stem and in the anterior horn of spinal cord, which in turn innervate effector muscles by cholinergic synapsis[2].

The lower MNs can be further classified into:

- brachial MNs, located in the brainstem and innervating face and neck area;
- visceral MNs, belonging to the autonomic nervous system;
- somatic MNs, which innervate skeletal muscles.

Their degeneration results in opposite outcomes based on the involvement of the upper or lower MNs. In particular, damage to the upper MNs results in uncontrolled movement and spasticity due to overactive muscle, while conditions involving the lower MNs have as typical outcome muscle weakening and loss of the ability to control voluntary movements[3]. MNDs can occur in all ages, etiology could be both inherited or sporadic, and they shall affect both the upper and/or lower MNs, and these features allow to better classify the specific disease.

The most common MNDs are:

- Amyotrophic Lateral Sclerosis (ALS);

- Spinal Muscular Atrophy (SMA);
- Progressive Bulbar Palsy (PBP);
- Primary Lateral Sclerosis (PLS);
- Hereditary Spastic Paraparesis (HSP);
- Progressive Muscular Atrophy (PMA).

2.2. *Spinal Muscular Atrophy with Respiratory Distress type 1*

2.2.1. Identification

The most frequent inherited MND is SMA, also called Werdnig-Hoffmann disease, an autosomal recessive pathology that causes the degeneration of the lower MNs in the anterior horn of the spinal cord resulting in proximal muscle weakness and atrophy in infants[4]. It is considered the major genetic cause of newborn mortality occurring in 1:10'000 live births[5]. The genetic etiology of SMA is the loss of the *Survival Motor Neuron-1* (*SMN1*) gene located on chromosome 5q[6].

Otherwise, in 1974, Mellins et al. described two atypical SMA cases that showed diaphragmatic respiratory distress. Peculiar is that this symptom, caused by bilateral diaphragmatic paralysis, occurred before the clinical evidence of progressive neuromuscular disease, an aspect that made these two patients significantly distinct from the SMA classical pathophysiology. This feature brought them also to speculate that the number of infants with this unknown disorder might have been underestimated, considering both the difficulty in the differential diagnosis from SMA and the possible sudden infant death that it could cause before clinical evidence of skeletal muscle involvement[7].

Fundamental to the disclosure of this pathology was another case report published in 1995, in which two SMA type 1 diagnosed infants showed once more diaphragmatic paralysis associated with spinal muscular atrophy. Interesting were the results from genetic analysis, which showed a lack of linkage to 5q11.2-q13, the region where the SMA causative gene *SMN1* is located[8]. For this reason, and the clinical discrepancy, since 1996, this pathology was considered a distinct disease to SMA, and called Spinal Muscular Atrophy with Respiratory Distress type 1 (SMARD1, OMIM #604320), as we know it nowadays. Different other definitions are still in use such as Distal Spinal-Muscular Atrophy 1 (DSMA1) or Distal Hereditary Motor Neuropathy type VI (dHMN6)[9].

Then, in 1999, two families were identified with cases of diaphragmatic SMA: patients showed greater impairment of the upper spinal cord, in contrast to SMA which affects the lower section, and, fundamentally different from the classical Werdnig-Hoffmann disease, it was discovered that the etiology of this pathology resides in mutations located in the 11q13-q21 region[10]. In particular, in

2001, Grohmann et al. defined the genetic defect specifically located in the *immunoglobulin μ DNA binding protein 2* gene (*IGHMBP2*, OMIM #600502, RefSeq NM_002180.2)[11].

Up to now the precise prevalence of this disease is still unknown, more than 100 cases have been reported in the literature, otherwise, retrospective studies hypothesized that 1% of the early onset SMA patients may be considered instead affected by SMARD1, also in light of the possible underestimation attributable to the newborn sudden death[9,12].

2.2.2. Clinical manifestation

SMARD1 pathology, such as SMA, induces the degeneration of α MNs located in the anterior horns of the spinal cord in infants. α MNs belong to the somatic lower MNs class, and they are the principal responsible for the voluntary movement generation, thus their death results in symmetrical muscle weakness of the trunk and limbs. Symptoms occur early, usually during the first year of life, and in some cases, the respiratory failure came out before any other muscular symptoms, making this pathology more difficult to be diagnosed[13].

Differently from SMA, there are few peculiar symptoms present only in SMARD1 described deeply by a retrospective study published by Grohmann in 2003 on 29 SMARD1 patients[14].

First of all, even if not so specific, it was possible to observe prenatal issues such as intrauterine growth retardation, which resulted in lower birth weight (<10th percentile) associated with possible premature birth (<37 weeks of gestation) and/or decreased fetal movement.

After birth, one of the most common symptoms is weak cry and/or inspiratory stridor caused by diaphragmatic complications, even when respiratory distress is still not present. Diaphragmatic involvement is the most prominent symptom, and it is the essential clinical difference between SMARD1 and SMA. The phenomenon starts usually with diaphragm eventration, diagnosed by a chest radiograph, in a period between the first week to the first month of life, giving rise to a rapidly progressive severe respiratory distress, that is considered a life-threatening issue that commonly requires mechanical ventilation[15]. The cohort considered by Grohmann showed an extensive range for the age of onset of respiratory distress between 3 days to 1 year of life[14].

An early effect is also the presence of foot deformities caused by initial involvement of the distal muscles of the lower limbs, then followed by symmetrical weakness progression to the upper limbs and trunk. Finger contractures and accumulation of adipose tissue on the proximal phalanges (fatty pads) develop only later. Only a few SMARD1 children reach the motor milestone to be able to sit without support. The neuromuscular pathogenesis in SMA patients is similar but not completely identical, in fact, in SMA the proximal limb muscles are the first involved, leading babies to assume a frog-leg position, and only later in life they develop respiration insufficiency, which is not caused

by diaphragmatic issues instead due to intercostal recession and paralysis of intercostal muscles, not present although in SMARD1 patients. These muscular symptoms are coherent concerning the laboratory findings which showed differences in electromyography, decreased motor nerve conduction speed, and lack of motor response after maximum stimulation, associated with neurogenic changes, visible in muscle biopsies, such as fibers hypertrophy and atrophy[16].

Later in life, with a range of around 3-68 months of life, is possible to observe, in SMARD1 patients, nervous system symptoms, without intellectual alterations, such as facial muscles weakening and tongue fasciculations caused by cranial nerves complications, and/or symptoms concerning sensory and autonomic nervous system as reduced pain sensitivity, excessive sweating, constipation, bladder incontinence, reflux nephropathy, and cardiac arrhythmia. The prognosis for SMARD1 patients is poor and the life expectancy is reduced with a mean age of death within the first 13 months of life even with the use of artificial ventilation[16].

Otherwise, in literature, three different forms of SMARD1 based on the age of onset were described:

- the classical severe form, with symptoms appearing usually after three months of life;
- the early-onset form, which emerges before three months of life, and is considered the most severe;
- the milder late-onset form, even if very rare, with onset after 12 months of life[17].

Considering this variability in the age of onset and the consequent severity of the pathology, the life expectancy is not so homogeneous, and, even if rarely, SMARD1 patients with ventilation support can reach adolescence and even early adulthood[18].

2.2.3. Diagnosis

In 2003 Pitt et al. designed a list of criteria for the clinical-pathological recognition, and thus the diagnosis, of SMARD1, that could be divided into three subgroups:

- clinical criteria: low birth weight (<3rd centile), onset of symptoms within the first 3 months of life, unilateral or bilateral diaphragmatic weakness, ventilator dependence within <1 month from onset with an inability to wean, and absence of other dysmorphology or other conditions;
- histopathological criteria: reduced myelinated fiber size in sural nerve biopsies (since the thickness of the myelin sheath is found to be appropriate for axon size, the fiber size change would depend on axon), small evidence of progressive myelinated fiber degeneration in biopsies taken up to 3–4 months, and lack of evidence of regeneration or of demyelination (which might be the cause of the change in fiber size);

- EMG criteria: evidence of distal denervation acute or chronic, and evidence of severe slowing (<70% of lower limit of normal range) in one or more nerves (motor and/or sensory)[19].

Additionally, Guenther et al. in 2007 used a mathematical algorithm of hierarchical cluster analysis to define the appropriate clinical criteria which could best predict the presence of SMARD1 causative mutations in the *IGHMBP2* gene. The best criteria combination (98% sensitivity and 92% specificity) resulted to be the presence of both respiratory failure between 6 weeks and 6 months of life and diaphragmatic eventration or preterm birth. However, these criteria are not always fulfilled in all the SMARD1 patients due to heterogeneous phenotype, making the clinical evaluation based on these parameters not sufficient[20].

Up to now, the easiest and most efficacious method is the direct genetic evaluation for the presence of *IGHMBP2* mutations on chromosome 11q. The most effective resolution will be molecular genetic prenatal screening, which was firstly used in 2004 on DNA extracted from chorionic villi samplings to disclose possible outcomes of twin pregnancy in a couple at risk with a precedent child who died at one month of age[21]. The next important work in this direction was a large-scale carrier-screening program conducted in 2008 on residents of an isolated Israelian village where 9.9% of the women tested resulted carriers for SMARD1, and a married couple who resulted positive for the carrier condition discovered that also their fetus was affected. In this specific case, which also reflects the general population condition, prenatal screening will be fundamental for both a guided decision process for the parents and/or the timely treatment of the affected baby after birth[22]. Today it is still not implemented in clinical practice as a routinary assessment due to the rarity of the disease, it is only performed in case of precedent familiar cases of SMARD1.

2.2.4. Genetic background

2.2.4.1. *IGHMBP2* gene and protein

IGHMBP2 is a protein-coding gene located on chromosome 11q13.2–q13.4 (*Figure 2*). It is 36748 bp long and composed of 15 exons. It is a conserved gene in vertebrates with more than 400 orthologous genes[23].

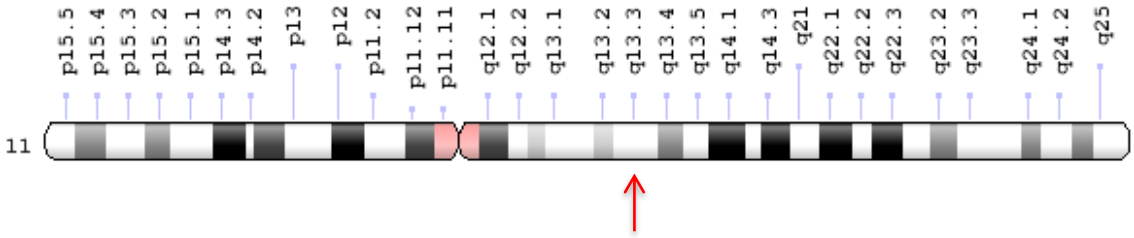

Figure 2. Human Chr 11 schematic representation. IGHMBP2 location (11q13.2-q13.4) is indicated by the red arrow

It encodes for the Immunoglobulin μ DNA Binding Protein 2 (IGHMBP2) also called DNA-binding protein SMUBP-2 (UniProt P38935), which is a 109 kDa protein of 993 amino acids with a ubiquitous expression and with low tissue specificity. Elevated expression was found in the cerebellar cortex after birth, reaching a constant level maintained during all adult life, suggesting a possible role in nervous system development[24]. At the subcellular level, it has been shown that it is present in the nucleus, but also cytoplasmically and in the axons of MNs, highlighting its function in the peripheral nervous system[25].

IGHMBP2 protein belongs to the helicase superfamily 1 (SF1), particularly to the Upf1-like/Dna2 family[26]. Helicases are a group of enzymes with an RNA or DNA unwinding function which work in an ATP-dependent manner, the mechanism at the bases of the most common genome processes as replication, repair, transcription, RNA maturation and splicing, and ribosome synthesis. They were classified on similarity bases on six big superfamilies of which the SF1 and the SF2 are the most numerous. They are both non-hexameric superfamilies in which the conserved core is composed of two recombinase A (RecA)-like domain folds. These functional domains in turn contain both the DEAD-box helicase domain and an ATPase-associated domain (AAA). The principal differences between them are located in the accessory domains at the C- and N- terminals that give them specificity[27,28].

The Upf1-like subfamily members, and thus IGHMBP2, are able to uncoil both DNA and RNA duplexes with a 5'→3' polarity[29]. IGHMBP2 contains, in addition to the two RecA-like helicase domains, two more regulatory regions at the C-terminal: an R3H motif, which recognizes the phosphorylated sequence at the 5-terminal of nucleic acids and enhances the RNA binding and the ATPase activity of the protein, and an AN1-type zinc-finger (ZnF) domain, which can bind and coordinates two zinc atoms (*Figure 3*)[30,31].

Figure 3. IGHMBP2 schematic representation. Helicase domain, R3H, nuclear localization signal, and AN1-ZnF were shown.

The cellular role of IGHMBP2 is still incompletely characterized, but its ATP-dependent 5'→3' catalytic activity was demonstrated to be linked to the translational process in different ways[32].

First of all, it was demonstrated that it is present in the cytoplasm as part of a large ribonucleoprotein complex binding ribosomal RNA (rRNA) and the eukaryotic translation initiation factor eIF4G2[32]. It

has been reported that IGHMBP2 interacts directly with the 80S ribosomal subunit, suggesting a possible role in the translation initiation of mRNA molecules. Its involvement in ribosomal biogenesis and translation was further consolidated by its association with Reptin and Pontin helicases, and thus in turn with U3 snoRNA, which regulates the rRNA biogenesis[25].

In addition, it has also been demonstrated the involvement of IGHMBP2 in the tRNA metabolism, in particular, it was shown to associate directly with tRNA, especially with tRNATyr, and also with the activator of basal transcription 1 (Abt1) and the transcription factor IIIC (TFIIIC220), essential for tRNA transcription, strongly supporting its role in the cellular translational machinery. Aberrant processing of tRNA was reported to mediate the accumulation of toxic tRNA fragments which could lead to the activation of the p53-mediated cell death pathway, suggesting another pathological mechanism at the bases of SMARD1 disease[25].

Another pathological feature, that otherwise needs further elucidation for SMARD1, is the presence of R-loop accumulation. R-loops are three-stranded nucleic acid structures that physiological are present in a transient way during transcription when an mRNA molecule hybridizes with a template DNA leaving the non-template DNA single strand free. Their functional role is linked to DNA replication, immunoglobulin switch recombination, and gene expression regulation. The mechanism with which they are generated is still not clear but their accumulation, caused probably by the lack of proteins able to resolve them, like DNA helicase, may result in DNA double-strand breaks, genomic instability, and at last cell death and neurodegeneration. Considering that in other MNs diseases such as ALS or ataxia with oculomotor apraxia type 2 (AOA2) this dysfunctional accumulation is present and that the protein mutated in AOA2, senataxin, is an RNA/DNA helicase very similar to IGHMBP2, the pathogenic role of R-loop could be important also in SMARD1 and needs to be further elucidated[33,34].

Overall, these pieces of evidence support the multifunctional role of IGHMBP2 protein in the cellular processes even further clarifications are needed to better understand the disease mechanisms.

2.2.4.2. *IGHMBP2* mutations

The majority of the known disease-causing mutations of *IGHMBP2* fall in its catalytic domains and thus affect the enzymatic activities of the protein which result in being deleterious, for neuronal cells and especially in MNs, even if the cause of this selective damage is still not clear[35].

Mutations in the *IGHMBP2* gene are at the bases of a spectrum of phenotypes. The first identification, by Grohmann in 2001, already demonstrated the presence of heterogeneity of mutations (recessive missense, nonsense, frameshift deletion, and splice donor-site) in SMARD1 patients[11]. These mutations are located mainly in the helicase domain or in the 5' on both the alleles resulting in a loss-

of-function condition. The same group in 2003 published a retrospective study in which all the mutations until then reported were summarized (*Figure 4*)[14]. They validated the heterogeneity of the type of mutations which resulted in being also distributed over quite all the exons (except for the 1st, 4th, and 14th) and not present as polymorphisms in unaffected unrelated individuals. They also confirmed that the two hot spots where they found the higher number of mutations were (i) the AAA domain or broader in the DEAD-like helicase domain (DEXDc) and (ii) between the nucleotides 1693 and 1758, suggesting then the presence in that location of an important functional domain for the protein still unidentified. No mutations were found in the R3H and AN1-like ZnF, leading to the belief that the helicase and the ATPase role of the protein are at the bases of the disease-causing mechanism[14].

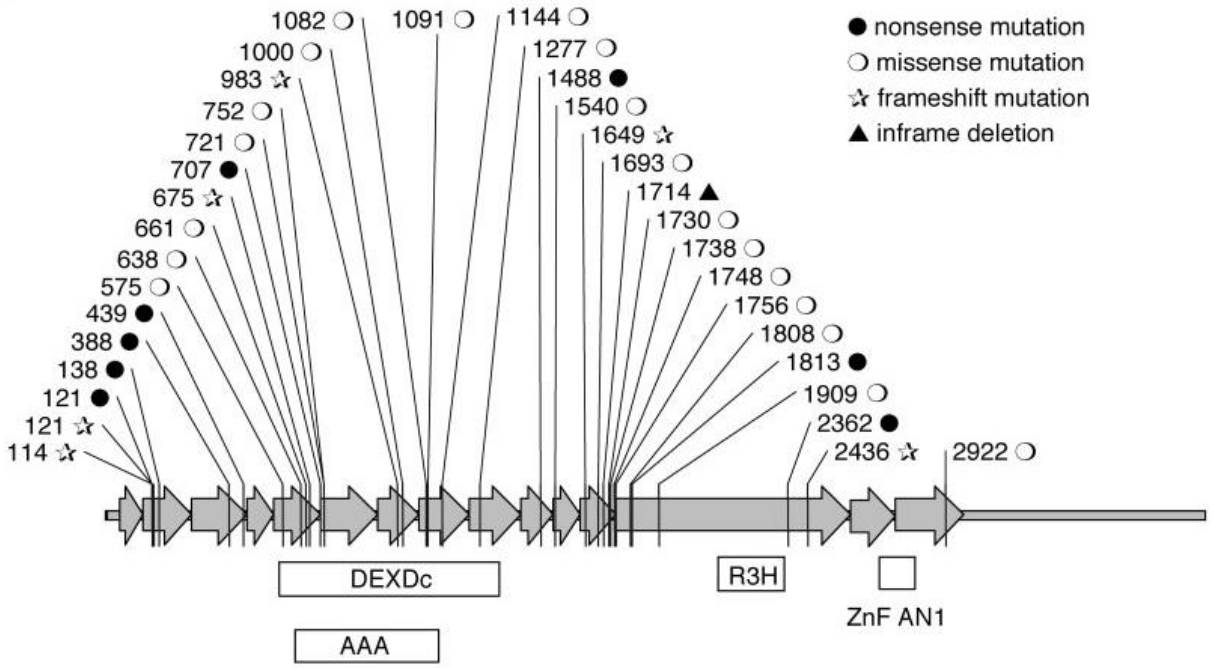

Figure 4. IGHMBP2 mutations localization reviewed by Grohmann et al. in 2003[14]. Exons are represented as arrows; mutations are indicated with nucleotide numbering.

Next, in 2004 other nine *IGHMBP2* novel mutations, of which seven located in the helicase domain, were reported, including seven missense and two nonsense[36], and by 2010 other 26 were added, the majority of which were found in the enzymatic domain, supporting the hypothesis that the loss of the helicase or ATPase activity of IGHMBP2 is the principal defect at the base of the SMARD1 pathology[14,37–39].

Few novel missense mutations in the following years have been found outside the helicase domain in SMARD1 patients. The principal hypothesis for their pathogenicity are (i) the formation of a premature stop codon in the mRNA, which results in a lack of translation and its elimination by nonsense-mediated mRNA decay and/or (ii) the production of a protein with altered aggregation and degradation features[36,40].

In 2014 compound heterozygous mutations in the *IGHMBP2* gene were also found correlated to a hereditary recessive motor and sensory neuropathy defined as Charcot-Marie Tooth disease axonal type 2S (CMT2S). They were identified as a combination of loss-of-function nonsense mutations in the 5' region and truncating frameshift, missense, or homozygous 3' frameshift mutations in the last exon. The phenotype of CMT2S is less severe than SMARD1 one. It is fundamental a slowly progressive weakness associated with sensory loss without diaphragm involvement and thus respiratory distress[24]. In 2018 Kulshrestha et al. published a case report presenting an atypical case of CMT2S with a diaphragmatic involvement caused by heterozygous missense mutations in exons 8 and 14 of the *IGHMBP2* gene, suggesting that the pathogenic alterations of the gene are responsible for a broader spectrum of disorders which comprise both SMARD1, CMT2S, and other intermediate phenotypes[41]. One hypothesis at the basis of the phenotypical difference between the two pathologies is the variation in the protein amount, which resulted higher in CMT2S compared to SMARD1, but this data is not supported by other works, which otherwise suggests the principal role of genetic modifiers in the modulation of the clinical phenotype[24,42].

Overall, up to now, even if in literature it is shown that the lower level of protein is predictive of higher severity, no correlation was found between genotype and phenotype, confirming the necessity of further study on IGHMBP2-related diseases to better understand the neuropathogenic effect of the mutations and the possible therapeutic approaches.

2.2.5. Clinical treatments

Unfortunately, there are no therapies approved for SMARD1 patients, but only palliate treatments to support vital function and mitigate symptoms. Being respiratory failure due to diaphragmatic paralysis the most invalidating feature of the disease, the principal treatment is lifelong permanent mechanical ventilation with associated airway clearance procedures, like cough augmentation devices. Life expectancy without external respiratory support is very poor, with a mean age of death around 9 months[17].

Bladder atonia was also observed in some patients and the subsequent urine retention is treated with regular catheterization. Alimentation and digestion issues caused by autonomic nervous system dysfunction are usually managed with gastrostomy or tube feeding[26].

Muscle weakness is handled with physical and occupational therapy especially to delay as much as possible the related orthopedic problems of the dorsal spine. Muscle atrophy results later in life in wheelchair dependence[16].

Recently, promising results of gene therapy in SMARD1 preclinical area paved the way for the launch of a Phase I/IIa clinical trial for IGHMBP2-related disease in December 2021.

2.3. *In vitro SMARD1 models*

2.3.1. Cellular models

Currently, to study neurodegenerative diseases, such as SMARD1, the principal issue is due to the limitation into study directly the affected cells, the neurons. For this reason, the most used human *in vitro* model for SMARD1 is based on induced pluripotent stem cells (iPSCs) derived from patients' skin biopsies or blood samples. This is possible thanks to the revolutionary Takahashi and Yamanaka method based on the retroviral expression of a specific set of transcriptional factors (cMyc, Oct3/4, Sox2, and Klf4) in somatic cells[43]. iPSCs are very similar in expression profile and differentiation potential to human embryonic stem cells (hESCs), but with the major advantage of being obtained by somatic cells overcoming the ethical issues, costs, and difficulties in the procedure and also giving the possibility to be obtained virtually from any patient resulting in a more personalized approach[35].
More precisely, the usefulness of iPSCs as a model for MNDs was confirmed in 2009 by Hu's group who described a multistep reproducible protocol to obtain spinal MNs based on the use of small molecules which directed the differentiation of iPSCs[44].
To reduce the possible insertional mutations caused by the use of viral transducers, in 2012 Corti's group validated a protocol for SMA patients' derived iPSC lines generation using a nonviral and non-integrating method founded on the use of plasmids nucleofection. These constructs encode for Oct4, Sox2, Nanog, Lin28, c-Myc, and KLF4 and were progressively lost from the cells making this approach more prone to translatability for the reduction of genetic undesired modifications[45].
This method was then used by Simone et al., who published in 2014 the first work regarding the reprogramming of SMARD1 and control skin fibroblasts in iPSCs followed by differentiation in MNs using Hu's protocol. In the same work, the authors demonstrated also that the SMARD1 iPSC-derived MNs are less in cell number and the axon length is reduced if compared to MNs obtained from healthy controls confirming the presence of a pathological phenotype in this *in vitro* model[46].
This kind of model brings with it also some limitations that have to be considered, due mainly to the high cost, the elaborate protocol for reprogramming and differentiation, and, as with every *in vitro* model, the lack of complexity and physiology that an *in vivo* model could give. On the other hand, fundamental is the possibility to reprogram iPSCs starting from a non-invasive skin biopsy, which leads also to the chance to study how the genetic background of each patient contributes to the pathogenesis, making the research more personalized. Another important aspect is the possibility to differentiate iPSCs in almost any cell types, giving the opportunity to study also other cells type that can interact with the MNs in the SMARD1 pathology, such as glial cells and muscle cells. All these

advantages make iPSCs and furthermore iPSCs-derived MNs the best *in vitro* models to study neurodegenerative disease and possible therapeutic interventions[35].

2.3.2. Saccharomyces cerevisiae

Another model used to study human neurodegenerative diseases is the budding yeast *Saccharomyces cerevisiae*. It is considered a very reliable model for specific mechanisms such as cell cycle control, signal transduction, cell growth and division, organelle function, homeostasis, stress response, DNA replication, transcription, translation, and repair for their similarity to the eukaryotes ones[47]. From what concerns the genetic point of view, about 30% of the human disease-associated genes have yeast orthologues and the yeast genome is easily manageable through gene disruption, mutation, overexpression, or tagging. The advantages of using this model are also linked to its fast, easy, and cheap cultivation, which could be addressed to perform high-throughput screenings. It has limitations that must be considered, especially linked to the inability to study physiology at the multicellular or tissue-specific level[35,48].

The conservation of cellular mechanisms from yeast to humans and the genetic features of *S. cerevisiae* make it suitable to study specific pathways also in IGHMBP2-related diseases. In particular, the *IGHMBP2* orthologue, *Hcs1* (HeliCaSe), has a 38% similarity with the human gene, and it shares also its function being an ATP-dependent DNA helicase with a 5'→3' polarity belonging to the SF1 Upf1-like family. The main difference with the human IGHMBP2 protein is the length, it is only 683 aminoacids long due to a truncation at the C-terminal which results in the lack of the R3H and the AN1 domains. This difference is only partially problematic because the majority of the mutations in SMARD1 fall in the conserved helicase domain still present in *Hcs1*[35].

S. cerevisiae could be exploited for SMARD1 research to study cellular mechanisms involved in the disease, such as transcription, translation, and rRNA and tRNA metabolism, but also to perform fast and easy high-throughput tests for new therapeutic molecules. Fundamental is to take into consideration that the complexity of the organism is too simple to analyze tissue-specific pathological issues or systemic therapeutic effects[35].

2.4. In vivo SMARD1 models

2.4.1. Caenorhabditis elegans

Caenorhabditis elegans is a free-living well-known non-parasitic transparent nematode used as a simple model in medical research. One of the most important advantages is the short life cycle, with a development 3 days long and a whole life span of about 2-3 weeks. In addition, it is also very small

in size, reaching a length of 1 millimeter, making it fast, cheap, and easily cultivated in petri dishes. Otherwise, the small size does not preclude the presence of organ systems such as the digestive system, nervous system, musculature, and reproductive system, which allow preliminary tissue-specific studies and analysis of complete organism physiology. The fixed number of 959 somatic nuclei (302 of which are neurons and 30 MNs) makes it also easily genetically tractable and its transparency allows real-time assessment of genetic modifications through non-invasive imaging methods[35,49].

Regarding specifically *IGHMBP2*, its orthologue, *ERI-6/7* (Enhanced RNAi), shares only 27% of similarity and does not produce a protein containing all the human IGHMBP2 domains with a slightly different function. It belongs, as the human IGHMBP2, to the SF1 helicase family, but it is mainly involved in the regulation of exogenous RNAi, generation, and stability of siRNA[50], and in the silencing mechanism of retrotransposons and integrated viral genes[51], functions that are still not demonstrated to be comprised in the one of the human protein. Therefore, even if the *C. elegans* could be a simple and excellent organism model to study toxicity, perform drugs evaluation in high-throughput studies, and analyze tissue-specific effects of a single mutation, the substantial different role of IGHMBP2 and ERI-6/7 precluded a more important role in the specific field of SMARD1 research[35].

2.4.2. Danio rerio

Another successful animal model is the zebrafish or *Danio rerio*. It is the first vertebrate model, a feature that gives it the possibility to be used to study the complete physiology of the organism and tissue-specific aspects. It is relatively fast, thanks to its short generation time, and also cheap and quite easy to maintain. As with *C. elegans,* it is possible to genetically manipulate it during its embryo stage and the modification can be followed non-invasively thanks to its transparency. Fundamental is also its usage, as a unique vertebrate, in high-throughput drug screening[35].

IGHMBP2 orthologue in zebrafish, *Ighmbp2*, is well conserved, sharing 71% of similarity with the human gene containing both the helicase domain and the regulatory R3H and AN1. By the way, currently, there are no published results about the use of *Danio rerio* as a model for SMARD1, even if it was already used to study SMA and mutations which results in SMARD1 phenotype[52,53].

2.4.3. Mus musculus

The most used and most advantageous animal model used in basic and preclinical research is the mouse model. It brings the possibility to study mammalian physiology that is remarkably similar to

the human one, both for anatomy, biology, and tissue specificity. *IGHMBP2* orthologue, *Ighmbp2*, is conserved in mice, it is located on Chr19 (19:3,309,076-3,333,011) and has the highest similarity (85%). Even the protein that it encodes for is very similar, both for the identical length (993 aa) and for the domains that it contains (helicase, R3H, and AN1)[23]. It is a ubiquitous protein largely expressed in elevated levels in the brain, heart, kidney, spleen, and testes. As the human protein, its role is still not completely understood, but its implication in transcriptional activation and immunoglobulin class switching was demonstrated[54].

2.4.3.1. B6.BKS-Ighmbp2$^{nmd\text{-}2J/J}$

The first *Ighmbp2* mutant animal appeared spontaneously in a diabetes type II mice model (BKS db) in 1987 at The Jackson Laboratory Mouse Mutant Resources[55]. Homozygous mutant *nmd^{2J}/nmd^{2J}*, currently named B6.BKS-Ighmbp2$^{nmd\text{-}2J/J}$ or more commonly *nmd* mice, show impaired movement and progressive paralysis, starting in the hindlimb, from 2 weeks of age. This impairment is not present in the forelimbs that they usually use to crawl forward. They are not able to stand erect and assume full posture on all paws, but their balance is not compromised. A typical sign is the clench of the hindlimb when suspended head down by the tail. Their mean death age is 3.5-4 weeks caused in the majority of the cases by secondary respiratory failure. Histopathological analysis of forelimb and hindlimb muscles show severe muscle atrophy with more severe lesions and adipose infiltrations in the distal areas. The atrophy is asymmetrical with random denervation of the fibers. The hematoxylin and eosin and the luxol fast blue-cresylecht violet stain result "faded away" in the affected MNs, a sign of reduced density, a feature present also in ALS patients, but they are not swollen, do not present altered shape and the organelles are normal. The most affected MNs are the αMN located in the lumbar section of the spinal cord, without signs of inflammatory infiltrations, while the ones positioned in the thoracic and cervical portions appear normal. Heterozygous animals do not show any anomalies[56].

Subsequent genetic mapping demonstrated that the mutation aroused in these animals (*nmd-2J*), does not fall in the coding region, but it is a single A to G transition located 23bp into intron 4 of the *Ighmbp2* gene on Chr 19. It creates a cryptic splice donor resulting in the inclusion of these 23 nucleotides in a mutated larger fragment and in turn leading to the formation of a frameshift and a premature stop codon. The result is a 21 kDa protein truncated at the C-terminal. Northern blot analysis showed a 20% reduction in the expression level of full-length *Ighmbp2* mRNA in the brain and spinal cord. RT-PCR revealed that also in the other tissues analyzed (liver, kidney, lung, heart, spleen, muscles, and thymus) there was a 20-25% wild type and 75-80% mutant splicing. The same group showed also that different phenotypic classes are present in the intersubspecific cross, with

animals reaching a longer survival time over 7 months and minimal muscle defects. They demonstrated that a positive modifier gene located on Chr 13, called *Mnm*, is responsible for a milder phenotype and that this region shares homology with four human chromosomal regions. This gene does not modify the *Ighmbp2* mRNA expression and/or splicing, and the actual mechanism with which it interacts with the protein and how it ameliorates the phenotype is still unknown[57].

In a next characterization of the model, another form of the protein, derived from alternative splicing, has been detected in wild-type (WT) and *nmd* mice brains. Its weight is about 55-60 kDa and it seems to have the same expression between the two groups suggesting that this specific protein does not correlate with the pathology[58].

Ighmbp2 localization is confirmed to be predominantly in the cytoplasm and axons of sciatic nerves while only weak signals come from the nucleolus. From the neuropathologic point of view, the study revealed that the number of MNs is not different in *nmd* mice with respect to WT at 5 days of age, but an important reduction (63%) is present at 10 days and remains constant until the pathological end stage where there is a further MNs degeneration. The histopathological analysis also evidenced the presence of axonopathy especially found in myelinated larger axons of sciatic and femoral nerves, which are numerously reduced after 3 weeks of mice life. This axonal loss is confirmed also by altered electrophysiological results, in gastrocnemius more than in quadriceps. Motor endplates innervation reduction is also detected in *nmd* mice quadriceps and gastrocnemius with a more severe degeneration at the end stage of the disease in correlation with MNs loss. Remarkably, no changes have been found in the diaphragm, organs instead affect in SMARD1 children. This is one of the biggest limitations of this model which does not represent severe respiratory distress, cause of death in human patients. Otherwise in *nmd* mice were found myopathic changes, as necrotic myofibers in the diaphragm, and a high number of fibers with central nuclei in both diaphragm and quadriceps, a sign of regeneration[57].

2.4.3.2. FVB/NJ-Ighmpb2^{D564N}

In 2022 another SMARD1 mice model was published by Smith et al., referred to as FVB/NJ-Ighmpb2^{D564N} or *Ighmbp2*^{D564N} or D564N. They initially generated six different SMARD1 mice models based on the most common human mutations (C46X, C496X, D565N, R603C, R605X, and H924Y). Two of them have been abandoned because of their embryonic lethality, while the remaining four showed phenotypes in the homozygous mutant animals. The characterization of these models started from the one containing the D564N (D565N in humans) mutation. The authors generated *Ighmbp2*^{D564N} mutation in FVB/NJ background using the CRISPR/Cas9 methodology. They demonstrated that there was not a reduction in protein level in contrast to *nmd* mice, suggesting that the introduced D564N mutation affects the Ighmbp2 protein functionality instead of its amount.

Homozygous mutant mice were indistinguishable at birth from heterozygous or homozygous negative for the mutation littermates. Their lifespan is between 16 and 22 days while heterozygous animals for the mutation did not show a detectable phenotype. Starting from one week of life homozygous affected mice appeared smaller and weighed less. Movement abnormalities showed up by postnatal day 16 (P16), along with reduced weight and worse coat quality. The hindlimb splay ability was severely affected starting from P7 associated with contractures and reduced forelimb strength after P16. The histopathological analysis demonstrates that, as the *nmd* mice, they displayed an important reduction in MNs number in the lumbar spinal cord, associated also with a reduced MNs area and perimeter. End plate innervation analysis confirmed severe denervation starting from P7. Reduction in muscle fibers area and perimeter has been demonstrated in gastrocnemius and surprisingly also in the diaphragm, which otherwise did not show alterations of neuromuscular junction (NMJ) innervation. A fundamental difference, if compared to the previous mouse model, was the presence of respiratory abnormalities, a typical sign of SMARD1 pathology. Under normoxia conditions, in fact, homozygous mutant mice showed a decreased respiratory frequency with respect to WT, and, when challenged, the respiratory frequency felled, while minute ventilation and mean inspiratory flow did not increase as happens in WT animals. Surprisingly D564N mutants had a higher tidal volume with respect to WT animals, which seemed to be an over-compensation mechanism of the failure to respond to respiratory challenges through the diaphragm and inspiratory muscles. It was also demonstrated that all these defects can be restored/avoided if the animals were treated at P2 intracerebroventricularly (ICV) with adeno-associated virus serotype 9 containing the wild type *IGHMBP2* confirming the functional defect caused by the inserted mutation[59].

Overall, this model, even if very recent and thus still not so diffused and not commercially available, recapitulates very well the human pathology and could be particularly useful especially to study the respiratory defect not present in the *nmd* mice, but the principal cause of death in human patients.

2.5. Preclinical therapeutic strategies

Currently, no therapies for IGHMBP2-related diseases are approved. Otherwise, at present few interesting therapeutic approaches are evaluated in preclinical and clinical studies. As for other systemic multiorgan diseases such as SMA, the therapeutic approaches can be divided into two distinct groups, the IGHMBP2-restoring therapies, and the IGHMBP2-independent strategies.

2.5.1. IGHMBP2-dependent approaches

The IGHMBP2-dependent therapies are focused on restoring the genetic defect at the basis of the pathology, thus the principal ideas are reintroducing a compensatory WT gene such as occurs in gene therapy, or modulating the expression of the endogenous mutated one, principle at the basis of mRNA modulation or gene editing.

2.5.1.1. Gene therapy

Gene therapy is a promising approach based on the delivery of the WT form of the mutated gene, making this technique especially efficacious for monogenic disorders[60]. This method could be performed *ex vivo* by modifying the cells before transplantation or *in vivo* using a vector that delivers the healthy gene. The viral vectors were identified as more efficacious than the less pathogenic nonviral compounds, and, for this reason, more than 70% of the trials have been performed with viral constructs. Currently, the most used are retroviruses, adenoviruses, herpes-simplex viruses, and adeno-associated viruses (AAV)[60–62]. In 2019 ongoing or completed gene therapy clinical trials were 2600, 5 of which ended with the commercial approval of the U.S. Food and Drug Administration (FDA)[63].

In the field of neurological diseases, in particular, the biggest issue is bypassing the blood-brain barrier (BBB) to reach targets such as brain and spinal cord. On this regard, in 2009, Foust et al., demonstrated that one AAV serotype (AAV serotype 9, AAV9) was the most efficacious into reach CNS with systemic intravenous (IV) administration, both in young mice with not fully developed BBB and in adult animals, making AAV9, since then, the favorite choice for neurological diseases treatment[64].

AAVs were first discovered in 1965 as non-pathogenic contaminants in adenovirus preparations. They are small single-stranded (ss) viruses belonging to the *Parvoviridae* family. The ssDNA which encodes for non-structural and capsidic proteins is 4.7 kb in length and it is contained in a non-enveloped icosahedral capsid. Endogenous AAVs establish latency by integrating into a specific site in Chr 19 (q13.4) and remain quiescent until the cell is super-infected with a helper virus which mediates AAVs replication and virion production[65].

In gene therapy, the non-structural viral sequence is substituted with the exogenous DNA of choice. These so-called recombinant AAV vectors, differently from the wild type do not integrate into the genome remaining in the episomal form, increasing thus their safety from the genotoxicity point of view. Safeness is the principal issue when viral vectors are used as therapy, but AAVs are not associated with human diseases, in fact, a large percentage of the population is seropositive to various

serotypes of AAV[66]. Nevertheless, some immune responses to the use of AAV-mediated therapy could be present such as the presence of preexisting neutralizing antibodies against the AAV capsid caused by the seropositivity, TLR2/9 innate immune response to capsid or genomic material, CD8+ T cells cytotoxic response, and humoral immune response against the encoded protein[67].

12 AAV serotypes and 108 isolates (serovars) have been identified so far, and their differences reside mainly in capsid structure which in turn are responsible for their divergence in tissue tropism[68].

AAV9, in particular, resulted to be specific for brain[64], cardiac tissue[69], liver[70], and lungs[71]. Its ability to overcome the endothelial barrier of BBB, when administered IV, makes it the elected choice to target the CNS. Even if today, CNS delivery is often exploited preferring a more local administration to overcome potential AAV9 off-target effects, immune responses, neutralizing antibodies, and to reduce dosage and thus hypothetical toxicity and costs[72].

Since 2015 the number of ongoing clinical trials based on the use of AAV9 has rapidly increased reaching today the number of 29 clinical trials (*Table 1*) mostly directed to the metabolic and the neurologic therapeutic area[73,74].

Table 1. List of clinical trials ongoing or completed based on AAV9 gene therapy (updated from Kuzmin et al. 2021[73])

NCT number	**Title**	**Drug ID**	**Administration route**	**Therapeutic area**	**Phase**
NCT02122952	Gene Transfer Clinical Trial for Spinal Muscular Atrophy Type 1	AVXS-101 Zolgensma	Intravenous	Neurology	1
NCT02240407	Re-administration of Intramuscular AAV9 in Patients With Late-Onset Pompe Disease	rAAV9-DEShGAA	Intramuscular	Metabolic	1
NCT02362438	Intrathecal Administration of scAAV9/JeT-GAN for the Treatment of Giant Axonal Neuropathy	scAAV9/JeT-GAN	Intrathecal	Neurology	1
NCT02716246	Phase I/II Gene Transfer Clinical Trial of scAAV9.U1a.hSGSH	ABO-102	Intravenous	Metabolic	1/2
NCT02725580	Gene Therapy for Children With Variant Late Infantile Neuronal Ceroid Lipofuscinosis 6 (vLINCL6) Disease	AT-GTX-501	Intrathecal	Neurology	1/2
NCT03306277	Gene Replacement Therapy Clinical Trial for Participants With Spinal Muscular Atrophy Type 1	Zolgensma	Intravenous	Neurology	3
NCT03315182	Gene Transfer Clinical Trial for Mucopolysaccharidosis (MPS) IIIB	ABO-101	Intravenous	Metabolic	1/2
NCT03362502	A Study to Evaluate the Safety and Tolerability of PF-06939926 Gene Therapy in Duchenne Muscular Dystrophy	PF-06939926	Intravenous	Musculoskeletal	1
NCT03368742	Microdystrophin Gene Transfer Study in Adolescents and Children With DMD	SGT-001	Intravenous	Musculoskeletal	1/2
NCT03381729	Study of Intrathecal Administration of Onasemnogene Abeparvovec-xioi for Spinal Muscular Atrophy	Zolgensma	Intrathecal	Neurology	1
NCT034	Single-Dose Gene Replacement	Zolgensma	Intrathecal	Neurology	3

61289	Therapy Clinical Trial for Patients With Spinal Muscular Atrophy Type 1				
NCT03505099	Pre-Symptomatic Study of Intravenous Onasemnogene Abeparvovec-xioi in Spinal Muscular Atrophy (SMA) for Patients With Multiple Copies of SMN2	Zolgensma	Intravenous	Neurology	3
NCT03566043	RGX-121 Gene Therapy in Patients With MPS II (Hunter Syndrome)	RGX-121	NA	Metabolic	1/2
NCT03580083	RGX-111 Gene Therapy in Patients With MPS I	RGX-111	Intracranial	Metabolic	1
NCT03770572	Gene Therapy for Children With CLN3 Batten Disease	AT-GTX-502	Intrathecal	Neurology	1/2
NCT03837184	Single-Dose Gene Replacement Therapy Using for Patients With Spinal Muscular Atrophy Type 1 With One or Two SMN2 Copies	Zolgensma	Intravenous	Neurology	3
NCT03882437	Gene Therapy for Male Patients With Danon Disease Using RP-A501; AAV9.LAMP2B	RPA-501	Intravenous	Metabolic	1
NCT03952637	Intravenous Gene Transfer With an AAV9 Vector Expressing Human Beta-Galactosidase in Type II GM1 Gangliosidosis	AXO-AAV-GLB1	Intravenous	Metabolic	1/2
NCT04088734	Gene Transfer Study of ABO-102 in Patients With Middle and Advanced Phases of MPS IIIA Disease	ABO-102	Intravenous	Metabolic	1/2
NCT04127578	Phase 1/2a Clinical Trial of PR001 (LY3884961) in Patients With Parkinson's Disease With at Least One GBA1 Mutation	LY3884961	Intracisternal	Neurology	1/2
NCT04240314	AAV9 U7snRNA Gene Therapy to Treat Boys With DMD Exon 2 Duplications	scAAV9.U7.ACCA	Intravenous	Musculoskeletal	1/2
NCT04408625	Phase 1/2 Clinical Trial of PR006 in Patients With Frontotemporal Dementia With Progranulin Mutations	PR006	Intracisternal	Neurology	1/2
NCT04411654	Phase 1/2 Clinical Trial of PR001 in Infants With Type 2 Gaucher Disease	LY3884961	Intracisternal	Endocrinology	1/2
NCT04737460	Study for the Treatment for CLN7 Disease	AAV9/CLN7	Intrathecal	Neurology	1
NCT04798235	First-in-Human Study of TSHA-101 Gene Therapy for Treatment of Infantile Onset GM2 Gangliosidosis	TSHA-101	Intrathecal	Metabolic	1/2
NCT04998396	A Study of AAV9 Gene Therapy in Participants With Canavan Disease	AAV9 BBP-812	Intravenous	Neurology	1/2
NCT05143307	Long-Term Follow-Up Study of HIV-1 Infected Adults Who Received EBT-101	EBT-101	Intravenous	Virology	1
NCT05144386	Study of EBT-101 in Aviremic HIV-1 Infected Adults on Stable ART	EBT-101	Intravenous	Virology	1
NCT05152823	Gene Therapy for IGHMBP2-Related Diseases	AAV9.IGHMBP2	Intrathecal	Neurology	1/2
NCT05394064	A Study to Evaluate Administration of SBT101 Gene Therapy in Adult Patients With Adrenomyeloneuropathy (AMN)	SBT101	Intrathecal	Neurology	1/2

NCT05419492	A Clinical Study to Evaluate the Safety and Efficacy of ETX101 in Infants and Children With SCN1A-Positive Dravet Syndrome	ETX101	Intracerebroventricular	Neurology	1/2
NCT05487599	A Clinical Trial of PR001 (LY3884961) in Patients With Peripheral Manifestations of Gaucher Disease	LY3884961	Intravenous	Endocrinology	1/2
NCT05507996	Recombinant Adeno-associated Virus Serotype 9 (LTGT06) Injection for Patients With Menkes Syndrome	AAV9 LTGT06	NA	Metabolic	Early 1

For MNDs, was initially demonstrated in 2009 the capability of AAV9 vectors to reach MNs by bypassing the BBB and maintaining a transgenic expression for up to 5 months[75]. Next, in 2011, Dominguez et al. demonstrated the efficacy of AAV9 vectors in rescuing SMA mice phenotype. The vectors carried an optimized human *SMN1* WT sequence and were administered at P1 by a single systemic injection ($4.5x10^{10}$ vector genome (vg)) through the temporal vein of the SMA mice model. The results obtained showed an increased amount of SMN protein in the spinal cord and muscles with values similar to WT animals. In the brain, there was also an increment of the expression but in less extent (40% compared to WT). This rescue mediated an extensive increase in the survival time reaching a median of 199 days (untreated SMA mice normally survive ∼13 days), linked to an improved phenotype with increased body weight and spontaneous motor activities. Although some necrotic changes were seen in the ears and tails of SMA-treated animals, these effects were not present in heterozygous mice treated with the same dosage of the AAV9, suggesting that this abnormality was not due to the construct but probably to a low level of SMN protein in these districts[76]. These results had been corroborated by other independent studies which confirm the efficacy of this approach in rescuing SMA pathology when administered systemically in the first days of life both in mice and nonhuman primates[77,78].

In the case of SMA, these successful data paved the way for the start in 2014 of the clinical trials which resulted in the approval, by the FDA in 2019 and by the European Medicines Agency (EMA) in 2020, of the first gene therapy for SMA known as AVXS-101 or Onasemnogene abeparvovec (commercially called Zolgensma). Zolgensma therapy consists of the administration of AAV9 containing a copy of the functional *SMN1* gene by vein infusion in patients younger than 2 years old, with a bi-allelic mutation in the *SMN1* gene and up to 3 copies of *SMN2*. Results up to now demonstrated reduced need for mechanical ventilation and the ability of the treated babies to sit for 30 seconds even after 18 months of life, a milestone that untreated SMA patients never reach[79]. Nevertheless, in a few subsequent studies some adverse effects showed up, such as dorsal root ganglia toxicity, a rare increase in serum aminotransferase levels (adequately treated with additional prednisolone) without other liver dysfunctionalities, respiratory illnesses, and immune reaction

against AAV9 caused by precedent infections, issue partially avoided pre-excluding patients with elevated anti-AAV9 antibodies titers (>1:50) from the trials and treatment[80,81].

The similarity between SMARD1 and SMA led to hypothesize that this approach could work also in the case of SMARD1 and in fact, Nizzardo et al., had firstly demonstrated in 2015 the efficacy of IV administration (facial vein) of AAV9 ($5x10^{11}$ vg) containing the WT human *IGHMBP2* under the control of the cytomegalovirus enhancer/chicken β-actin promoter (CAG) in *nmd* mice at P1. The treatment efficiently mediated a higher expression level of IGHMBP2 protein in the spinal cord of treated mice which resulted in a preservation of MNs and axons numbers, an amelioration of the NMJs innervation, and restored skeletal muscles and heart myofibers size. The mean life span increased by 450% compared to the *nmd* mice treated with the empty vector, with the majority of animals still alive at P300 and a weight similar to WT littermates. In addition, improvement in motor phenotype was also assessed with the hindlimb and rotarod tests[82].

Another independent work by Shababi et al., has been published one year later evaluating a more local route of administration and dosing effect, in particular, a lower dose was evaluated administering ICV at P2 and P3 $1,25x10^{11}$ vg of AAV9-*IGHMBP2* under the control of chicken β-actin promoter (CBA). In parallel, they evaluated also a high dose consisting of the ICV delivery of $2,5x10^{11}$ vg at P2, P3, and P4. Data showed an important survival extension especially with the lower dosage, differently from the high dose which, as a result of unclear toxic effects, resulted in early mortality between P19-22 (30%) and a shorter life span. Low-dose-treated mice displayed additional weight gain, muscle fibers ameliorations, preservation of MNs and axons number and diameter, and NMJs innervation improvement correlated with a phenotypical motor upgrade[83].

Subsequentially the same group compared the efficacy of different routes of administration using the previously determined low dosage of AAV9-*IGHMBP2* vector administered ICV at P2 and P3 or IV at P2. Data demonstrated that both the injection routes mediated a comparable extension of the survival and body weight, but that only the ICV treatment can improve the motor abilities of the *nmd* mice, consistent with a lower IGHMBP2 expression in the spinal cord provided by the systemic administration. Otherwise, they confirmed that the positive effect on the cardiac function mediated by the injection of AAV9-*IGHMBP2* through the IV route was sufficient to extend survival[84].

Surprisingly, in both these works, the nmd^{2J} phenotype was different with respect to what was described by the supply company for the survival time, with untreated affected animals having a variable median life span between 2-5 months of life, suggesting the presence of possible more complex genetic background in the strain.

In 2019 Shababi et al., to overcome the issue of hypothetical modifier allele in the C57BL/6 strain which led to longer survival time, developed a new *nmd* mouse on the FVB background (FVB-*nmd*). The model resulted to be similar to the original *nmd* mouse, but more severe, with a shorter life expectancy (18-21 days), fundamental to test treatments in a timely manner[85]. Then FVB-*nmd* model was exploited by the same group to define the therapeutic window of AAV9-*IGHMBP2* delivery. They tested both low dose (single injection at P2, P4, P6, or P8) and high dose (double injection at P2-3, P4-5, P6-7, or P8-9) administering them ICV at different time points both pre- and post-symptomatically. The results demonstrated that an early treatment led to a more important rescue of the phenotype and of the typical disease hallmarks, although also a delayed injection in the symptomatic phase of the disease mediated an amelioration expanding the potential therapeutic window of this approach[86].
Overall, these results demonstrated the promising application of gene therapy in the treatment of a monogenic disease such as SMARD1, leading to an extended survival time, improvement in the phenotype, and in the neuropathological hallmarks of the disease, without severe complications. Otherwise, the therapeutic window aspect needs further assessment, in fact, up to now, the delayed treatment was evaluated only with ICV local injection, and data on a systemic less invasive route of administration are still lacking.

The preclinical results presented in this work in collaboration with the Center for Gene Therapy at Nationwide Children's Hospital, The Ohio State University, and Jackson Laboratories paved the way for the launch in December 2021 of a Phase I/IIa clinical trial focused on the use of gene therapy for IGHMBP2-related diseases (NCT05152823). It consists of an open-label, single intrathecal injection of AAV9-*IGHMBP2*, in children with a pathogenic variant of the *IGHMBP2* gene (comprising both SMARD1 and CMT2S patients). The principal eligibility criteria are age between 2 months to 14 years, the presence of *IGHMBP2* pathogenic mutations, and the ability of the patient to cooperate for the functional tests. While the major exclusion criteria are correlated to the use of AAV9 such as the presence of active infection or serological evidence of past HIV, Hepatitis B/C and JCV infection, leukopenia/leukocytosis, alterations in liver functionality, prior participation in a gene or cell therapy, autoimmune diseases, and high titer of AAV9 binding antibody (>1:50). Currently the study is enrolling by invitation and its estimated completion date is in November 2028[74].

2.5.1.2. mRNA modulation

Like other neurodegenerative diseases, also in SMARD1, some causative mutations lead to premature termination codons or alteration of the splicing. Currently, a stop codon readthrough therapy,

Ataluren, is available for Duchenne muscular dystrophy[87], while oligonucleotide-based therapy able to modulate the splicing, Nusinersen, is approved for SMA[88]. Recently for SMA was also approved the use of Risdiplam which is a small molecule that mediates the same effect on the affected gene with the advantage that could be administered orally[89].
Considering especially SMARD1, these approaches could be very promising but is necessary to take into consideration that not all the mutations in SMARD1 should be addressed with these therapeutic mechanisms and this leads to the necessity of extensive *in vitro* screening for each patient and a more personalized therapy, which today is still not feasible.

2.5.1.3. Gene editing

The recent discovery of the technology based on the use of clustered regularly interspaced short palindromic repeats (CRISPR) and the associated CRISPR-associated protein-9 nuclease (Cas9) makes genetic editing a promising approach for genetic diseases. The CRISPR-Cas9 system is founded and involved in the prokaryotic immune system and is based on a guide RNA that recognizes the target DNA and then recruits the endonuclease Cas9 which in turn mediates double-strand breaks to eliminate the dangerous DNA. The application of this mechanism in gene editing is exploited by providing a specific RNA guide for a specific gene (knockout) or a template DNA that can be repaired by homologous recombination (knock-in)[90].
Currently, this approach is used mostly to obtain *ex vivo* isogenic corrected iPSCs lines from patients, to have a control model which is completely identical to the patients except for the disease-causative mutation, which could help to better understand the pathological mechanisms at the bases of the disease. Already demonstrated is the possibility to use this technique in other neurodegenerative MN diseases such as ALS, allowing to study the early pathological molecular hallmarks of the disease[91]. Being SMARD1 a monogenic disorder the application of this approach could be very promising, however as mRNA modulation, it will require personalized study of each mutation making it still not practicable on large scale.

Further preclinical studies have also demonstrated the efficacy of this method as a potential therapeutic application in *in vivo* mouse model of Duchenne muscular dystrophy. The authors delivered the CRISPR-Cas9 components through an AAV virus targeting the mutated exon of the dystrophin gene, leading to a recovery of the corrected dystrophin protein and partial rescue of the disease[92].

The most problematic issue is the possible presence of off-target unpredictable consequences which can in turn result in catastrophic effects. Being a very recent and promising method, further studies are needed to assure the safety of this approach before being translated to humans.

2.5.2. IGHMBP2-independent approaches

The treatments based on protein restoration, even if very promising, are probably not sufficient to cure completely the disease, as already demonstrated in SMA, and for this reason, the development of complementary IGHMBP2 independent strategies occurred.

2.5.2.1. Insulin-like growth factor 1

Insulin-like growth factor 1 (IGF1) is a hormone growth factor synthesized by the liver and in less extent also by other peripheral tissues, such as bone, after the stimulation of growth hormone, and then delivered into the blood system. Its transport is mediated by six different IGF binding proteins (IGFBDs) and its function by the presence of peripheral tyrosine kinase IGF1 receptor (IGF1R)[93]. In the central nervous system, the presence of a developmental and tissue-specific expression of IGF1 and its receptor was already demonstrated, suggesting a neuroprotective effect of the pathway. In particular, it was demonstrated how IGF1 increase can stimulate growth cone motility and neurite outgrowth and diminish neuron apoptosis[94].

Regarding MNs, it was demonstrated *in vitro* that IGF1 stimulates axon growth, axonal sprouting in denervated or paralyzed muscles, and prevents muscle damage and atrophy after injury[95–97]. A recent study demonstrates that in ALS patients the circulating level of IGF1 is equivalent to control, but the concentration in the cerebrospinal fluid is significantly reduced suggesting a possible role in the pathology[98]. Its real role in the disease needs further clarification. Few preclinical studies on progressive motor neuropathy[99], ALS[100], and Duchenne muscular atrophy[101] mice models obtained beneficial effects and promising results in treating animals with polyethylene glycol-coupled IGF1 (PEG-IGF1).

A preliminary study in SMARD1 mice described how the activation of tyrosine kinase receptor C simulating the presence of IGF1 by the use of an agonistic monoclonal antibody showed good results into prevent the early decline of muscular ability, but failed in fiber preservation or survival extension, suggesting the need of optimization of this therapeutic approach[102].

In 2014, Krieger et al. investigated the effect of PEG-IGF1 in the SMARD1 *nmd* mice model. In particular, they observed at P14 and also later at P42 that the serum level of IGF1 is endogenously reduced in *nmd* mice, IGFBPs resulted increased, while the transcript expression in the liver is preserved. Therefore, they treated *nmd* mice with multiple subcutaneous injections of PEG-IGF1

from the second week of life every second day obtaining, first of all, an increased serum IGF1 in treated *nmd* mice, and a balanced level of IGFBPs. IGHMBP2 level is not affected by the treatment. PEG-IGF1 administration did not mediate improvement in length and weight of the mice but mutated treated animals showed an amelioration of the muscular phenotype assessed with grip and rotarod tests. Gastrocnemius and diaphragm histopathological analysis demonstrated also that the treatment induced a significant effect on restoring the fiber area on both the muscles analyzed without alteration of the fiber type contribution and distribution, and that the number of cells with central nuclei, a typical feature of *nmd* mice, was reduced after PEG-IGF1 administration. Cardiac hypertrophy present in mutated mice tended to decline after IGF1 injection. Otherwise, no beneficial effects were seen on MNs' survival. Data of this study suggest that the early pathology in *nmd* mice could be associated with an impairment in peripheral IGF1 homeostasis, thus supporting the PEG-IGF1 treatment as a good candidate for future combined treatment in combination with the more effective gene therapy[103].

2.5.2.2. Neural stem cell transplantation

Another promising approach for neurodegenerative treatment is the neuroprotective transplantation of healthy cells in the CNS. Already demonstrated is the ability of embryonic cell-derived MNs to survive and populate the spinal cord if transplanted *in vivo*. They were able also to extend axons and innervate target muscles[104]. This approach was already demonstrated to be beneficial in the ALS model especially when a selected family of neural stem cells (NSCs) were transplanted into the spinal cord[105].

Regarding SMARD1, in 2006 it was first demonstrated the efficacy of transplantation of high expressing aldehyde dehydrogenase embryonic murine NSCs in *nmd* mice. The transplanted mice showed a milder phenotype, extended survival rate, and reduced neural cell death when compared to the untreated ones, even if moderately lower than the WT siblings. Indeed, the MNs substitution was limited and did not allow a complete functional recovery[106].

A different group of murine NSC (Lewis X positive) derived MNs were subsequently tested alone or in combination with pharmacological treatment promoting axonal growth. The transplantation alone led to an extended survival time further improved if associated with pharmacological treatment, which if administered alone is not able to modify the *nmd* phenotype. The beneficial effects were also visible in motor tests and MNs number and size, NMJs, and anti-inflammatory neuroprotection[107].

More recently Simone et al. demonstrated the neuroprotective effects mediated by the transplantation of human iPSCs-derived NSCs in the SMARD1 mice model. The group firstly revealed the capability of iPSCs-derived NSCs to acquire motor neuronal specific characteristics after the transplantation in

nmd mice at P1. In parallel, they demonstrated also that the transplantation of these cells ameliorated the SMARD1 phenotype and extends the animals' survival time. The beneficial result was obtained especially thanks to the neuroprotection of the endogenous MNs mediated by the NSCs released factors such as glial cell-derived neurotrophic factor (GDNF), brain-derived neurotrophic factor (BDNF), transforming growth factor-α (TGF-α), and neurotrophin-3 (NT3)[46]. The advantages of using iPSCs are both ethical and immunological, they make possible autologous transplantation reducing the possibility of rejection. Otherwise, one serious limitation is surprisingly their capability to differentiate in many tissue types, which could be both positive, to complete support the endogenous degeneration, but also a limit due to their high tumorigenic potential[108].

Overall, these results support positively the efficacy of murine and human-derived NSCs transplantation in modifying the phenotype in *in vivo nmd* model, nevertheless, the biggest limitation is their inability to mediate a complete rescue of the pathology, suggesting a possible application of this approach only if combined with gene therapy.

3. Aim of the thesis

SMARD1 is a rare genetic autosomal recessive neurodegenerative disease with infantile onset and fatal course, caused by mutations in the *IGHMBP2* gene. It is considered a MND being the MNs the cells that selectively degenerate in the pathology. Currently, the prognosis is poor, life expectancy is reduced, and no therapies are approved, only palliative treatments.

Gene therapy emerges in the last years as a promising tool for monogenic diseases. It is founded on the replacement of the mutated gene with a copy of the WT one carried by an AAV construct. In SMARD1 specificity, even if how IGHMBP2 decreased protein level leads to MNs degeneration is still not completely understood, an AAV9 vector with CNS tropism was used efficaciously in preclinical studies to deliver the human WT *IGHMBP2* gene.
This approach has already obtained encouraging results in SMARD1 mice when administered pre-symptomatically, otherwise, the promoter choice, a fundamental aspect to have better control of the transgenic expression, has never been investigated. In this work, we want to assess if the use of distinct promoters which modulate differently the protein expression could affect the efficacy of the treatment administered ICV, with the aim of optimize the gene therapy technique for the clinical translation (in collaboration with Ohio Nationwide Children's Hospital).
Another essential point for clinical application is the definition of a therapeutic window. Currently, preclinical data are available only for the local ICV route of administration in the more severe *FVB-nmd* model. For this reason, here we want also to evaluate how a less invasive systemic administration, such as the subcutaneous (SC) one, is able to rescue SMARD1 disease when administered in an already symptomatic *nmd* model.

In particular, the aims of this thesis are:

- Compare blindly the efficacy of two different promoters in AAV9-*IGHMBP2* constructs administered in pre-symptomatic *nmd* mice via ICV injection. The best construct will be assessed by evaluation of IGHMBP2 protein level, survival time, phenotypical rescue, and neuropathological changes, with a parallel evaluation of toxicity and long-term effects;
- Concomitantly assess the efficacy of a different route of administration with respect to the already validated systemic (IV) one, in particular, evaluating a more local injection (ICV) which could result in reduced dosage, dispersion, toxicity, and costs if compared to a more systemic one;

- Define the therapeutic window for the efficacy of gene therapy in *nmd* mice, treating animals during the symptomatic phase of the disease systemically SC with the construct already validated by Nizzardo et al. 2015, essential for future implication in the clinic application.

4. Materials and methods

4.1. Murine model

The B6.BKS-*Ighmbp2*^{nmd2J}/J mouse strain is the SMARD1 murine model selected to perform the experiments described in this work. Animals were purchased from The Jackson Laboratory (Bar Harbor, ME, USA) as stock #002521. All animal experiments were approved by the University of Milan and Italian Ministry of Health review boards according to the institutional guidelines, in compliance with national (D.I. no. 116, G.U. suppl. 40, February 18th, 1992, Circular no. 8, G.U., July 14th 1994) approved protocol 707/2019-PR. Heterozygous mice for the *Ighmbp2* mutation were bred together to obtain affected mice with homozygous mutation (*nmd*^{2J}*/nmd*^{2J} commonly called *nmd*) and WT littermates were used as healthy controls.

4.1.1. Genotyping

Mice genotyping was performed on a 2 mm tail biopsy taken from newborn pups. DNA extraction was performed using the salting-out method based on the removal of contaminants using a high salt concentration solution followed by the alcoholic precipitation of the DNA. Tail biopsies were incubated overnight (ON) at 55°C with 0.27 mg/ml Proteinase K (Thermofisher) resuspended in 300 ul of Tris-EDTA buffer (20 mM EDTA, 400 mM NaCl, 0.5% SDS, 50 mM Tris). The next day, 180 ul of NaCl 3M were added. 5 min centrifugation at 13'000 round per min (rpm) was then performed to precipitate and discard the digested proteins and collect in a new tube 200 ul of the supernatant containing the nucleic acids. The precipitation was subsequentially performed by adding 200 ul of cold ethanol 100% and centrifugating for 5 min at 13'000 rpm. The pellet was then again resuspended in 150 ul of ethanol 75% and re-centrifuged for 3 min at 13'000 rpm. Next, the supernatant was discarded, and the pellet was let air dried for 10 min before being resuspended in 50 ul of deionized water and incubated for 30 min at 65°C.

100 ng of the obtained DNA were amplified using the following primers (Sigma Aldrich):

- Forward: 5'-CCT GAT TTT GGC TCT GGT CC-3'
- Reverse: 5'-GCT CCT GAT GAT CCA ATG GT-3'.

The primers were designed to amplify a 356 bp region on Chr 19 containing the mutated nucleotidic position in the intron 4 of *Ighmbp2*. The amplification was performed using the following mix (*Table 2*) and a TouchDown (TD) polymerase chain reaction (PCR) cycling protocol (*Table 3*).

Table 2. PCR solution mix

Reaction component	Final concentration
ddH20	Up to final volume
10X PCR Buffer, Minus Mg (Invitrogen)	1X
MgCl2 (Invitrogen)	2 mM
Primer Forward	0.75 uM
Primer Reverse	0.75 uM
Betaine, 5M (Thermo Scientific)	1 M
Platinum Taq DNA Polymerase (Invitrogen)	1.3 U
DNA	100 ng

Table 3. PCR cycling protocol

Step #	Temperature (°C)	Time	Note
1	97	3 minutes (min)	
2	95	30 seconds (s)	
3	65	30 s	-0.5 °C per cycle decrease
4	72	45 s	
5			Repeat steps 2-4 for 10 cycles (TD)
6	95	30 s	
7	55	30 s	
8	72	45 s	
9			Repeat steps 6-8 for 20 cycles
10	72	3 min	
11	4		Hold

The A to G transition mutation resulted in the creation of a unique restriction site for the DdeI enzyme making only the mutated allele susceptible to its action. For this reason, the PCR amplification product was then digested with 0.2 U/ul DdeI (Promega) in Buffer D 1X (Promega) added with 0.1 ug/ul BSA (Promega) for 45 min at 37°C. The digestion results were visualized in a 2% agarose gel with the use of GelRed™ (Sigma Aldrich). Affected animals were recognized by the homozygous presence of the mutated allele digested in two segments of 147 and 209 bp, while the WT allele, insensitive to the DdeI digestion, produced a single product of 356 bp. Genotyping categorized animals in WT, heterozygous or homozygous for *Ighmbp2* mutation.

4.2. Viral vectors structure and administration

In the first part of the work, three AAV9 constructs provided by our collaborator at Nationwide Children's Hospital (Columbus, Ohio) were tested. Two contain human *IGHMBP2* cDNA under the control of different promoters, specifically the chicken beta actin (CBA) or a truncated form of the

Methyl CpG binding protein 2 (MeCP2) called P546, and the third one empty, randomly assigned as virus A, B or C (*Figure 5*).

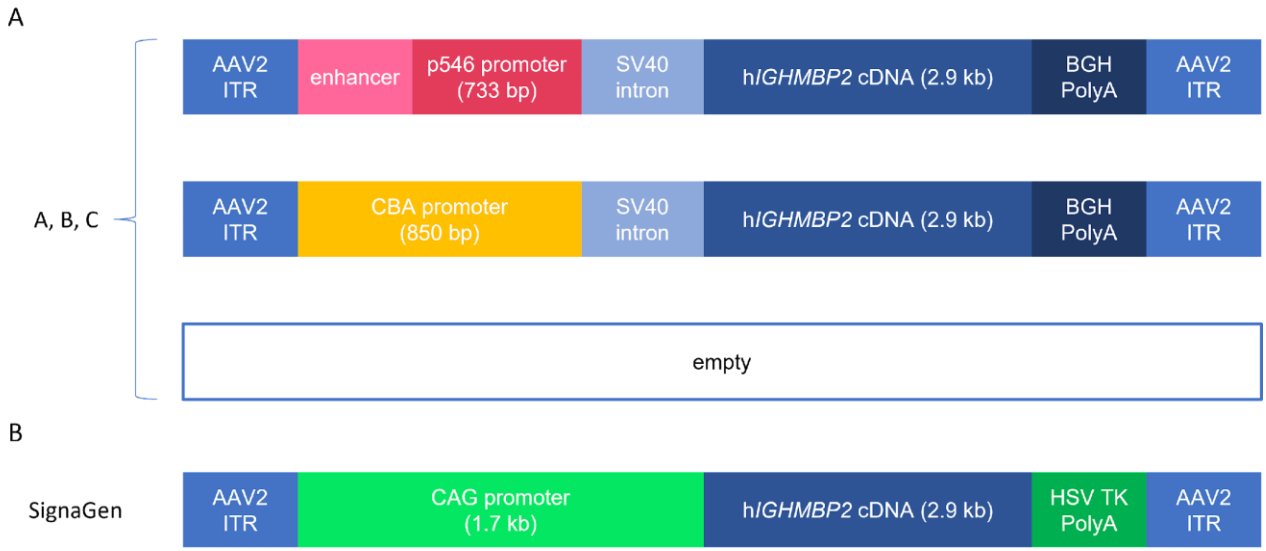

Figure 5. Schematic representation of AAV9 constructs tested. (A) virus A, B and C structure was shown. Two constructs contain the human IGHMBP2 cDNA under the control of CBA or p546 promoter while the third is empty. (B) Structure of the AAV9 construct produced by SignaGen Laboratories containing the human IGHMBP2 cDNA under the control of CAG promoter. Abbreviations: simian virus 40 (SV40) intron, Inverted Terminal Repeats (ITR), bovine growth hormone (BGH), Herpes simplex virus thymidine kinase (HSV TK).

The treatment with virus A, B, and C during the presymptomatic phase consists of a single ICV injection, performed as previously described[109], of $5x10^{10}$ vg of virus A (n=28), B (n=26), or C (n=28) at P1. The operator was blind to promoter selection. WT littermates (n=28) were used as controls, and *nmd* mice treated with virus B were used as pathological baseline (negative control).

The second part of the project was performed using an already validated AAV9 construct[82–84] carrying the human *IGHMBP2* cDNA under the control of the CAG promoter (SignaGen Laboratories, Maryland, USA) consisting of the cytomegalovirus enhancer fused to the CBA promoter (*Figure 1B*). An empty construct (AAV9null) was used as negative control. The dosages preliminarily tested were indicated in *Table 4*.

Table 4. Treatment dosage

Route of administration	**Dosage (vg)**
Subcutaneous low dose	$6.25x10^{10}$
Subcutaneous high dose	$1.26x10^{11}$
Intraperitoneal low dose	$8.75x10^{10}$
Intraperitoneal high dose	$1.5x10^{11}$
ICV	$7.5x10^{10}$

The symptomatic treatment was then performed in *nmd* mice at P7 treated subcutaneously (SC) with the high dose ($1,26x10^{11}$ vg) (n=51). WT mice (n=39) were used as control and *nmd* mice treated with the empty vector (n=7) as pathological baseline.

4.3. Western Blot analysis

Spinal cords of the mice treated at P1 and harvested at P20 (n=3/group) and P200 (WT and virus A n=3, virus C n=1) and WT mice treated at P7 (n=1/condition) harvested at P20, were directly frozen in liquid nitrogen, and stored at -80°C. The lysis of 20 mg of frozen tissues was performed using NuPAGE™ LDS Sample Buffer pH 8.4 (ThermoFisher) added with Protease Inhibitor Cocktail (ThermoFisher) a set of protease inhibitors. The samples were then sonicated for 10 s at 40 watts twice, boiled for 4 min, and then centrifuged for 13 min at 13'200 rpm. 20 µg of the extracted proteins were collected with the use of a reducing agent (dithiothreitol) and separated on a 4-12% gradient polyacrylamide gel (Invitrogen NuPAGE Bis-Tris). Next, they were electrophoretically transferred to a nitrocellulose membrane (GE Healthcare Amersham) at 100V for 1 hour (h) at 4°C. The membrane was then saturated with the Intercept® Blocking Buffer in PBS (LI-COR) for 1h at room temperature (RT). Next, it was incubated ON at 4°C with primary antibody anti-human IGHMBP2 (Millipore, 1:800) and anti-α-actin (Sigma-Aldrich, 1:1'000) as control protein in TBS solution (20mM Tris-HCl, 0.5 M NaCl). The next day the membrane was washed with TBS additioned with 0.05% Tween 20 (Sigma-Aldrich) (TBS-T) and then incubated with the secondary antibody anti-mouse (IR-DYE 800 CW, 1:10'000) diluted in TBT-T 1.30 h at RT. The membrane was then washed again with TBS-T and the visualization of the bands was performed with LI-COR Bioscience, Odyssey FC, and the densitometric analysis of the signals was conducted with the Image Studio™ (LI-COR Biosciences). The IGHMBP2 levels were normalized on the α-actin ones.

4.4. Phenotype and survival analysis

Each animal was monitored once a week for morbidity and mortality, then, starting from 2 weeks of age, body weight and behavioral motor responses were also registered. At P45 the rotarod performance test was added and performed monthly.

Motor function was tested through the hindlimb splay test, the rotarod test, and the grip strength measurement.

4.4.1. Hindlimb splay test

The hindlimb splay test was used to evaluate the ability of the mice into open the hindlimb when suspended head down for the tail classified on a 5 steps scale from 0 to 4. The 0 score corresponds to the complete inability to open the hindlimb when suspended for the tail, a characteristic sign of *nmd* mice phenotype, while the 4 score indicates the maximum extension typically obtained from WT mice.

4.4.2. Rotarod test

Monthly, starting from P45, the Rotarod performance test (Rotarod 7650, Ugo Basile) was performed to assess the motor ability and the balance of the mice. The protocol used consisted of an increasing speed from 4 to 40 rpm in 300 s (with an increase of 1 rpm each ~8.3 s). At the maximum trial duration of 300 s, the percentage of the mice that completed the test without falling was recorded.

4.4.3. Grip strength

Grip strength of all four paws was measured weekly with Stoelting Ugo Basile Grip Strength Meter. Animals were placed on a grid (1 cm^2) and dragged for the tail horizontally measuring the resistance that the mice opposed in Gram Force (gf).

4.5. Histological and immunohistochemistry analysis

Tissues of P1 and P7 treated animals were collected at P20 (n=3/group). P1 treated samples were also harvested at P200 from adult mice (WT and virus A n=3, virus C n=1).

Gastrocnemius and cardiac muscles were directly frozen on dry ice and stored at -80°C. Spinal cords were fixed in a 4% paraformaldehyde solution for 24h at 4°C and then immersed ON at 4°C in a 30% sucrose solution. The next day spinal cords were removed from their backbone part, the lumbar part was frozen on dry ice immersed in the Optimal Cutting Temperature compound (OCT, Tissue Tek), and then stored at -80°C. Each tissue was sectioned by cryostat (Leica) and mounted on a glass slide conserved at -80°C for at least one night before staining.

4.5.1. MN count

MN specific staining was performed on lumbar spinal cord slides sectioned with a thickness of 20 μm. Slides were let defrost for 15 min at RT, washed one time in PBS 1X, and permeabilized in 0.25% Triton-X-100 in PBS 1X for 5 min. The sections were then blocked for 1 h with blocking solution (0.25% Triton-X-100, 10% Normal Donkey Serum) in PBS 1X at RT. Slides were incubated ON at 4°C with the primary antibody against choline-acetyltransferase (ChAT, Millipore, Goat, 1:250) in the blocking solution. The next day the tissues were washed with PBS 1X and incubated for 1 h at RT with the secondary biotinylated anti-goat antibody (Vector Laboratories, 1:400) in PBS 1X. Then sections were washed with PBS 1X and incubated for 1 h at RT with Streptavidin Cy3 (Sigma Aldrich, 1:400) in PBS 1X. After the incubation, the samples were washed and incubated for 5 min at RT with 4',6-diamino-2-phenylindole (DAPI, Invitrogen, 1:1000) in PBS 1X. Lastly, the slides were washed again, and the coverslips were mounted with the use of Fluor Save Reagent (Calbiochem). Images were acquired with confocal microscope (Leica SP8) at 10X and 20X

magnification. 30 serial sections taken at least 100 μm apart were analyzed counting the mean number of ChAT-positive MNs in the ventral horns of the lumbar spinal cord (L1-L5).

4.5.2. Astrocyte gliosis and microglia activation analysis

Astrocyte and microglia assessment was performed on lumbar spinal cord slides sectioned with a thickness of 20 μm. Slides were let defrost for 15 min at RT, washed one time in PBS 1X, and permeabilized in 0.25% Triton-X-100 in PBS 1X for 5 min. The sections were then blocked for 1 h with blocking solution (0.25% Triton-X-100, 10% Normal Goat Serum) in PBS 1X at RT. Slides were incubated ON at 4°C with the primary antibody against Glial fibrillary acidic protein (GFAP, Millipore, Mouse, 1:600) for astrocyte or Ionized calcium binding adaptor molecule 1 (Iba1, Wako, Rabbit, 1:500) for microglia in blocking solution. The next day the slides were washed with PBS 1X and incubated for 1 h at RT with the specific secondary antibody (Alexa Fluor 488, goat anti-mouse, Invitrogen 1:1000 or Alexa Fluor 568, goat anti-rabbit, Invitrogen, 1:1000) in PBS 1X. After the incubation, the samples were washed and incubated for 5 min at RT with DAPI (Invitrogen, 1:1000) in PBS 1X. Lastly, the slides were washed again, and the coverslips were mounted with the use of Fluor Save Reagent (Calbiochem). Images were acquired with a confocal microscope (Leica SP8) at 63X magnification. Astrocyte gliosis and microglia activation were evaluated by counting the percentage of the cells for each slice surrounded by more than 50% of their perimeter by GFAP or Iba1 signal.

4.5.3. NMJs innervation analysis

NMJ staining was performed on gastrocnemius muscle slides sectioned with a thickness of 20 μm. Slides were let defrost for 15 min at RT, washed one time in PBS 1X, and permeabilized in 0.25% Triton-X-100 in PBS 1X for 5 min. The sections were then blocked for 1 h with blocking solution (0.25% Triton-X-100, 10% Normal Goat Serum) in PBS 1X at RT. Slides were incubated ON at 4°C with the primary antibody anti neurofilament medium chain (NF-M, Millipore, Rabbit, 1:250) in the blocking solution. The next day the muscles were washed with PBS 1X and incubated for 1.30 h at RT with the specific conjugated secondary antibody anti-rabbit (Alexa Fluor 488, Invitrogen, Goat, 1:1000) in PBS 1X. Then sections were washed with PBS 1X and incubated for 3.30 h at RT with α-bungarotoxin conjugated with Alexa 555 (Invitrogen, 1:200) in PBS 1X. After the incubation, the samples were washed, and the coverslips were mounted with Fluor Save Reagent (Calbiochem). Images were acquired with confocal microscope (Leica SP8) at 40X and 63X magnification. The total number and the innervated percentage, identified by the colocalization of NF-M and the α-bungarotoxin, of randomly selected NMJs were counted (n=100 junctions/animal).

4.5.4. Histological analysis

12 μm thick gastrocnemius and cardiac muscle slides were stained with hematoxylin-eosin (HE). The samples were let defrost for 15 min at RT and then immersed for 5 min in hematoxylin. The slides were then washed with water, immersed for 30 s in eosin, and rewashed. Next, the muscles were immersed for 1 min in ethanol 96%, and then for 1 min in other two consecutive jars containing ethanol 100%. Lastly, they were immersed twice in xylene for 1 minute, mounted with the use of DPX Mounting Media (Thermo Scientific), and stored at RT. Images were acquired at 20X with optical microscope Leica DMi8.

The cross-sectional area (CSA) of each fiber was obtained by a manual trace of their perimeter using LAS software version 4.9.0 (n=600 muscular fibers/animal).

The fibrotic and necrotic percentage of each image was calculated by using the HE colors deconvolution plugin of ImageJ software.

4.6. RNA isolation and Real-Time qPCR

The liver of the mice treated at P1 or P7 (n=3/group) harvested at P20 and the cardiac muscle (n=1/group) at P200 (WT and virus A n=3, virus C n=1), were frozen directly in liquid nitrogen and stored at -80°C. Total RNA was extracted from 20 mg of tissue using ReliaPrep™ RNA Tissue Miniprep System (Promega). 1 μg of RNA was retrotranscribed in cDNA using the Ready-to-Go™ kit (GE Healthcare) using random hexamer primers. The expression level of *Igf1* (Mm00439559-m1, ThermoFisher Scientific) and *Igfals* (Mm01962637_s1, ThermoFisher Scientific) were assessed by quantitative analysis on a 7500 Real-Time PCR System (Applied Biosystems) with ΔΔCt protocol. Data were normalized to the average levels of 18S (Hs99999901_s1).

4.7. Toxicity evaluation

The toxicity of the treatment was evaluated on the serum of WT mice, and animals treated with virus A, B, and C (n=4/group). Blood was collected from the mice's facial vein in MiniCollect™ Tube, Gold Cap, CAT Serum Sep Clot Activator (Greiner Bio One) and let coagulate for 30 min at RT. Then the samples were centrifuged for 10 min at 2500 g and the resulting supernatants serums were collected and stored at -20°C. Serums were then analyzed by the Charles River Laboratories (Italia) for the following toxicity biomarkers: alanine transaminase (ALT), aspartate aminotransferase (AST), alkaline phosphatase (ALP), creatine kinase (CK), lactate dehydrogenase (LDH), total bilirubin, bile acids, glucose, creatinine, urea, albumin, total proteins, total cholesterol.

4.8. Statistical analysis

Statistical analyses were performed with the software GraphPad Prism® version 6.0 (GraphPad Software Inc.). The survival data were represented with the Kaplan-Meier curve and analyzed with the log-rank test. The remaining data were expressed as mean ± standard error of the mean (SEM). Each data group was normalized on the mean of the control group (WT). Multiple values were examined using one-way analysis of variance (ANOVA) for multi-comparison analysis followed by Tukey's post hoc test. Two-tailed, unpaired Student's t-test was employed to compare two groups. The NMJ innervation was analyzed by the Contingency test followed by Fisher's exact test. For all the analyses a *P*-value <0.05 was considered statistically significant.

5. Results

2.6. Presymptomatic AAV9-IGHMBP2 administration

2.6.1. IGHMBP2 protein increased expression after local injection

Homozygous mutated B6.BKS-*Ighmbp2*^{nmd2J}/J (named *nmd*), were blindly treated with three constructs, two containing different promoters and the third one empty, defined as virus A, B, and C. The animals were treated ICV with a single injection containing $5x10^{10}$ vg at P1. To assess the efficacy of the constructs in rescuing the IGHMBP2 protein level, WB was performed on spinal cords of WT mice and *nmd* mice treated with virus A, B, and C ICV at P1 harvested at P20 (*Figure 6A*). The results showed that both virus A and C led to a huge increase in protein expression especially virus A, confirming that the administration of AAV9-*IGHMBP2* vectors ICV at P1 efficaciously rescued the level of the lacking protein (*Figure 6B*, ANOVA $P<0.01$). Virus B showed a lower level of IGHMBP2 compared both to WT animals and to mice treated with the other two constructs, leading us to suppose that it was the empty vector. For this reason, with the aim to reduce the number of animals used, the virus B treatment was kept as negative control.

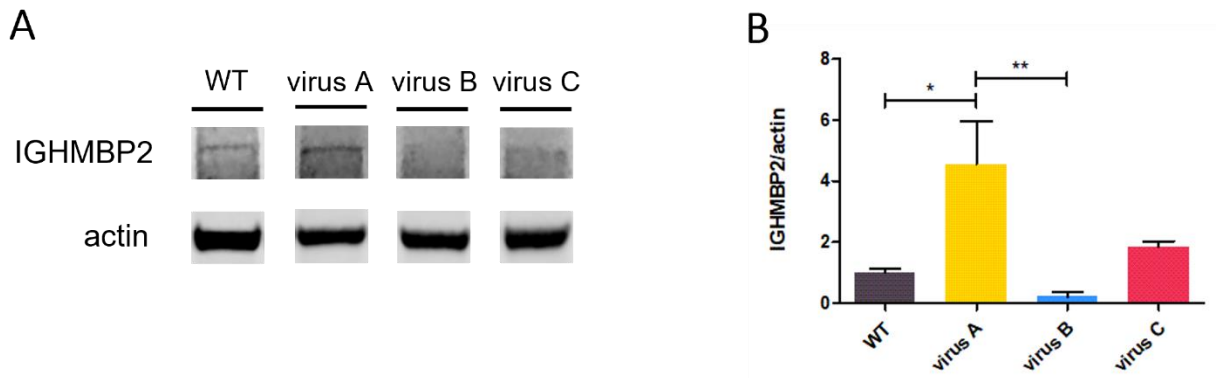

*Figure 6. IGHMBP2 protein expression. (A) Expression level was detected by WB analysis performed on P20 spinal cords of WT mice and nmd mice treated ICV at P1 (n=3/group). Representative immunoblots were shown (B). Relative values normalized on α-actin. The values are represented as mean value ± SEM. Statistical analysis was performed with one-way ANOVA followed by Tukey's post hoc test. *P<0.05, **P<0.01.*

2.6.2. Survival extension and phenotypical amelioration

After having demonstrated that the A and C constructs were both able to mediate an increase of the IGHMBP2 protein in the spinal cord of *nmd* treated animals when administered ICV at P1, the next step was to assess if changes in the IGHMBP2 level corresponded to an amelioration of the phenotype and modification of the mice survival time. To this extent WT animals, and *nmd* animals treated with virus A, B, and C were monitored for mortality and phenotypical motor ability starting from P15.

Survival data showed an important and significant extension of the survival proportion with both virus A ($P<0.001$) and C ($P<0.001$), with a median survival of 162 days for virus A treated animals and 138 days for virus C treated animals, while the virus B treated animals reached only a median value of 25 days (*Figure 7A*). Virus A treated group showed an important early mortality rate around P20, not present in the virus C cohort.

Affected *nmd* animals were already described to be smaller compared to the WT littermates. For this reason, body weight was the next parameter that have been assessed. Weight analysis showed that both the compounds A and C led to weight values very similar to the WT littermates, confirming their efficacy into rescue the pathological phenotype after the treatment, especially considering that the virus B treated *nmd* mice died very early and thus they can be weighted only a few times (*Figure 7B*, $P<0.01$, $P<0.001$).

The motor behaviors of the animals were evaluated with the hindlimb splay test (*Figure 7C* and *E*). A typical characteristic of *nmd* mice is to show hindlimb contractures which results in the complete inability to open their hindlimb when suspended head down for the tail (0 score on the test scale). A similar result was in fact obtained compared to WT in our virus B treated cohort, in which the animals can be tested only in the early phases before their natural early death. Otherwise, the mice treated with virus A and C obtained a significantly better score close to WT one, demonstrating the efficacy of both the compounds into rescue the motor ability of the mice through increasing IGHMBP2 protein ($P<0.001$).

Lastly, the rotarod performance test was exploited to evaluate the motor functionalities and the equilibrium of the animals when positioned on a rotating tube in acceleration. The mice treated with both virus A and C reached the age to perform it (at least P45) while the virus B treated animals did not. The results of the rotarod test demonstrated that an important percentage of the animals treated with virus A and virus C completed the test without falling, again a sign of an improved motor ability mediated by the treatment (*Figure 7D*).

Overall, the data obtained so far demonstrated that an increase in the level of IGHMBP2 protein in the spinal cord mediated by AAV9-*IGHMBP2* ICV administration at P1 corresponded also to a parallel impressive extension of the life span and an important amelioration of the motor phenotype in the *nmd* mice model.

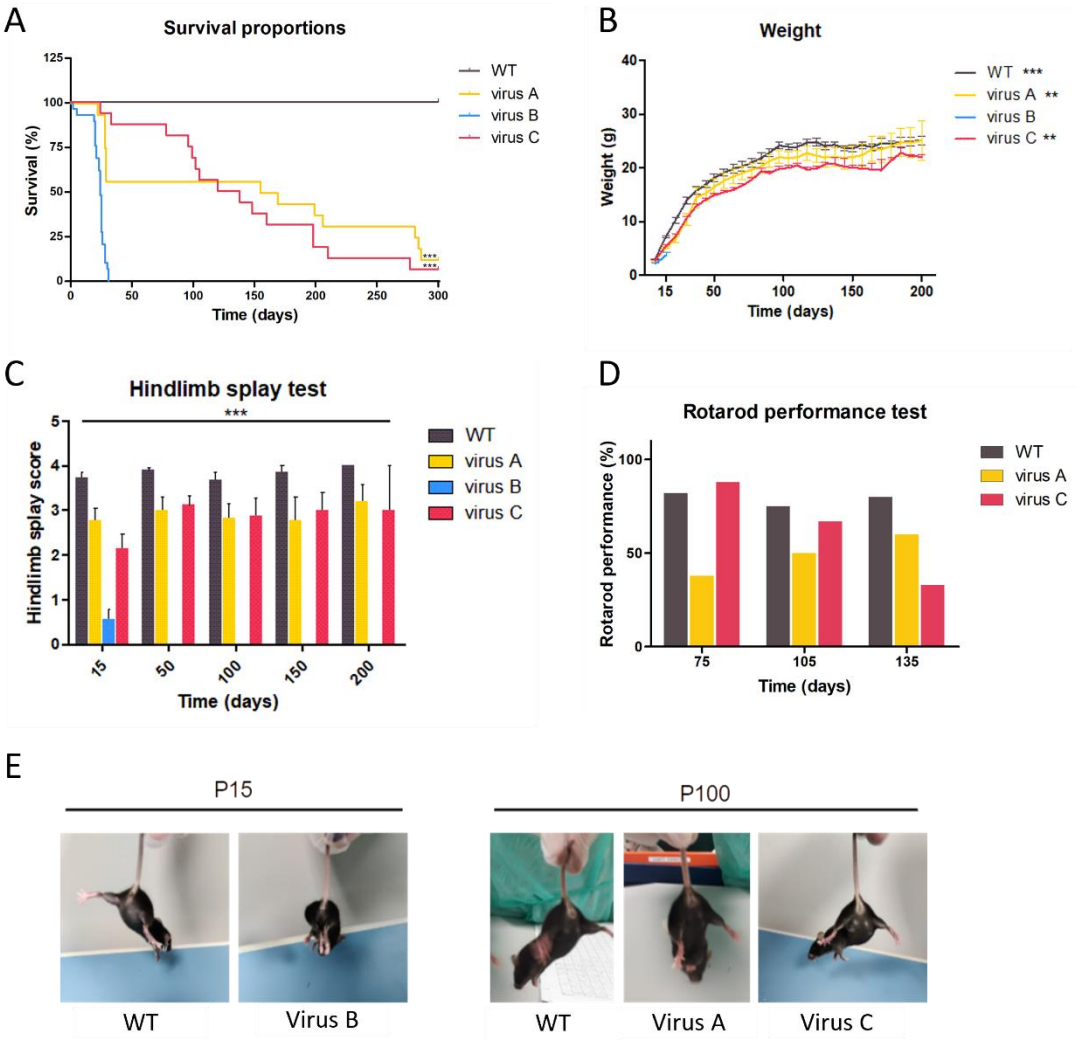

*Figure 7. Survival and phenotypical test of WT mice (n=19), mice treated with virus A (n=19), B (n=20), and C (n=19). (A) Kaplan-Meier survival curve. (B) Body weight curve in grams. The values are represented as mean value ± SEM. Statistical analysis performed with one-way ANOVA in comparison to the virus B group (C) Hindlimb splay test score at different time points. The values are represented as mean value ± SEM. Statistical analysis was performed with one-way ANOVA. (D) Rotarod performance recorded monthly starting from P75. (E) Representative images of macroscopic phenotypical difference between WT and virus B treated mice at P15 (left) and between WT and virus A and C treated animals at P100 (right). **P<0.01, ***P<0.001.*

2.6.3. Neuropathological hallmarks rescue

To determine if the motor functional and phenotypical macroscopic amelioration correspond to a histopathological change in the most affected tissues, spinal cord, and gastrocnemius muscles were analyzed.

2.6.3.1. MN number

By definition, in MNDs, and thus SMARD1, the cells that selectively degenerate are the MNs. To detect changes in the number of MNs in mice spinal cord the MN-specific antibody against choline acetyltransferase (ChAT) enzyme was used to stain serial sections of the most affected area, the lumbar spinal cord (L1-L5), harvested at P20 of WT, and treated mice (*Figure 8A*). The quantification of ChAT-positive MNs in the ventral horn of the spinal cord demonstrated a global reduction of MNs number in virus B treated mice (mean = 6.4±0.6) compared to WT (mean = 9.3±1.3), and a partial rescue in virus A (mean = 8.9±0.9) and virus C (mean = 9.7±1.4) treated mice (*Figure 8B*, $P<0.05$).

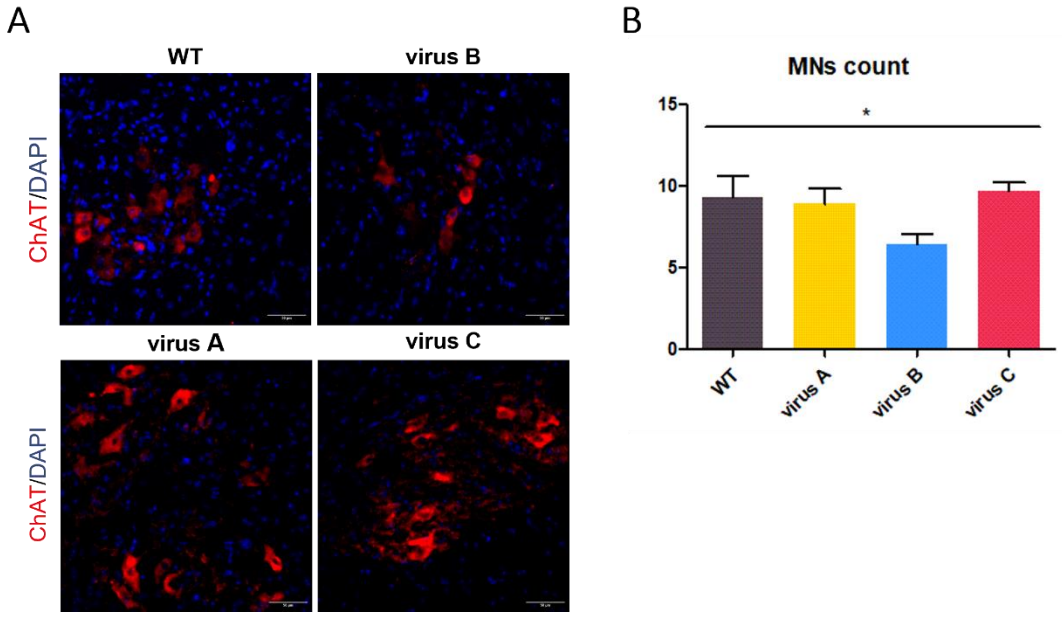

*Figure 8. MN count in lumbar spinal cord. (A) Representative immunofluorescence images of 20 µm spinal cord's ventral horn sections of WT, and nmd treated mice (n=3/group) stained for ChAT (red) and DAPI (blue) and acquired with a confocal microscope with a magnification of 20X. (B) Average MN number in the lumbar spinal cord. The values are represented as mean value ± SEM. Statistical significance was determined by one-way ANOVA. * P<0.05. Scale bar = 50 µm.*

This result confirmed that the increase of IGHMBP2 protein in the spinal cord led to a preservation of the MN number in the virus A and C treated animals if compared with the virus B treated mice in which the degeneration of the MNs was clearly visible.

2.6.3.2. Astrocyte gliosis and microglia activation

The presence of neuroinflammation has already been demonstrated in neurodegenerative diseases. In particular, in SMA, astrogliosis was shown to be present in the spinal cord in animal models and human patients at the end stage of the disease resulting in both morphological and functional changes in astrocytes. In parallel, the presence of activated microglia was also demonstrated in the SMA mice model starting from the early symptomatic stage. Fundamental, in this contest, is the activation of the neuroinflammatory pathways which could induce neuronal and glial apoptosis spreading

neurodegeneration. The temporal relationship between neuroinflammation and MN degeneration is still debating[110].

For similarity, the presence of astrocyte gliosis and microglia activation was here evaluated to observe the modifications induced by the treatment. Astrogliosis was studied by immunofluorescence analysis of mice spinal cord using a specific antibody against the glial fibrillary acidic protein (GFAP) (*Figure 9A*). Quantification expressed as a percentage of GFAP-positive cells on the total cell number demonstrated a significative alteration of astrocytes number with an important increase of GFAP signal in virus B treated animals (28.2%±1.6) compared to WT (6.6%±1.1), which otherwise resulted

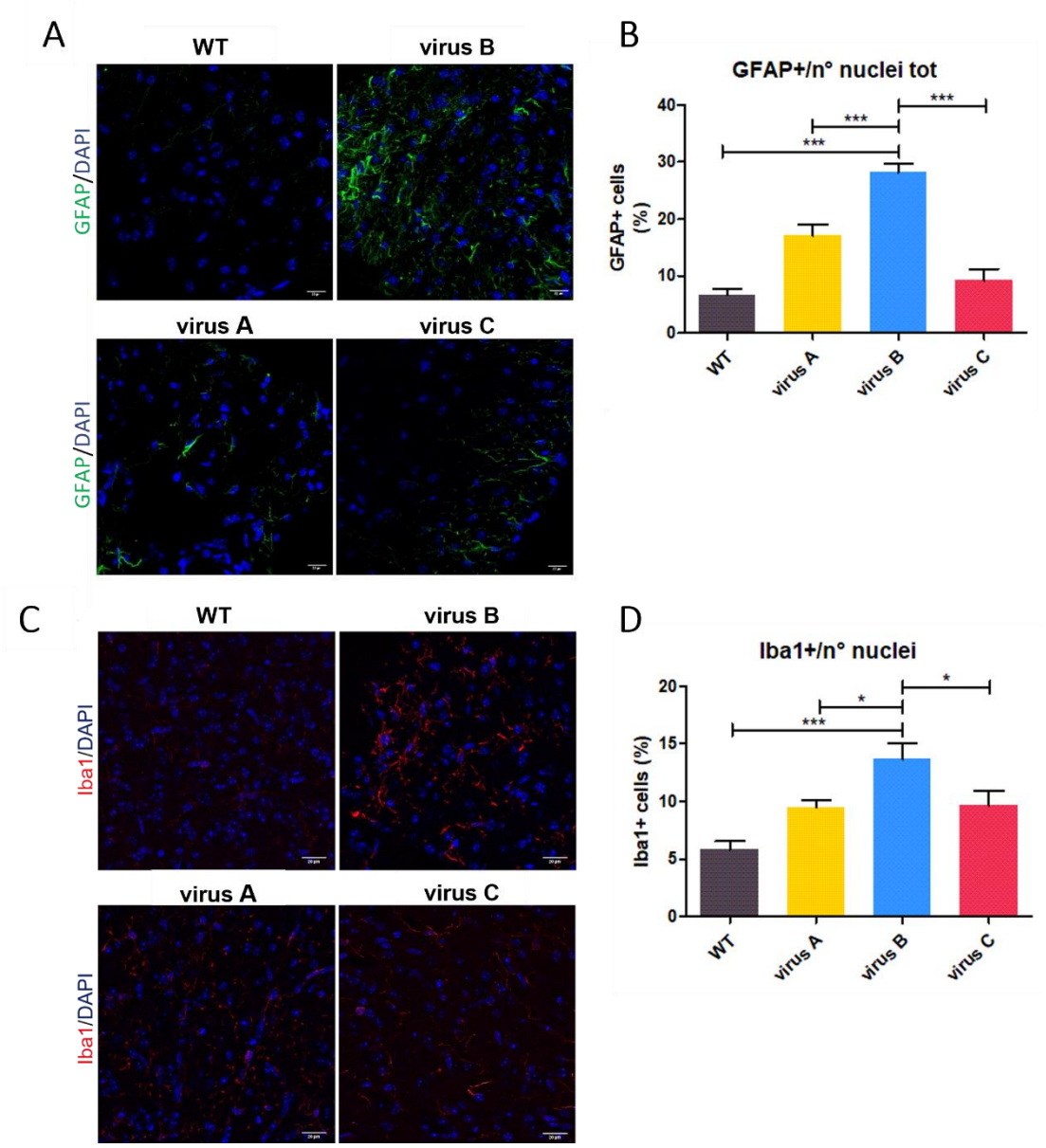

*Figure 9. Astrocyte gliosis and microglial activation analysis. (A-C) Representative immunofluorescence images of 20 µm spinal cord sections of WT, and nmd treated mice (n=3/group) stained for GFAP (green) (A) or Iba1 (red) (C) and DAPI (blue) and acquired with confocal microscope with a magnification of 63X. (B-D) Quantification represented as percentage of GFAP (B) or Iba1 (D) positive nuclei divided for the total number of cells. The values are represented as mean value ± SEM. Statistical significance was determined by one-way ANOVA followed by Tukey's post hoc test. *P<0.05, ***P<0.001. Scale bar = 20 µm.*

significatively rescued in virus A group (17.1%±2.0) and furthermore in virus C cohort (9.2%±2.0) (*Figure 9B*, *P*<0.001).

Microglia status was assessed by spinal cord staining against ionized calcium-binding adaptor molecule 1 (Iba1) (*Figure 9C*). The quantifications expressed as the percentage of Iba1-positive cells on the total cell number demonstrated the presence of a significative difference between the mice groups, in particular, increased Iba1 microglial expression was present in virus B treated mice (13.7%±1.4) if compared to WT (5.8%±0.8), and that the treatment with both the constructs, mediated a partial rescue of this activation (virus A 9.5%±0.7, virus C 9.6%±1.3, *Figure 9D*, *P*<0.001).

2.6.3.3. NMJ innervation

Another important feature of MNDs diseases and SMARD1 is the reduced innervation of the skeletal muscles which results in muscular atrophy and paralysis. To assess the denervation level after the treatment, immunofluorescence analysis on the gastrocnemius of the mice investigating the NMJ innervation was performed (*Figure 10A*). The neuronal presynaptic compartment was stained using the antibody against the neurofilament medium chain (NF-M) while the muscular post-synaptic one was targeted with α-bungarotoxin (BTX). The NMJs were considered innervated when the two signals colocalized. Results were expressed as the percentage of innervated NMJs on their total number.

This experiment confirmed that both the A and C treatments led to a significant increase in the innervation of the NMJs if compared to virus B, reaching values very similar to the WT mice.

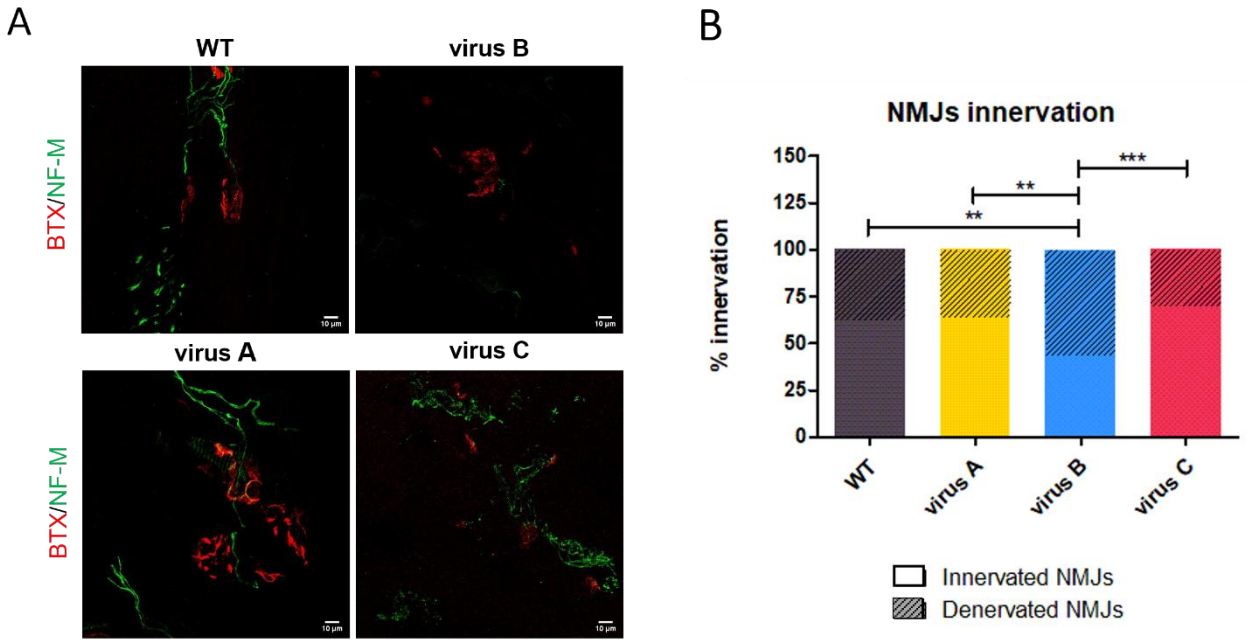

*Figure 10. Neuromuscular junction immunofluorescence analysis. (A) Representative immunofluorescence images of 20µm gastrocnemius sections of WT, and nmd treated mice (n=3/group) stained for NF-M (green) and BTX (red) and acquired with a confocal microscope at a 47 magnification of 63X. (B) Stacked bar plot of NMJs percentage innervation. Statistical significance was determined by the Contingency test (Fisher's exact test). **P<0.01, ***P<0.001. Scale bar = 10 µm.*

Treated mice showed a significant increase in average NMJ innervation if compared to the *nmd* animals treated with the empty vector (43.4%), in fact, virus A treated animals reached an NMJ innervation percentage of 63.5% (chi-square = 8.863) and virus C cohort 69.9% (chi-square = 14.83) both comparable to the WT animals results (62.2%), demonstrating one of the neuropathological modifications at the basis of the phenotypical muscular improvement (*Figure 10B*).

2.6.3.4. Muscle histology

The results up to now demonstrated the degeneration of the presynaptic compartment in the motor signal pathway. To evaluate the presence of muscle alterations caused by decreased innervation, hematoxylin-eosin (HE) staining on transversal sections of gastrocnemius was performed (*Figure 11A*). Both viruses A and C led to a qualitative reduction of macroscopic muscular damage signs, mediating an amelioration of fibers distribution and organization if compared to virus B treated animals.

The first parameter analyzed was the cross-sectional area (CSA) of muscle fibers which resulted to be drastically reduced in virus B mice and partially restored in size after the treatment with virus A and furthermore with virus C (*Figure 11B*, $P<0.001$).

The second measurement performed was the quantitative evaluation of fibrosis (fatty connective tissue) and necrosis (cellular infiltrates) in gastrocnemius muscles, expressed as non-muscular percentage area. The data confirmed that virus B treated mice had a significant increase in the amount of fibrotic tissue and infiltrates compared to WT, while the percentage in virus A and C treated animals was lower even not significantly different from virus B (*Figure 11C*, $P<0.001$).

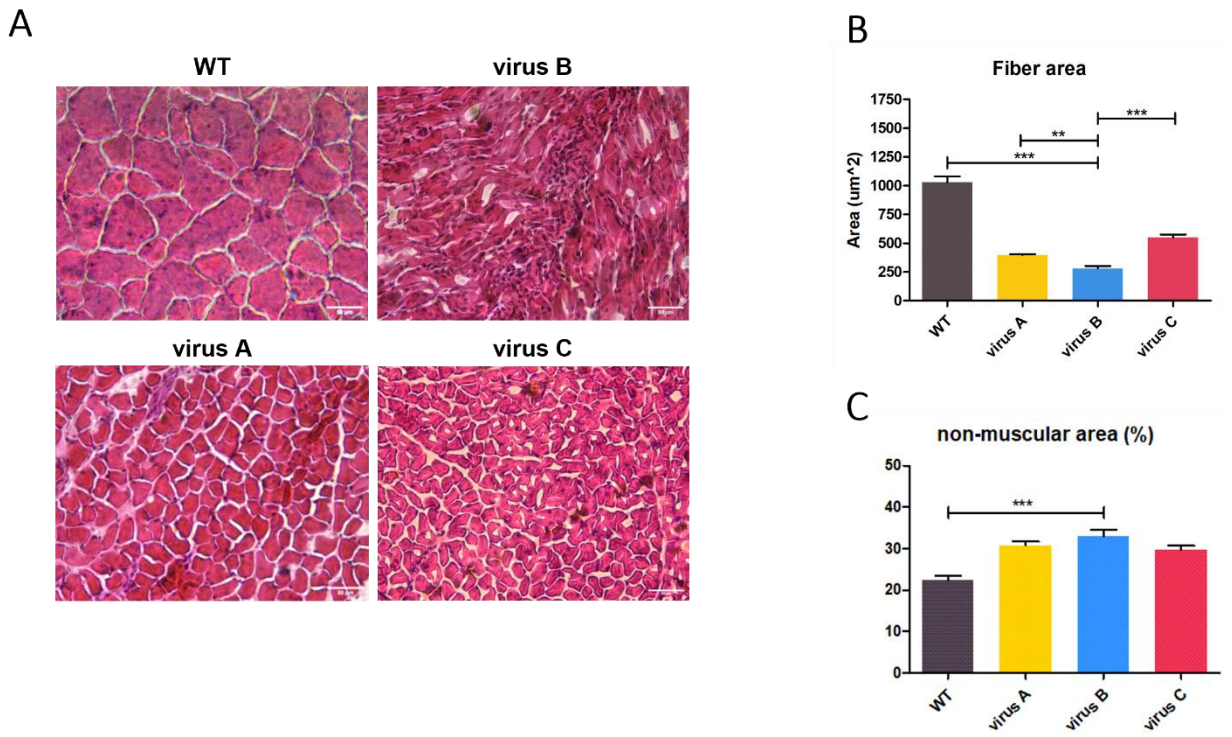

*Figure 11. Hematoxylin-eosin staining on gastrocnemius muscles. (A) Representative muscle fibers of WT and nmd treated animals (n=3/group) stained with HE and acquired with optical microscope with a magnification of 20X. (B) Fibers CSA quantification expressed in μm^2. (C) Fibrotic and necrotic tissue quantification expressed as non-muscular area percentage. The values are represented as mean value ± SEM. Statistical significance was determined by one-way ANOVA followed by Tukey's post hoc test. **P<0.01, ***P<0.001. Scale bar = 50 µm.*

2.6.4. IGF1 axis dysregulation and rescue

Next, the IGF1 axis, which was already demonstrated to be altered in *nmd* mice[103], was analyzed. The evaluation was performed by searching for alterations in two of the major components of the axis by quantitative polymerase reaction (qPCR) for IGF1 and the insulin-growth factor binding protein acid labile subunit (IGFals), in the liver of WT, and treated mice at P20.

A significant reduction in the mRNA expression of IGF1 was observed in virus B treated mice compared to WT animals, result also correlated with a rescue of the level after the treatment, especially with virus A (*Figure 12A*, $P<0.05$).

The analysis of one of its major binding proteins, IGFals, demonstrated the presence of a similar significative trend with very low values in virus B treated mice and a huge increase after both the treatments, again higher with virus A (*Figure 12B, P*<0.05).

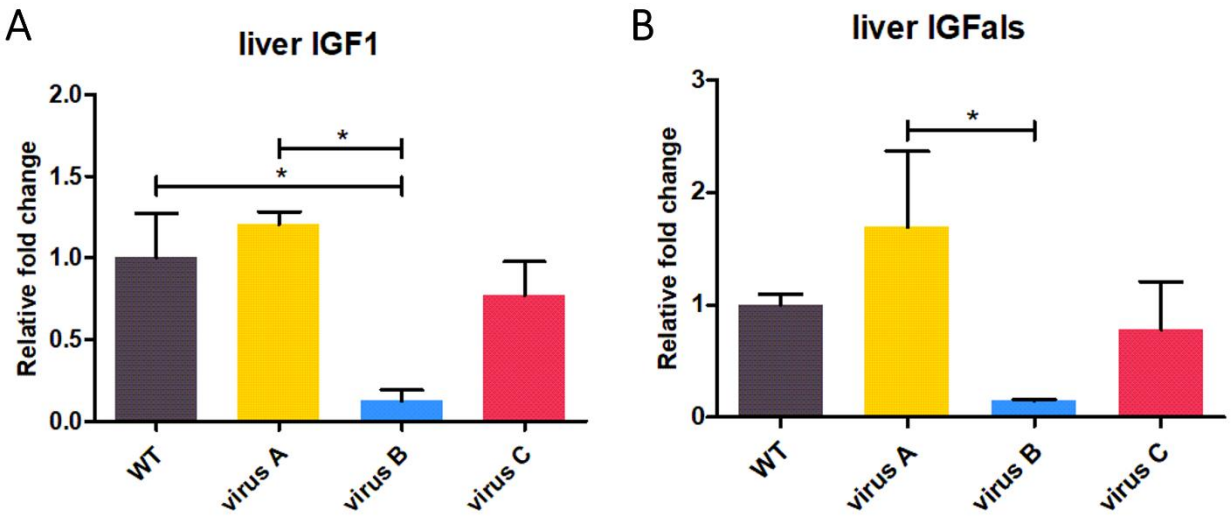

*Figure 12. IGF1 axis expression analysis. Bar plot of liver IGF1 (A) and IGFals (B) expression analyzed by qPCR in WT, and nmd treated animals at P20 (n=3/group). Values are presented as means ± SEM. Statistical significance was determined by one-way ANOVA followed by Tukey's post hoc test. *P<0.05.*

2.7. Long-term effects of presymptomatic treatment

For the clinical translation of the therapy, fundamental is to understand the long-term consequences of the treatments, and for this purpose, animal tissues were analyzed also later in life (P200). It is necessary to consider that mice treated with virus B did not reach the age to be considered in this group of analysis.

2.7.1. IGHMBP2 expression is maintained in adult mice

To confirm the ability of the constructs into maintaining the expression level of IGHMBP2 along mice's life span, WB analysis of the spinal cord at P200, to assess the level of the protein in WT animals and mice treated with virus A and C, was performed (*Figure 13A*).

The results confirmed that the rescue of IGHMBP2 protein level was still present even later in life with expression levels comparable to WT animals, confirming the long-term efficacy of the gene therapy (*Figure 13B*).

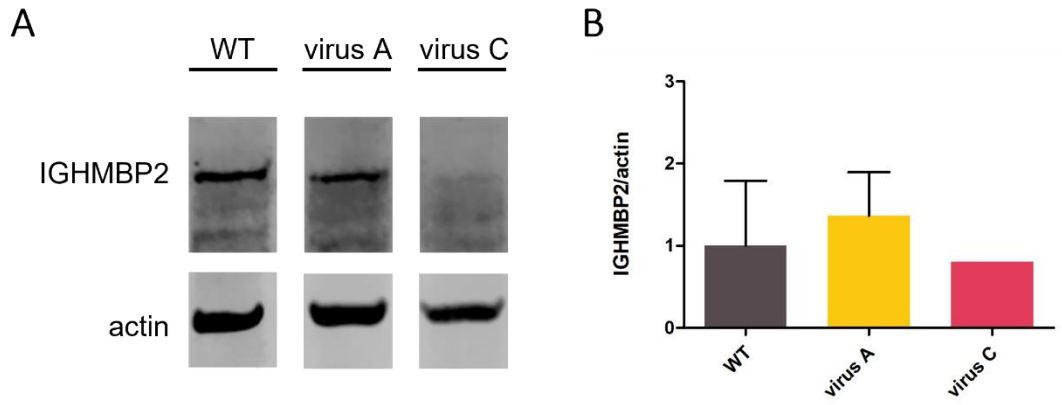

Figure 13. IGHMBP2 protein expression. (A) Expression level was detected by WB analysis performed on P200 spinal cords of WT mice (n=3) and nmd mice treated ICV at P1 with virus A (n=3) and virus C (n=1). Representative immunoblots were shown (B) Relative values normalized on α-actin. The values are represented as mean value ± SEM. Statistical analysis was performed with one-way ANOVA followed by Tukey's post hoc test.

2.7.2. Neuropathological rescue is conserved

Next, neuropathological analyses were performed to assess if the amelioration mediated by the treatment was stable in time or led only to a delay of phenotype appearance.

2.7.2.1. MN count

First of all, the principal SMARD1 degeneration of the MNs was evaluated by the count of MN number in the lumbar spinal cord of the WT animals and the mice treated with virus A and C at P200, performing an immunostaining against the MN specific ChAT enzyme (*Figure 14A*).

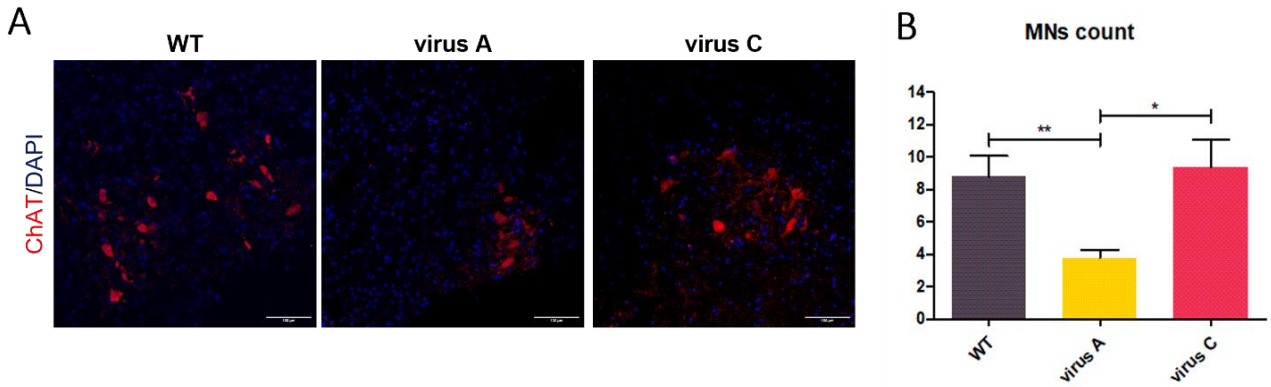

*Figure 14. MN count in the lumbar spinal cord. (A) Representative immunofluorescence images of 20 µm spinal cord's ventral horn sections of WT (n=3) and mice treated with virus A (n=3) and virus C (n=1) at P200 stained for ChAT enzyme (red) and DAPI (blue) and acquired with a confocal microscope with a magnification of 10X. (B) Average MN number in the total lumbar spinal cord. The values are represented as mean value ± SEM. Statistical significance was determined by one-way ANOVA followed by Tukey's post hoc test. *P<0.05, **P<0.01. Scale bar = 100 µm.*

The results demonstrated that the number of MNs was preserved in virus C treated mice (9.4±1.7) at P200 and was comparable later in life to the healthy littermates. While for virus A treated group, there was a significant reduction in the MN number (3.8± 0.5) compared to P20, which resulted at P200 in a significative lower MN number compared to adult WT and virus C treated mice (*Figure 14B*, $P<0.01$).

2.7.2.2. Adult astrocyte gliosis and microglia activation

Starting from the assumption that the major signs of astrocytosis were seen in the end-stage of SMA mice pathology, and that its timing correlation to MN death is still unclear, it is crucial to observe how neuroinflammation develops also later in *nmd* mice life after gene therapy administration[110]. Thus, the presence of astrocyte gliosis and microglia activation was evaluated by immunofluorescence analysis of P200 mice lumbar spinal cord searching for GFAP (*Figure 15A*) and Iba1 (*Figure 15C*) positive cells.

Quantification of GFAP-positive cells percentage demonstrated that there were no significant differences between the WT and the treated mice confirming similar values to the ones seen at P20. In particular here was possible to observe again a slightly higher astrocytosis with virus A treatment (11.1%±2.2) while the virus C cohort obtained a value (9.0%±0.5) nearer to WT mice (4.7%±1.1), taking into consideration that the level of GFAP in virus B treated mice was greatly higher at P20 (28.2%±1.6) (*Figure 15B*).

Comparable results were obtained also for microglia activation, with values similar to P20 mice, and a lack of significative variation in virus A (10.4%±0.7) and C (6.5%±0.6) treated animals if compared to WT (7.7%±0.7), considering the higher value obtained by virus B treated animals at P20 (13.7%±1.4) (*Figure 15D*).

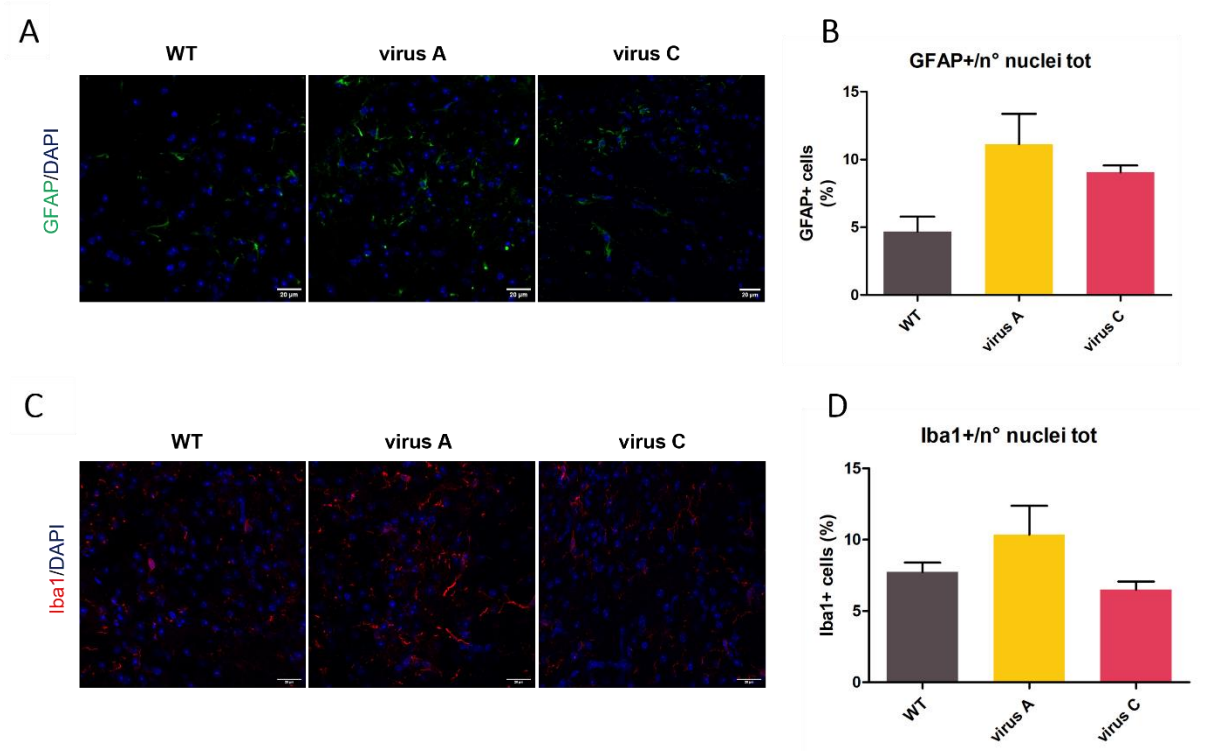

Figure 15. Astrocyte gliosis and microglial activation analysis. (A-C) Representative immunofluorescence images of 20 µm spinal cord sections of WT (n=3) and virus A (n=3) and C (n=1) treated mice stained for GFAP (green) (A) or Iba1 (red) (C) and DAPI (blue) and acquired with a confocal microscope with a magnification of 63X. (B-D) Quantification represented as percentage of GFAP (B) or Iba1 (D) positive nuclei divided for the total number of cells. The values are represented as mean value ± SEM. Statistical analysis was performed with one-way ANOVA followed by Tukey's post hoc test. Scale bar = 20 µm.

2.7.3. Long term cardiac effects

The survival and functional analysis made possible to observe that the *nmd* treated animals who reached the adult age, died suddenly and without a clear phenotypical deterioration before their death. In this regard, interesting could be the investigation of the sudden death causes in adult life. One of the hypotheses was the presence of alterations in the cardiac muscle, another commonly affected organ in SMARD1 patients and animal models.

To confirm this hypothesis, the cardiac muscles of WT animals and mice treated at P1 with virus A and C and sacrificed at P200 were firstly evaluated by HE staining.

In this case, the myofibers arrangement made not feasible the evaluation of the CSA, but only the presence of infiltrates and fibrosis. As baseline cardiac tissues of WT and virus B treated animals were firstly evaluated at P20, and a significant increase in non-muscular tissue was observed in virus B treated mice compared to WT (*Figure 16A* and *B*, Student t-test $P<0.01$). Otherwise, at P200 a significant increase in the amount of fibrotic tissue and cellular infiltrates in virus A treated animals was detected. Differently, the quantification of virus C treated mice was comparable to WT one (*Figure 16C* and *D*).

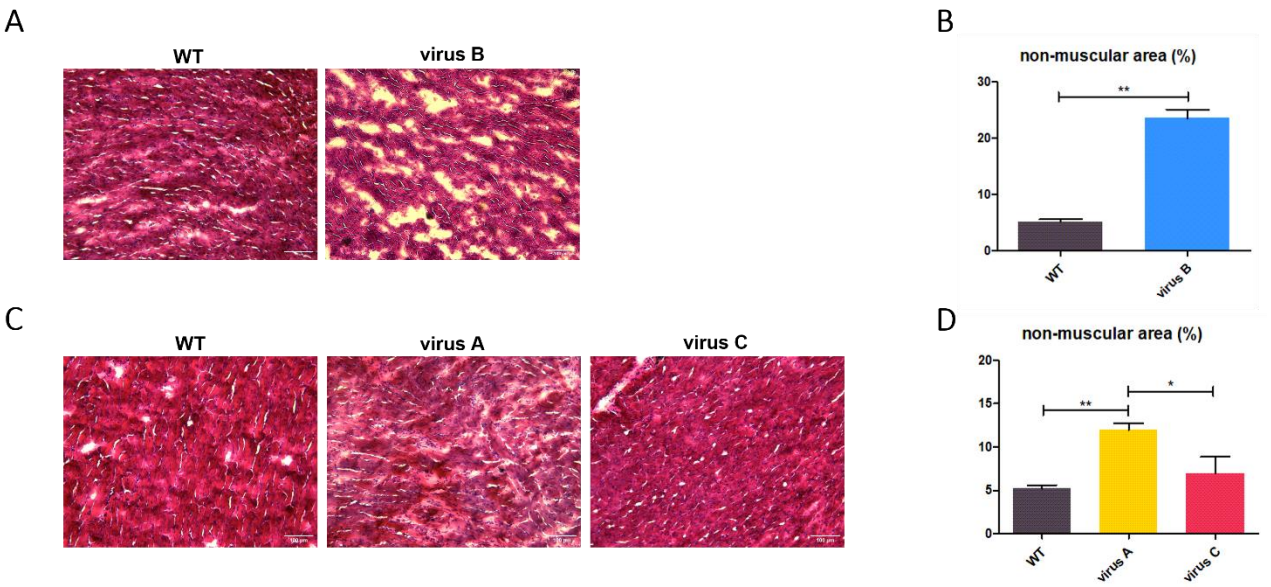

*Figure 16. Hematoxylin-eosin analysis on cardiac muscles. Representative cardiac muscle fibers of P20 WT and virus B treated animals (n=3/group) (A) and P200 WT (n=3), virus A (n=3) and C (n=1) treated mice (C) stained with HE and acquired with optical microscope with a magnification of 10X. (B-D) Fibrotic and necrotic tissue quantification expressed as non-muscular area percentage in P20 (B) and P200 (D) animals. Statistical significance was determined by Student t-test (B) and by one-way ANOVA followed by Tukey's post hoc test (D). *P<0.05, **P<0.01. Scale bar = 100 µm.*

Then the possible presence of alterations in the IGF1 axis was evaluated, as already seen at P20 in the liver, but also in the heart. In fact, if the liver is the supplier of the investigated hormone, the cardiac tissue is one of the most important target tissue for IGF1, which promotes there cardiac growth, cardiac contractility improvement, and tissue remodeling after myocardial infarction[111].

As a baseline, qPCR on cardiac tissued of WT and virus B treated animals harvested at P20 was performed. This result led to the observation that both IGF1 and IGFals resulted slightly reduced, even if not statistically significatively, in virus B treated animals if compared to WT (*Figure 17A* and *C*). Otherwise at P200 IGF1 level resulted more similar to WT levels after virus A and C treatment and the same result was obtained also with IGFals, even if virus C value was importantly higher than WT level (*Figure 17B* and *D*).

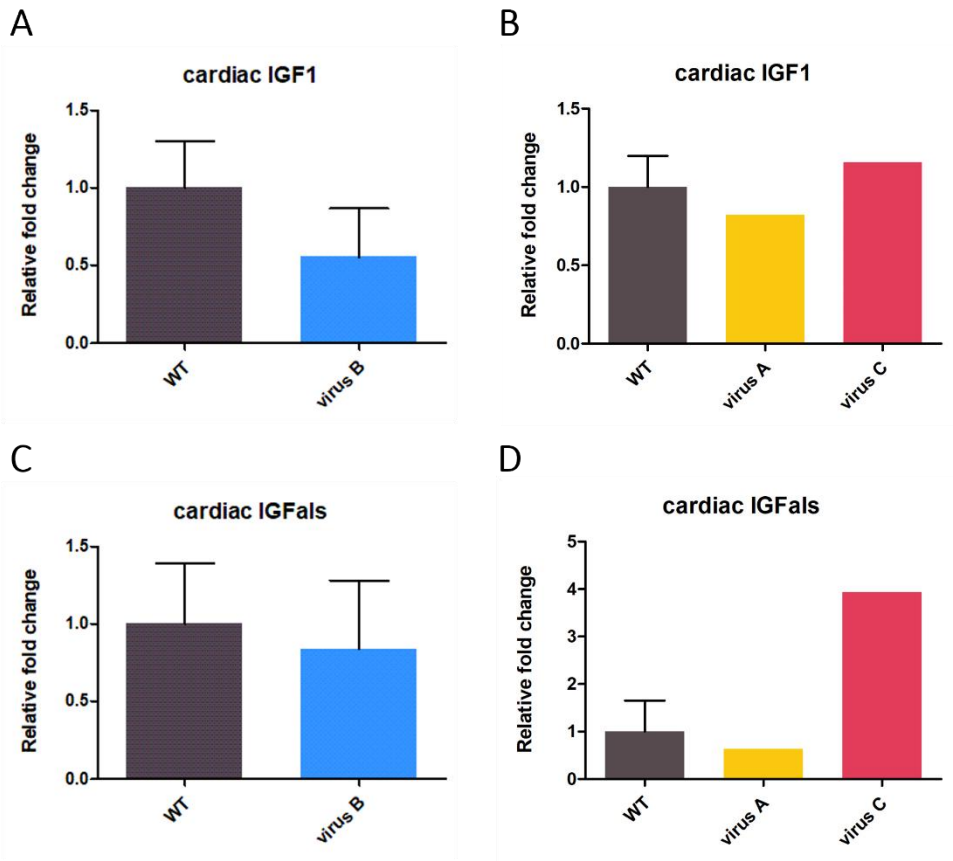

Figure 17. IGF1 axis expression analysis. Bar plot of cardiac IGF1 (A) and IGFals (B) analyzed in P20 cardiac tissue from WT and virus B treated mice (n=3/group) and cardiac IGF1 (B) and IGFals (D) from WT animals (n=3) and mice treated with virus A and C sacrificed at P200 (n=1/group). Values are presented as means ± SEM. Statistical significance was determined by Student t-test (A-C) and by one-way ANOVA followed by Tukey's post hoc test (B-D)

2.8. Toxicity effects evaluation

Another fundamental aspect especially for the clinical translation of the therapy is the evaluation of possible toxic effects after the treatment. To this aim, the evaluation of the principal toxicity biomarkers in the mice serum was performed.

The majority of the markers tested resulted not significantly changed (creatinine, total bilirubin, ALT, AST, total proteins, bile acids, LDH, and CK) after the treatment suggesting that the constructs did not mediate a toxicity effect in the mice analyzed.

Otherwise, some markers resulted to be altered in the virus B treated group and restored with the virus A and virus C treatment, suggesting an alteration of the basal value of these hallmarks in the SMARD1 pathology not linked to the vector used. For example, glucose level resulted significantly reduced in virus B treated animals if compared to WT, while in virus A and C cohorts the levels were

significantly restored, probably a sign of an improved metabolism of the animals with lack (WT) or reduced phenotype (virus A and C groups) (*Figure 18*, $P<0.001$).

The same trend was present also in the urea levels, with significative higher values in virus B treated animals, a sign of kidney malfunctioning, which was rescued in both the virus A and virus C treated groups.

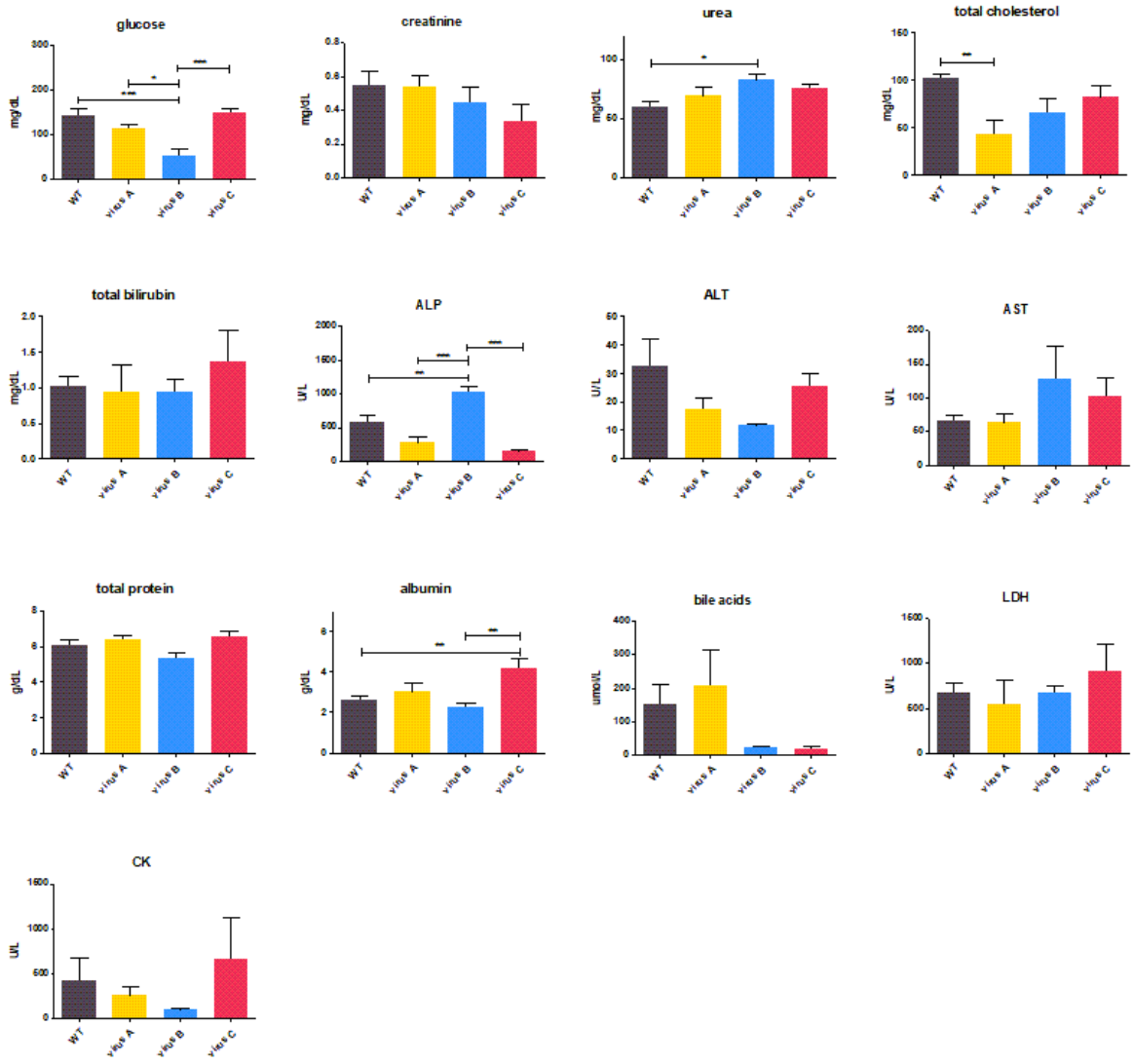

*Figure 18. Toxicity evaluation. Serum concentration of toxicity biomarkers in WT, virus A, B and C nmd treated animals (n=4/group). Values are presented as means ± SEM. The statistical significance was determined by one-way ANOVA followed by Tukey's post hoc test. *P<0.05, **P<0.01, ***P<0.001.*

Particular attention in this regard needed the hepatotoxicity and thus transaminases levels described higher in SMARD1 patients and animal model, and in SMA patients who have received gene therapy. Here, AST and ALT did not show significant changes between the groups. Otherwise, ALP resulted increased in virus B treated mice, but was completely restored to WT level with both virus A and C treatment ($P<0.001$).

A value that needs further examination was the albumin level resulted increased significantly only after virus C treatments ($P<0.01$).

2.9. *Symptomatic AAV9-IGHMBP2 administration*

2.9.1. *IGHMBP2 protein increased expression after systemic injection*

The second part of the work consisted of a better definition of the therapeutic window. Only a single work regarding the possibility of extending the therapeutic window with a local ICV injection was published in literature, but on the more severe mice model, still not commercially available and providing data not comparable at all to the one performed on the validated *nmd* mice model[85]. Here, the aim was to assess if the therapeutic efficacy was present also when the treatment is administered with a more systemic route of administration during the symptomatic phase of the disease of *nmd* mice. To this aim, the CAG-AAV9-*IGHMBP2* vector, already validated in presymptomatic mice[82], was administered in WT mice at P7 to define the best systemic route and the best dosage.

A single local, ICV, and two systemic routes, SC and intraperitoneal (IP), at low and high dosages were tested at P7 on WT animals. Spinal cords were harvested at P20 and analyzed by WB for IGHMBP2 (*Figure 19A* and *B*).

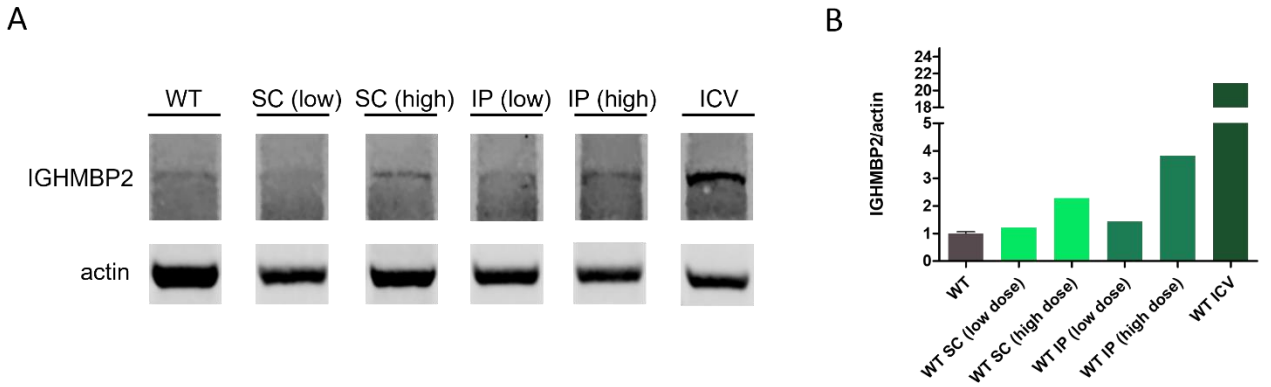

Figure 19. IGHMBP2 protein expression. (A) Expression level was detected by WB analysis performed on P20 spinal cords of WT mice untreated (WT) and treated at P7 with CAG-AAV9-IGHMBP2 (n=1/group) through SC, IP and ICV route at low and high dosage. Representative immunoblots were shown. (B) Relative values normalized on α-actin and on untreated WT values. The values are represented as mean value.

The ICV treatment resulted in an expression too high respect the physiological one with consequent important toxic effects (data not shown), thus the route selected to be tested was the systemic SC at a high dose ($1,26x10^{11}$ vg). An empty AAV9 vector was used as negative control (*nmd* AAV9null).

2.9.2. Survival extension and phenotypical partial amelioration

Survival data showed a significant extension of the survival time in *nmd* mice treated with gene therapy at the symptomatic phase (named *nmd* SC P7), with a median value of 30 days of life, with a great percentage of the animals still alive after 100 days (*Figure 20A*, $P<0.001$) if compared to *nmd* mice treated with the empty vector (*nmd* AAV9null). Also in this case there was a large percentage of the animals treated which died before P30.

Body weight was also measured and showed a significant improvement, even if the values were not so close to the WT ones (*Figure 20B*, $P<0.01$).

The same partial rescue was visible also in motor behavioral tests such as hindlimb splay (*Figure 20C*, $P<0.01$) and grip strength test (*Figure 20D*).

In particular, for the hindlimb splay test was possible to observe a significative difference with an important amelioration of the motor performance growing up already one week after the treatment reaching the highest value at P50, followed by a slight decrease of the motor abilities if compared to the WT animals which remain almost constant during their life.

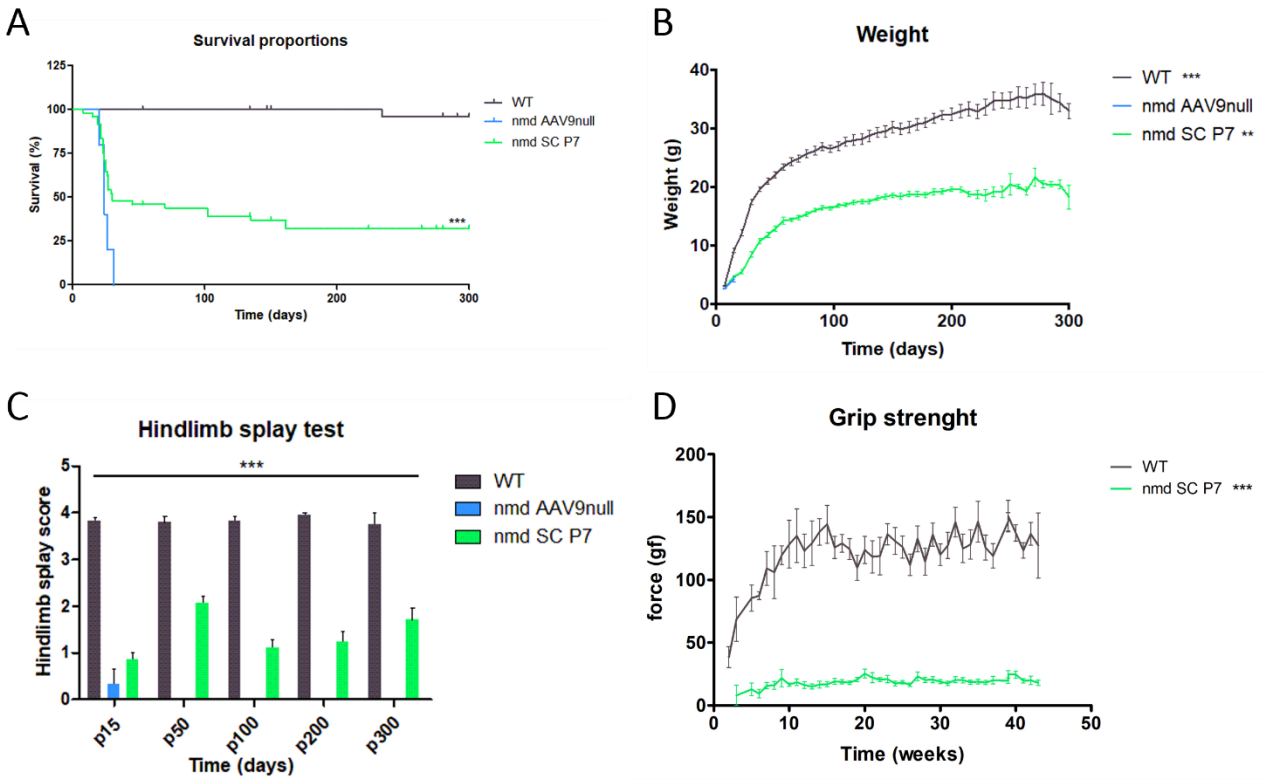

*Figure 20. Survival and phenotypical test of WT (n=36), nmd AAV9 null (n=4) and nmd SC P7 (n=48) animals. (A) Kaplan-Meier survival curve. (B) Body weight curve in grams. The values are represented as mean value ± SEM. Statistical analysis performed with one-way ANOVA respect to the nmd AAV9null group (C) Hindlimb splay test scored at different time points. The values are represented as mean value ± SEM. Statistical analysis was performed with one-way ANOVA. (D) Grip strength measure of all four limbs. The statistical significance was determined by Student t-test. **P<0.01, ***P<0.001.*

Regarding the grip strength test, the data showed only a partial rescue of the limbs force in the treated group, statistically different from the WT, but fundamental in this contest is to consider that the *nmd* AAV9null mice were never able to perform this test during their short life span.
These data supported the efficacy of the compounds to partially rescue the motor dysfunctions of the *nmd* mice even when treated after the appearance of the symptoms.

2.9.3. Neuropathological beneficial effects

2.9.3.1. MN count

To determine the effect of the delayed treatment on the MNs, serial section of mice spinal cord were stained for ChAT enzyme (*Figure 21A*) to count the number of MNs in the ventral horn (*Figure 21B*) Results demonstrated that the delayed treatment did not result at P20 in an increased amount of MNs in the spinal cord, with average values of *nmd* treated mice comparable to the group treated with the empty vector.

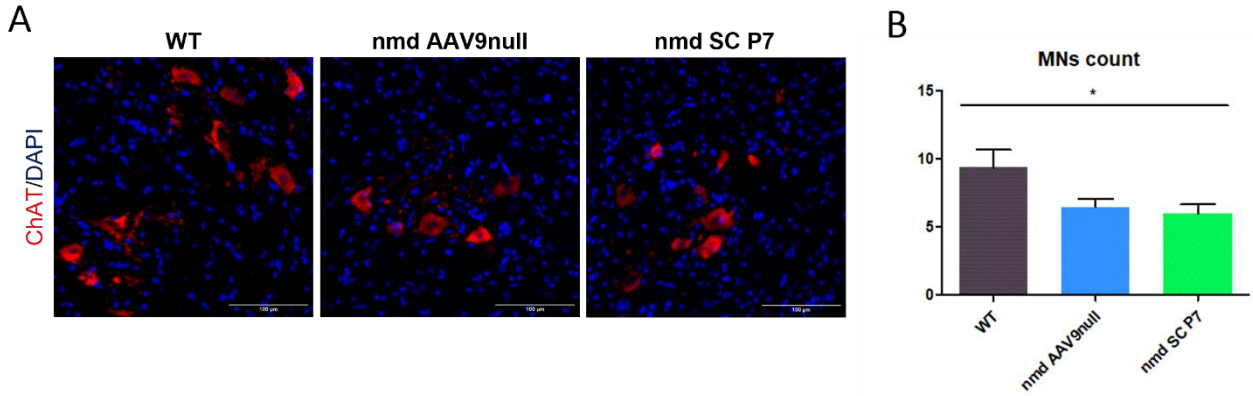

*Figure 21. MNs immunostaining. (A) Representative immunofluorescence images of 20 µm lumbar spinal cord's ventral horn sections of WT, nmd AAV9null and nmd SC P7 (n=3/group) animals stained for ChAT enzyme (red) and DAPI (blue) and acquired with a confocal microscope with a magnification of 20X.(B) Average MN number in the total lumbar spinal cord. The values are represented as mean value ± SEM. The statistical significance was determined by one-way ANOVA. *P<0.05. Scale bar = 100 µm.*

2.9.3.2. Inflammatory markers restoration

The evaluation of GFAP and Iba1 markers were also performed on P20 spinal cord of WT and treated animals (*Figure 22A* and *C*). Data demonstrated the presence of an important significative rescue of both the neuroinflammatory markers analyzed, even when a systemic administration of the treatment was performed during the symptomatic phase of the disease (*Figure 22B* and *D, P*<0.001).

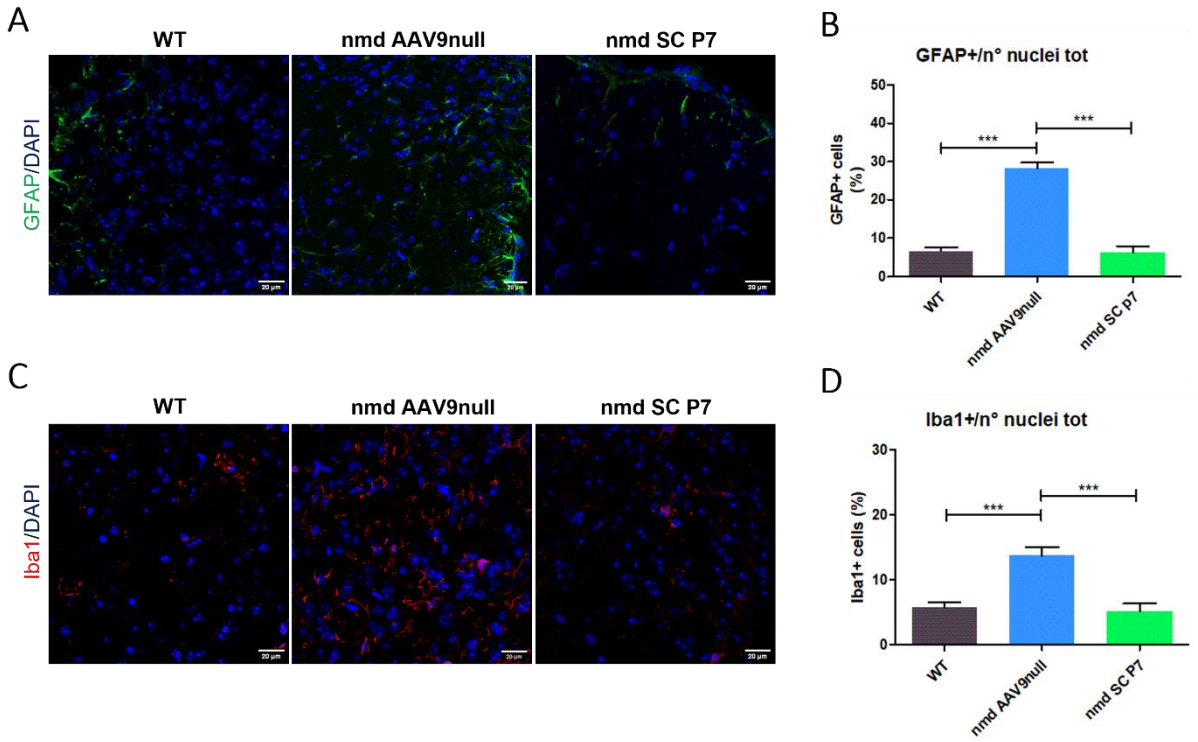

*Figure 22. Astrocyte gliosis and microglial activation. (A-C) Representative immunofluorescence images of 20 µm lumbar spinal cord sections of WT, nmd AAV9null and nmd SC at P7 (n=3/group) animals stained for GFAP (green) (A) or Iba1 (red) (C) and DAPI (blue) and acquired with confocal microscope with a magnification of 63X. (B-D) Quantification represented as percentage of GFAP (B) or Iba1 (D) positive nuclei divided for the total number of cells. The values are represented as mean value ± SEM. Statistical significance was determined by one-way ANOVA followed by Tukey's post hoc test. ***P<0.001. Scale bar = 20 µm.*

2.9.3.3. NMJ innervation

A subsequent analysis of NMJ innervation in gastrocnemius muscles of WT and *nmd* treated animals was then performed (*Figure 23A*). Results demonstrated that the innervation percentage after the treatment was slightly increased but not significantly higher than the *nmd* mice treated with the empty vector (*Figure 23B*).

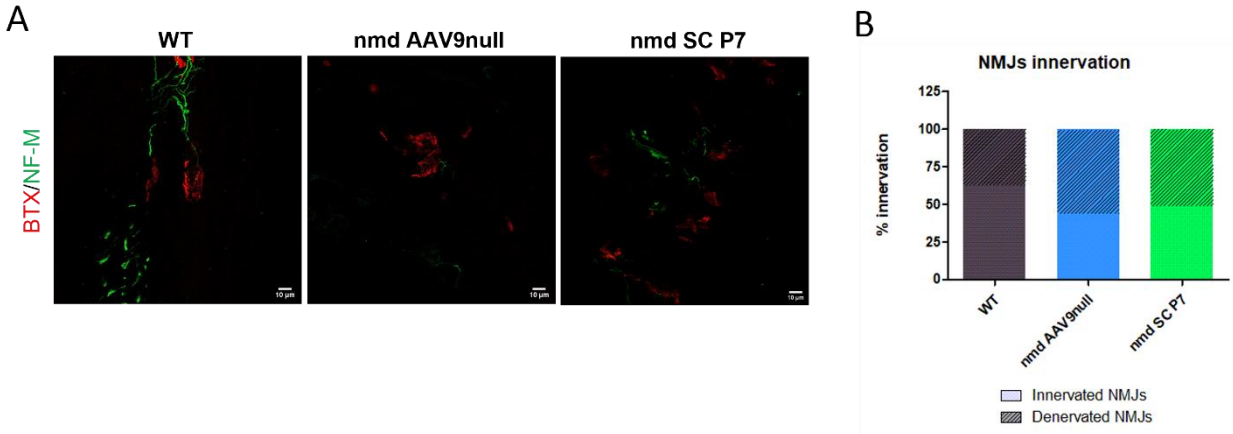

Figure 23. Neuromuscular junction immunofluorescence analysis. (A) Representative immunofluorescence images of 20µm gastrocnemius sections of WT, nmd AAV9null, and nmd SC P7 (n=3/group) animals stained for NF-M (green) and BTX (red) and acquired with confocal microscope with a magnification of 63X. (B) Stacked bar plot of NMJs percentage innervation. Scale bar = 10 µm

2.9.3.4. Muscle histology

Analyses of the postsynaptic compartment were performed through HE staining on gastrocnemius (*Figure 24A*) and cardiac muscle (*Figure 25A*).

On gastrocnemius muscles, the CSA evaluation showed a statistical significant restoration of muscle fibers dimension after the treatment (*Figure 24B*, $P<0.001$), correlated to a not significant percentage of fibrotic/necrotic infiltrates between WT and *nmd* AAV9null animals (*Figure 24C*).

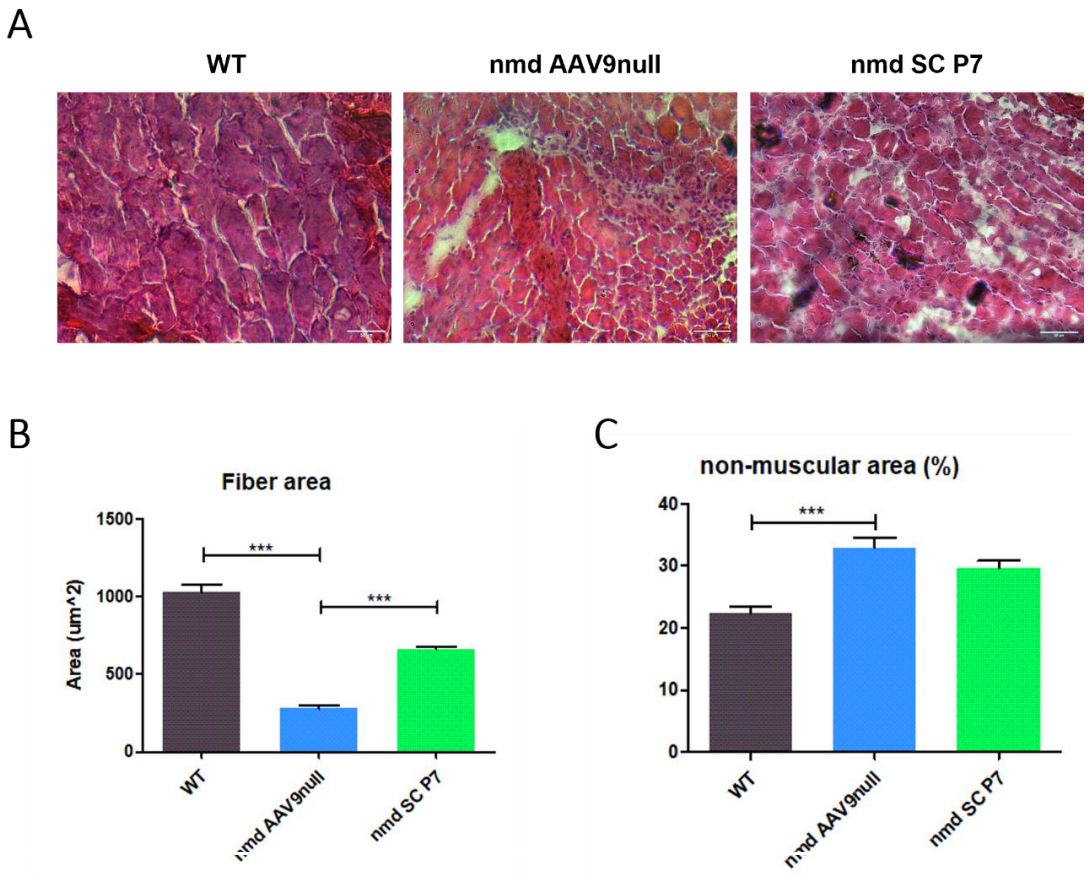

*Figure 24. Hematoxylin-eosin staining on gastrocnemius muscles. (A) Representative muscle fibers of WT, nmd AAV9null and nmd SC P7 (n=3/group) animals stained with HE acquired with optical microscope with a magnification of 20X. (B) Fibers CSA quantification expressed in μm^2. (C) Fibrotic and necrotic tissue quantification expressed as non-muscular area percentage. The values are represented as mean value ± SEM. Statistical significance was determined by one-way ANOVA followed by Tukey's post hoc test. ***P<0.001. Scale bar = 50 µm.*

On cardiac muscle, the evaluation of the fibrotic/necrotic tissue resulted otherwise in an increased amount of non-muscular tissue in the *nmd* AAV9null cohort already at P20 and a complete and statistically significative rescue in the AAV9-*IGHBMP2* treated group (*Figure 25B, P*<0.001).

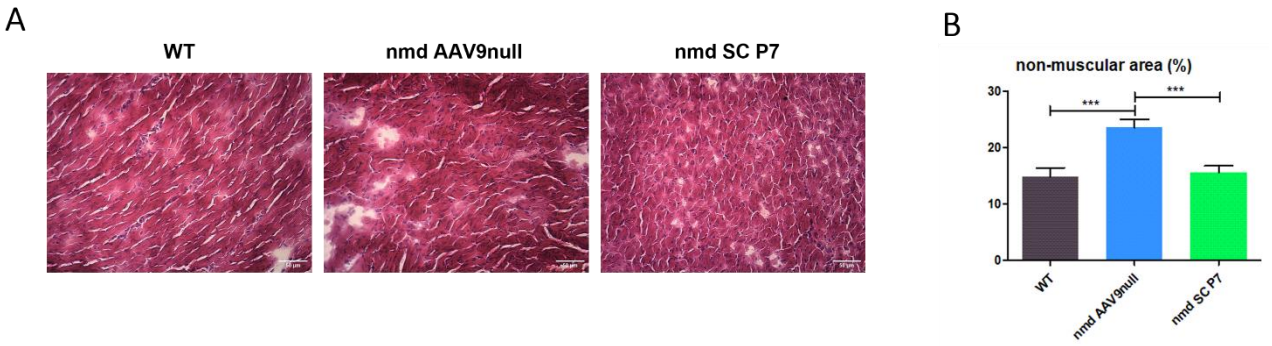

*Figure 25. Hematoxylin-eosin analysis on cardiac muscles. (A) Representative muscle fibers of WT, nmd AAV9null and nmd SC P7 animals (n=3/group) stained with HE and acquired with optical microscope with a magnification of 10X. (B) Fibrotic and necrotic tissue quantification expressed as non-muscular area percentage. ***P<0.001. Scale bar = 50 μm.*

2.9.4. IGF1 axis alterations

To determine if also the delayed treatment could mediate changes in the IGF1 axis components, previously demonstrated altered in virus B treated *nmd* mice in liver and heart, an evaluation of IGF1 expression by qPCR was performed at P20 on liver (*Figure 26A*) and heart (*Figure 26B*).

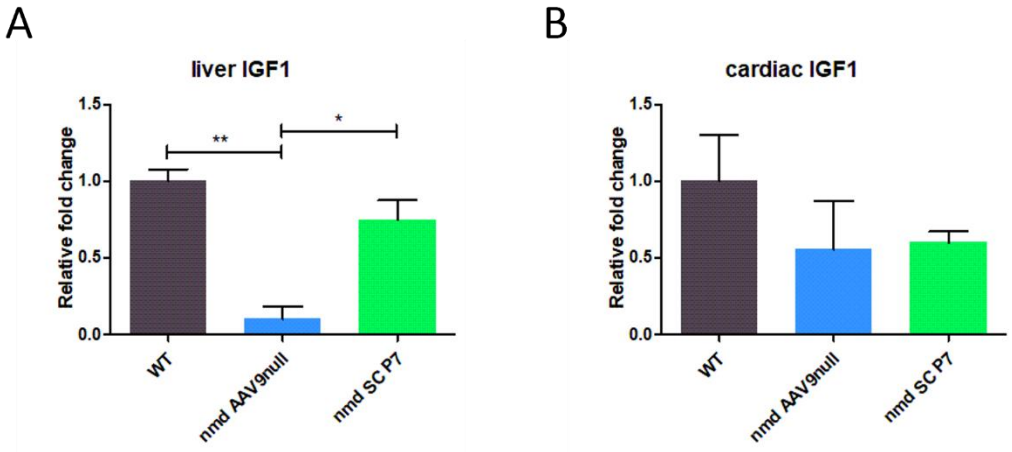

*Figure 26. IGF1 axis expression analysis. Bar plot of liver (A) and cardiac (B) IGF1 expression analyzed by qPCR at P20 in WT, nmd AAV9null and nmd SC P7 (n=3/group except for heart nmd SC P7 n=1) animals. Values are presented as means ± SEM. Statistical significance was determined by one-way ANOVA followed by Tukey's post hoc test. *P<0.05, **P<0.01.*

Results confirmed the reduction in hepatic IGF1 in the animals treated with the empty vector and demonstrated the significant restoration of the level after the treatment ($P<0.01$). Otherwise, in line with the presymptomatic treatment results, the cardiac level of IGF1 resulted reduced in *nmd* AAV9null mice even not significantly and with high variability, and the level found after the treatment was not restored.

6. Discussion

SMARD1 is a genetic autosomal recessive MND caused by mutations in the *IGHMBP2* gene. It is an infantile disease characterized by muscle atrophy and respiratory distress occurring in the first year of life, associated with a reduced life expectancy. Up to now, prenatal diagnosis is not implemented in routinary genetic tests, and the prognosis is poor. Currently, only palliate therapies are approved.

Recently, gene therapy approach has obtained promising results in the treatment of monogenic diseases, and, especially for neurological disorders, the use of AAV9-based vectors with CNS tropism and able to bypass the BBB has taken hold. Regarding MNDs in particular, the FDA and EMA had already approved respectively in 2019 and 2020 the first gene therapy for SMA, Zolgensma[79]. The pathological similarity between SMA and SMARD1 led to the hypothesis that gene therapy could be beneficial also for SMARD1 disease. In this regard, Nizzardo et al., already demonstrated in 2015 the efficacy of a single IV administration of AAV9, containing the WT human *IGHMBP2* gene under the control of CAG promoter, in rescue pathological SMARD1 phenotype in presymptomatic (P1) *nmd* mice[82]. In the same year also the group of Shababi obtained comparable results using a similar construct containing the CBA promoter, by administering it through double ICV injections, pre-symptomatically at P2 and P3[83].

A fundamental benefit given by the ICV route is the possibility to reduce the dosage of AAV9 administered because the vector does not have to overcome the BBB. This decrease, in addition, will result (i) in limitation of compound dispersion, which could lead to peripherical toxic effects, especially in the liver, already compromised in SMARD1 patients, and (ii) in a reduction of treatment costs, which could be prohibitive in humans.

Another important aspect in the field of gene therapy is the fine regulation of transgenic expression, which was already demonstrated to be a critical issue in SMA AAV9-mediated gene therapy. Van Alstyne et al., observed in fact that the *SMN* overexpression leads to a dose-dependent long-term toxic gain of function in mouse model[112]. To have a better transgenic expression control, fundamental is the promoter choice, which has never been investigated for the AAV9-*IGHMBP2* construct. With this aim, in this work in collaboration with Ohio Nationwide Children's Hospital, we want to determine if the use of different promoters controlling the *IGHMBP2* gene carried by an AAV9 vector and administered pre-symptomatically ICV in P1 *nmd* mice could result in distinct therapeutic outcomes, a fundamental aspect for the clinical translation of this approach.

In this regard, two constructs containing different promoters that correlate to a different expression of the transgene, and an empty vector, were here compared. The two promoters evaluated, the CBA and P546, are both safe, well tolerated, and already used in clinical trials. The first one is a strong

promoter, while the second leads to a more endogenous expression of the transgene in the nervous system and muscles, with a generally lower expression, especially in astrocytes.

First, we confirmed by WB that both the A and C constructs, when administered with a local injection (ICV) in *nmd* mice at P1, were able to mediate an important increase of the IGHMBP2 protein. In particular, data demonstrated that while virus C led to an IGHMBP2 expression in the spinal cord very similar to WT animals, virus A resulted in significantly higher expression compared to the healthy control. This confirmed the efficacy of both the vectors into increase the level of the protein even when administered ICV at a lower dosage in *nmd* mice at P1. Although, virus B treated mice showed an extremely low level of the protein, leading us to suppose that it was the empty vector.

Both virus A and virus C resulted in a striking extension of survival time if compared to virus B treated mice, confirming the hypothesis that it was the empty vector. This information brings us to decide to use the *nmd* mice treated with virus B as negative controls, being the AAV9 construct safety profile previously assessed and the vector already used in both clinical trials and approved therapies[66,73]. To be noted was the early mortality present only in virus A treated animals around P20 (44% of the animals treated died before P30). This effect was similarly seen also by Shababi et al., in 2016[83], when they demonstrated that a higher dosage of AAV9 administered ICV by multiple injections in presymptomatic *nmd* mice resulted in premature mortality between P19-22, hypothesizing the presence of an early toxic effect only in the high dose group. In line with the previously discussed WB data in which virus A mediated a higher increase in the IGHMBP2 protein level with respect to virus C, we could speculate that this was the cause also of the early mortality observed in our study.

The survival extension was also linked to comparable body weight between treated animals and WT littermates and an important amelioration of the motor phenotype. Fundamental is to take into consideration that virus B treated animals could be tested only a few times for weight and hindlimb splay before their early death and that they never reach the age to perform the rotarod test. Results demonstrated that the ability to open the hindlimb was significantly rescued and conserved in time in virus A and virus C animals with values very similar to the WT mice. In this test, the two compounds did not show major differences between the two groups, while in the rotarod performance test it was possible to see differences in the two trends. In particular, virus C treated mice obtained a response almost equal to the WT at P75 with a low decline in time, on the contrary virus A treated group obtained a lower value at P75 but showed an increase in motor performance during life. We hypothesized that this divergent trend was again linked to the different amounts of protein produced by the transgenes. Our results, in fact, suggested that the high dosage of transgene expression mediated by virus A led to some detrimental effects in the early phases, as demonstrated by the higher

mortality at P20, while virus C, which led to a protein level more similar to the WT one, mediate an almost complete rescue of the motor phenotype earlier in time delaying the insurgence of the most evident motor defects.

This difference in the phenotypical outcome however was not present in the histological results performed on MN count in the lumbar spinal cord. Our data showed in fact a significant and comparable rescue of MN number in the ventral horn of the lumbar spinal cord without major differences between the two constructs and correlated also to reduced neuroinflammation. Fundamental to this regard in fact was the demonstration, for the first time in the SMARD1 mice model, of the presence of increased astrogliosis and activated microglia in the empty virus treated mice (negative control) compared to WT, suggesting the involvement of neuroinflammation in the pathology. Little is known about the time correlation between neuroinflammation and MNs degeneration, but our data demonstrated that both the treatments were able to rescue astrocytes number and microglia activation in mice spinal cord. GFAP was extremely reduced after both the treatments, in particular, in the virus C treated cohort, its level reached a percentage more similar to WT than the virus A, while Iba1 levels resulted rescued with both the constructs even if in less extent compared to GFAP.

The effect of the treatment on muscle innervation was assessed on gastrocnemius muscle demonstrating the presence of complete rescue of the NMJs innervation with both the A and C constructs, even if it was possible to observe that the percentage reached with virus C was higher and more significative if compared to virus A treated cohort.

In addition, histological analysis on gastrocnemius demonstrated firstly that the mice treated with the empty vector had an important reduction in the myofibers' size correlated to an increased presence of fibrotic and necrotic tissue and secondly that both the treatments and especially virus C, were able to mediate a significative improvement in the fiber size even if not correlated to a significative reduction in muscle infiltrates.

A novel pathway already known to be altered in *nmd* mice was the IGF1 axis[102]. Ruiz et al. in 2005, demonstrated in fact that in the *nmd* mice the level of IGF1 was reduced in the animal serum linked also to an increased level of IGF1 binding protein, while the IGF1 transcription in the liver resulted unaltered. On the contrary, we found in the liver of virus B treated animals a significant reduction of the IGF1 and IGFals transcripts, and levels restored with the other two treatments, even if significantly only with virus A. These data need to be further expanded also analyzing IGF1 receptor expression and IGF1 circulating serum levels.

Next, we analyzed the long-term effects of presymptomatic ICV treatments, during adult life, at P200. We aimed to assess the potential causes of sudden death that we observed in adult mice that receive

the presymptomatic treatment, being their motor functionality and weight at P200 in the normal range and the animals macroscopically indistinguishable from WT animals. Firstly, we confirmed that both the constructs maintained the transgene expression in the spinal cord also later in life with values comparable to WT.

Otherwise, histopathological analysis of adult mice spinal cords demonstrated that the number of MNs in the ventral horn was importantly reduced in virus A treated animals while remained high in the virus C cohort, suggesting that this treatment was more efficient into preserve the degeneration of MNs in time, contrary to virus A. Data correlated also with a lack of changes in neuroinflammatory markers.

The lack of evident muscular and phenotypical degeneration before the sudden death of *nmd* treated animals in adult life, led us to hypothesize the presence of possible late-onset cardiac pathological hallmarks, being the heart an organ already demonstrated compromised in SMARD1 patients and animal models[16,70]. For this reason, we first evaluated the fibrotic/necrotic area percentage in virus B treated mice at P20 as a baseline and we could observe that there was a significant increase in infiltrates percentage compared to WT littermates. At P200 otherwise was possible to see the presence of significative increased fibrosis in virus A animals if compared to WT mice, while virus C treated animals showed a value more similar to WT. This result led us to hypothesize that if for virus A treated cohort, the possible cause of sudden death could be the lack of rescue of fibrosis and necrosis in the cardiac tissue, this could not be applied also to virus C treated animals, even if further analysis must be performed to assess if in addition to the infiltrates presence, other cardiac parameters could be altered, important for the possible application of combined therapies. In this regard, a subsequent analysis performed was to assess the possible presence of alterations in the IGF1 axis, being the heart one of its target tissues, where it is involved in cardiac growth, cardiac contractility, and tissue remodeling[111]. For this reason, we analyzed if the expression level of IGF1 in the cardiac tissue was altered. A little reduction even not significant in both IGF1 and IGFals could be observed in *nmd* cardiac muscle if compared to WT at P20, while at P200 IGF1 levels resulted comparable between WT and treated mice, and IGFals resulted increased, even not significantly, only with virus C treatment. However, to have a more comprehensive view of the IGF1 axis alterations and their effects on the heart condition, the expression evaluation of the IGF1 receptor and circulating IGF1 is needed. The results obtained so far on the P200 mice treated at P1 demonstrated a better beneficial effect in the virus C treated cohort with respect to the virus A group. This led us to suppose that the higher expression of IGHMBP2 mediated by virus A could results in high toxicity early after the treatment and long-term negative consequences if compared to a more physiological expression, as the one

stimulated by virus C, a similar effect to the one already seen in adult SMA mice treated with gene-therapy[112].

Overall, our results confirmed the efficacy of a more local route of administration such as the ICV, without relevant issues. Even if the IV administration could be less invasive than the ICV, the latter has the big advantage to bypass directly the BBB, allowing an important reduction of the viral dosage, which is fundamental for both limiting the dispersion of the construct in the peripherical tissues, and for managing the cost-effective aspect, issue especially important in term of clinical translation.
In addition, the comparison between the two constructs carrying different promoters led us to say that both the viral vectors were efficient into mediate a striking extension of survival, an improvement of the motor phenotype, and an amelioration of the pathological hallmarks of the disease, without relevant effects for what concern the toxicity point of view. In addition, we speculated that a more endogenous expression of the transgene, as the one mediated by virus C, could be more efficacious and less toxic as treatment in the long term, leading in our case to better results both in survival time and in terms of neuropathological rescue.

Fundamental in the contest of gene therapy based on AAV9 vectors are the analyses of the possible toxicity effects. The majority of serum toxicity biomarkers analyzed were not significantly altered between WT, and mice treated with virus A, B, and C, suggesting the lack of evident toxic effect mediated by the treatment. In addition, some parameters that were altered in our negative control were restored after virus A and C administration, suggesting the ability of the treatments to restore the altered hallmarks present in the disease. Relevant is the transaminases evaluation which are known to be altered both in SMA patients who have received gene therapy and in SMARD1 patients and animal models. In our case, the serum analysis performed on treated mice did not reveal important changes in ALT and AST, and both treatments mediated a complete rescue of ALP resulted increased in virus B treated animals. On the contrary, glucose resulted reduced in virus B treated animals compared to WT, but the level was significantly restored with virus A and furthermore with virus C, result probably linked to the improved metabolism due to improved motility. The urea level resulted higher in SMARD1 mice treated with the empty vector but in the WT range for both virus A and virus C groups. Values that need further validation were the total cholesterol which resulted significantly reduced only in virus A treated group and albumin which, even if not correlated to changes in the total protein amount that could suggest kidney or liver malfunctioning, resulted significantly increased in virus C treated cohort.

These preclinical data on the ICV administration of AAV9-IGHMBP2 at P1 in *nmd* mice conducted in collaboration with the Center for Gene Therapy at Nationwide Children's Hospital at the Ohio State University and with Jackson Laboratories, paved the way for the launch of the first Phase I/IIa clinical trial in December 2021 for IGHMBP2-related pathology (SMARD1 and CMT2S). It consists of a single intrathecal injection of an AAV9 containing the WT human *IGHMBP2* gene in 10 children between 2 months to 14 years carrying a pathogenic variant of the *IGHMBP2* gene. Currently, the study is enrolling participants by invitation and up to now, 3 patients have already received the treatment. The primary outcome measure of this study is the evaluation of possible insurgence of unacceptable toxicity effects in a period of 3 years after the treatment, while the secondary outcome measure is the change in neuromuscular gross motor outcome, in the 100-meter timed test and in the revised upper limb module.

Considering that the ongoing clinical trial for IGHMBP2-related diseases is enrolling participants of a wide range of ages, comprising patients whose symptoms have already shown up, the last aim of this work was to better define the presence of a therapeutic window for AAV9-*IGHMBP2* gene therapy-based treatment, to understand the efficacy of a more delayed treatment performed during the symptomatic phase of the disease. This is a fundamental aspect in the field of rare genetic disease as SMARD1, which usually are diagnosed only after the appearance of the symptoms. In this regard, preclinical experiments on a delayed ICV treatment using AAV9-*IGHMBP2* were only performed on a recently developed severe SMARD1 mouse model (*FVB-nmd*), still not commercially available, and no data were present on the original *nmd* mouse[85].
Starting from this premise, we aimed to test the already validated[82] CAG-AAV9-*IGHMBP2* vector, administering it during the early symptomatic phase of the disease, at P7, in the *nmd* model. The dosage and the route of administration were defined by testing them on WT mice. The results demonstrated that ICV administration led to an extreme increase in the IGHMBP2 protein expression in the spinal cord two weeks after the treatment, which although caused higher mortality rates in *nmd* mice early after the injection (data not shown), probably linked to a toxicity effect similar to the one seen in the virus A presymptomatic treatment. Therefore, we firstly tested a systemic route of administration, in line with the experimental plan performed also for the presymptomatic treatment, in particular selecting the SC route at a high dosage which resulted in an average increase of the protein in WT animals. The SC injection was preferred with respect to the IP and IV, first, for the easiest translation to the clinic, secondly, for the reduced dosage needed which makes it less expensive for the translational perspective, and lastly, to avoid the dispersion of the construct in the

organs near the injection site, as liver and kidneys, already partially compromised in *nmd* animals and a major target of gene therapy-mediated toxicity.

The SC treatment at P7 on *nmd* mice mediated first of all an important improvement in survival time, even if was possible to observe again an important early mortality around P20 (50% of the animals treated died before P30). We speculated that the early death, in this case, was probably caused by an insufficient distribution of the vector in the tissues mainly affected in the pathology, an idea supported also by lack of improvement in the classical neuropathological hallmarks of SMARD1 as MN number and NMJ innervation. The efficacy of the treatment otherwise was supported by the results obtained in weight value measurement, which, even not equal to WT, were significantly higher than animals treated with the empty vector, suggesting that also the systemic and delayed treatment mediated a partial rescue of the pathological phenotype. Significative results were also obtained in motor behavioral tests. In particular, with the hindlimb splay test, was possible to observe a significant improvement already one week after the treatment with the highest peak reached at P50, important amelioration considering that the *nmd* AAV9null mice can be tested only a few times before their early death. For what concern the grip strength, the values reached by treated mice are significantly different from WT, but it is necessary to take into account that it was an important amelioration with respect to the *nmd* AAV9null treated that had never been able to perform the test along their short lifespan. The macroscopic aspect of these animals at the adult stage otherwise resulted in a more severe phenotype if compared to the one treated at P1, leading us to think that here the rescue was not complete.

The neuropathological analysis did not demonstrate a correlation of the phenotypical improvement with a significative increased MN number in the lumbar spinal cord and showed only a slight increase in the NMJ innervation, suggesting that these alterations occur early in *nmd* mice and are difficulty reversible. Otherwise, a striking rescue of the neuroinflammatory markers in the spinal cord was observed for both the astrocyte gliosis and microglia innervation, suggesting a possible role of these cells, not only as a secondary effect of MNs degeneration but also directly involved in the pathology. In addition, we also demonstrated the presence of amelioration of the myofiber area in gastrocnemius, even if not correlated to a diminished fibrosis/necrosis as already seen for the presymptomatic treatment, and a significant reduction of fibrotic infiltrates in the heart. These results suggest the possible involvement of cardiac muscle in the outcome of the pathology, and that the increase of the IGHMBP2 protein by the use of gene therapy is able to rescue also this peripherical hallmark.

The analysis of the IGF1 axis demonstrates also here a significant rescue mediated by the treatment in the expression level of IGF1 in the liver, reduced in the *nmd* mice treated with the empty vector,

while no significant changes were observed in the cardiac level, in line with the precedent results. These results need to be further completed by analyzing the circulating level of IGF1 and the expression of its receptor.

Overall, our results suggest that the delayed treatment through a systemic injection was efficacious in partially rescuing the pathological phenotype of already symptomatic *nmd* mice. The data led us to speculate that the effects of this administration were more peripheral, especially on muscles than acting at the level of the CNS. In particular, no or small effects were seen in the principal affected components in the pathology, such as the MN number and the NMJ innervation, while helpful benefits were seen peripherally and in the CNS neuroinflammation, leading us to suppose that the positive amelioration in the phenotype could be linked to a better nervous microenvironment which supports the remained MNs.

This is a crucial result in the field of a rare pathology as SMARD1, usually diagnosed after the insurgence of the symptoms, and especially important considering the difficulties into rescue an already evident phenotype. Interesting will be also the evaluation of the delayed treatment administered more locally with an ICV injection, reducing the dosage with respect to the one tested in the preliminary experiments on WT which results too high in terms of toxicity and early mortality. These results support the possibility of a clinical translation of the treatment also during the symptomatic phase of the disease, in particular, opening future perspectives to the potentiality of a combined therapy acting on different targets. The combinatorial approach in fact has already obtained promising results for SMA, in which the approved gene therapy and antisense oligonucleotides acting on splicing were combined with inhibitors of histone deacetylase, ubiquitination inhibitors, and myostatin inhibitors obtaining better outcomes compared to single therapy[113–115]. In this regard, an RNAseq analysis on mice tissues is ongoing to detect possible pathways which could be involved in the pathology and targeted by a second therapeutic agent in combination with gene therapy.

7. Bibliography

1. National Institute of Neurological Disorders and Stroke. https://www.ninds.nih.gov/.
2. Natali, A. L., Reddy, V. & Bordoni, B. Neuroanatomy, Corticospinal Cord Tract. in *StatPearls* (StatPearls Publishing, 2022).
3. Ivanhoe, C. B. & Reistetter, T. A. Spasticity: The Misunderstood Part of the Upper Motor Neuron Syndrome. *American Journal of Physical Medicine & Rehabilitation* **83**, S3 (2004).
4. Shababi, M., Lorson, C. L. & Rudnik-Schöneborn, S. S. Spinal muscular atrophy: a motor neuron disorder or a multi-organ disease? *J Anat* **224**, 15–28 (2014).
5. Miniño, A. M., Xu, J. & Kochanek, K. D. Deaths: preliminary data for 2008. *Natl Vital Stat Rep* **59**, 1–52 (2010).
6. Lefebvre, S. *et al.* Identification and characterization of a spinal muscular atrophy-determining gene. *Cell* **80**, 155–165 (1995).
7. Mellins, R. B., Hays, A. P., Gold, A. P., Berdon, W. E. & Bowdler, J. D. Respiratory distress as the initial manifestation of Werdnig-Hoffmann disease. *Pediatrics* **53**, 33–40 (1974).
8. Novelli, G. *et al.* Neonatal spinal muscular atrophy with diaphragmatic paralysis is unlinked to 5q11.2-q13. *J Med Genet* **32**, 216–219 (1995).
9. Rudnik-Schöneborn, S., Forkert, R., Hahnen, E., Wirth, B. & Zerres, K. Clinical spectrum and diagnostic criteria of infantile spinal muscular atrophy: further delineation on the basis of SMN gene deletion findings. *Neuropediatrics* **27**, 8–15 (1996).
10. Grohmann, K. *et al.* Diaphragmatic Spinal Muscular Atrophy with Respiratory Distress Is Heterogeneous, and One Form Is Linked to Chromosome 11q13-q21. *Am J Hum Genet* **65**, 1459–1462 (1999).
11. Grohmann, K. *et al.* Mutations in the gene encoding immunoglobulin mu-binding protein 2 cause spinal muscular atrophy with respiratory distress type 1. *Nat Genet* **29**, 75–77 (2001).

12. Stalpers, X. L. *et al.* Clinical and mutational characteristics of spinal muscular atrophy with respiratory distress type 1 in The Netherlands. *Neuromuscul Disord* **23**, 461–468 (2013).
13. Fenichel GM. *Clinical pediatric neurology. A signs and symptoms approach*. (Saunders, 2001).
14. Grohmann, K. *et al.* Infantile spinal muscular atrophy with respiratory distress type 1 (SMARD1). *Ann Neurol* **54**, 719–724 (2003).
15. Kaindl, A. M. *et al.* Spinal Muscular Atrophy With Respiratory Distress Type 1 (SMARD1). *J Child Neurol* **23**, 199–204 (2008).
16. Eckart, M. *et al.* The Natural Course of Infantile Spinal Muscular Atrophy With Respiratory Distress Type 1 (SMARD1). *Pediatrics* **129**, e148–e156 (2012).
17. Viguier, A. *et al.* Spinal muscular atrophy with respiratory distress type 1: A multicenter retrospective study. *Neuromuscul Disord* **29**, 114–126 (2019).
18. Pierson, T. M. *et al.* Infantile-onset spinal muscular atrophy with respiratory distress-1 diagnosed in a 20-year-old man. *Neuromuscul Disord* **21**, 353–355 (2011).
19. Pitt, M. *et al.* Severe infantile neuropathy with diaphragmatic weakness and its relationship to SMARD1. *Brain* **126**, 2682–2692 (2003).
20. Guenther, U.-P. *et al.* Clinical and mutational profile in spinal muscular atrophy with respiratory distress (SMARD): defining novel phenotypes through hierarchical cluster analysis. *Hum Mutat* **28**, 808–815 (2007).
21. Sangiuolo, F. *et al.* Prenatal diagnosis of spinal muscular atrophy with respiratory distress (SMARD1) in a twin pregnancy. *Prenatal Diagnosis* **24**, 839–841 (2004).
22. Basel-Vanagaite, L. *et al.* Genetic Carrier Screening for Spinal Muscular Atrophy and Spinal Muscular Atrophy with Respiratory Distress 1 in an Isolated Population in Israel. *Genetic Testing* **12**, 53–56 (2008).
23. UniProt. https://www.uniprot.org/.
24. Cottenie, E. *et al.* Truncating and missense mutations in IGHMBP2 cause Charcot-Marie Tooth disease type 2. *Am J Hum Genet* **95**, 590–601 (2014).

25. de Planell-Saguer, M., Schroeder, D. G., Rodicio, M. C., Cox, G. A. & Mourelatos, Z. Biochemical and genetic evidence for a role of IGHMBP2 in the translational machinery. *Hum Mol Genet* **18**, 2115–2126 (2009).
26. Jędrzejowska, M. *et al.* Severe phenotypes of SMARD1 associated with novel mutations of the IGHMBP2 gene and nuclear degeneration of muscle and Schwann cells. *Eur J Paediatr Neurol* **18**, 183–192 (2014).
27. Gorbalenya, A. & Koonin, E. V. Helicases: amino acid sequence comparisons and structure-function relationships. *Current Opinion in Structural Biology* (1993) doi:10.1016/S0959-440X(05)80116-2.
28. Singleton, M. R., Dillingham, M. S. & Wigley, D. B. Structure and Mechanism of Helicases and Nucleic Acid Translocases. *Annual Review of Biochemistry* **76**, 23–50 (2007).
29. Fairman-Williams, M. E., Guenther, U.-P. & Jankowsky, E. SF1 and SF2 helicases: family matters. *Curr Opin Struct Biol* **20**, 313–324 (2010).
30. Lim, S. C., Bowler, M. W., Lai, T. F. & Song, H. The Ighmbp2 helicase structure reveals the molecular basis for disease-causing mutations in DMSA1. *Nucleic Acids Res* **40**, 11009–11022 (2012).
31. Jaudzems, K. *et al.* Structural basis for 5'-end-specific recognition of single-stranded DNA by the R3H domain from human Sμbp-2. *J Mol Biol* **424**, 42–53 (2012).
32. Guenther, U.-P. *et al.* IGHMBP2 is a ribosome-associated helicase inactive in the neuromuscular disorder distal SMA type 1 (DSMA1). *Human Molecular Genetics* **18**, 1288–1300 (2009).
33. Perego, M. G. L., Taiana, M., Bresolin, N., Comi, G. P. & Corti, S. R-Loops in Motor Neuron Diseases. *Mol Neurobiol* **56**, 2579–2589 (2019).
34. Perego, M. G. L. *et al.* Current understanding of and emerging treatment options for spinal muscular atrophy with respiratory distress type 1 (SMARD1). *Cell Mol Life Sci* **77**, 3351–3367 (2020).

35. Rzepnikowska, W. & Kochański, A. Models for IGHMBP2-associated diseases: an overview and a roadmap for the future. *Neuromuscul Disord* **31**, 1266–1278 (2021).
36. Maystadt, I. *et al.* Allelic heterogeneity of SMARD1 at the IGHMBP2 locus. *Hum Mutat* **23**, 525–526 (2004).
37. AlSaman, A. & Tomoum, H. Infantile Spinal Muscular Atrophy With Respiratory Distress Type 1: A Case Report. *J Child Neurol* **25**, 764–769 (2010).
38. Guenther, U. P. *et al.* Genomic rearrangements at the IGHMBP2 gene locus in two patients with SMARD1. *Hum Genet* **115**, 319–326 (2004).
39. Wong, V. C. N., Chung, B. H. Y., Li, S., Goh, W. & Lee, S. L. Mutation of gene in spinal muscular atrophy respiratory distress type I. *Pediatr Neurol* **34**, 474–477 (2006).
40. Guenther, U.-P. *et al.* Clinical variability in distal spinal muscular atrophy type 1 (DSMA1): determination of steady-state IGHMBP2 protein levels in five patients with infantile and juvenile disease. *J Mol Med (Berl)* **87**, 31–41 (2009).
41. Kulshrestha, R. *et al.* Charcot Marie Tooth disease type 2S with late onset diaphragmatic weakness: An atypical case. *Neuromuscul Disord* **28**, 1016–1021 (2018).
42. Pedurupillay, C. R. J. *et al.* Clinical and molecular characteristics in three families with biallelic mutations in IGHMBP2. *Neuromuscul Disord* **26**, 570–575 (2016).
43. Takahashi, K. & Yamanaka, S. Induction of pluripotent stem cells from mouse embryonic and adult fibroblast cultures by defined factors. *Cell* **126**, 663–676 (2006).
44. Hu, B.-Y. & Zhang, S.-C. Differentiation of spinal motor neurons from pluripotent human stem cells. *Nat Protoc* **4**, 1295–1304 (2009).
45. Corti, S. *et al*. Genetic Correction of Human Induced Pluripotent Stem Cells from Patients with Spinal Muscular Atrophy. *Science Translational Medicine* **4**, 165ra162-165ra162 (2012).
46. Simone, C. *et al.* iPSC-Derived neural stem cells act via kinase inhibition to exert neuroprotective effects in spinal muscular atrophy with respiratory distress type 1. *Stem Cell Reports* **3**, 297–311 (2014).

47. Oliveira, A. V., Vilaça, R., Santos, C. N., Costa, V. & Menezes, R. Exploring the power of yeast to model aging and age-related neurodegenerative disorders. *Biogerontology* **18**, 3–34 (2017).
48. Foury, F. Human genetic diseases: a cross-talk between man and yeast. *Gene* **195**, 1–10 (1997).
49. Apfeld, J. & Alper, S. What Can We Learn About Human Disease from the Nematode C. elegans? *Methods Mol Biol* **1706**, 53–75 (2018).
50. Fischer, S. E. J. *et al*. The ERI-6/7 Helicase Acts at the First Stage of an siRNA Amplification Pathway That Targets Recent Gene Duplications. *PLOS Genetics* **7**, e1002369 (2011).
51. Fischer, S. E. J. & Ruvkun, G. Caenorhabditis elegans ADAR editing and the ERI-6/7/MOV10 RNAi pathway silence endogenous viral elements and LTR retrotransposons. *Proc Natl Acad Sci U S A* **117**, 5987–5996 (2020).
52. Babin, P. J., Goizet, C. & Raldúa, D. Zebrafish models of human motor neuron diseases: advantages and limitations. *Prog Neurobiol* **118**, 36–58 (2014).
53. Butterfield, R. J. *et al.* Congenital lethal motor neuron disease with a novel defect in ribosome biogenesis. *Neurology* **82**, 1322–1330 (2014).
54. Mizuta, T. R., Fukita, Y., Miyoshi, T., Shimizu, A. & Honjo, T. Isolation of cDNA encoding a binding protein specific to 5'-phosphorylated single-stranded DNA with G-rich sequences. *Nucleic Acids Res* **21**, 1761–1766 (1993).
55. 002521 - neuromuscular degeneration 2 Jackson Strain Details. https://www.jax.org/strain/002521.
56. Cook, S. A., Johnson, K. R., Bronson, R. T. & Davisson, M. T. Neuromuscular degeneration (nmd): a mutation on mouse chromosome 19 that causes motor neuron degeneration. *Mamm Genome* **6**, 187–191 (1995).
57. Cox, G. A., Mahaffey, C. L. & Frankel, W. N. Identification of the mouse neuromuscular degeneration gene and mapping of a second site suppressor allele. *Neuron* **21**, 1327–1337 (1998).

58. Grohmann, K. *et al.* Characterization of Ighmbp2 in motor neurons and implications for the pathomechanism in a mouse model of human spinal muscular atrophy with respiratory distress type 1 (SMARD1). *Hum Mol Genet* **13**, 2031–2042 (2004).
59. Smith, C. E. *et al.* The Ighmbp2D564N mouse model is the first SMARD1 model to demonstrate respiratory defects. *Human Molecular Genetics* **31**, 1293–1307 (2022).
60. Robbins, P. D., Tahara, H. & Ghivizzani, S. C. Viral vectors for gene therapy. *Trends Biotechnol* **16**, 35–40 (1998).
61. Bulcha, J. T., Wang, Y., Ma, H., Tai, P. W. L. & Gao, G. Viral vector platforms within the gene therapy landscape. *Sig Transduct Target Ther* **6**, 1–24 (2021).
62. Ghosh, S., Brown, A. M., Jenkins, C. & Campbell, K. Viral Vector Systems for Gene Therapy: A Comprehensive Literature Review of Progress and Biosafety Challenges. *Applied Biosafety* **25**, 7–18 (2020).
63. Petrich, J., Marchese, D., Jenkins, C., Storey, M. & Blind, J. Gene Replacement Therapy: A Primer for the Health-system Pharmacist. *J Pharm Pract* **33**, 846–855 (2020).
64. Foust, K. D. *et al.* Intravascular AAV9 preferentially targets neonatal neurons and adult astrocytes. *Nat Biotechnol* **27**, 59–65 (2009).
65. Atchison, R. W., Casto, B. C. & Hammon, W. McD. Adenovirus-Associated Defective Virus Particles. *Science* **149**, 754–756 (1965).
66. Smith, R. H. Adeno-associated virus integration: virus versus vector. *Gene Ther* **15**, 817–822 (2008).
67. Chowdhury, E. A. *et al.* Current progress and limitations of AAV mediated delivery of protein therapeutic genes and the importance of developing quantitative pharmacokinetic/pharmacodynamic (PK/PD) models. *Adv Drug Deliv Rev* **170**, 214–237 (2021).
68. Colella, P., Ronzitti, G. & Mingozzi, F. Emerging Issues in AAV-Mediated In Vivo Gene Therapy. *Mol Ther Methods Clin Dev* **8**, 87–104 (2018).

69. Pacak, C. A. *et al.* Recombinant adeno-associated virus serotype 9 leads to preferential cardiac transduction in vivo. *Circ Res* **99**, e3-9 (2006).
70. Inagaki, K. *et al.* Robust systemic transduction with AAV9 vectors in mice: efficient global cardiac gene transfer superior to that of AAV8. *Molecular Therapy* **14**, 45–53 (2006).
71. Zincarelli, C., Soltys, S., Rengo, G. & Rabinowitz, J. E. Analysis of AAV serotypes 1-9 mediated gene expression and tropism in mice after systemic injection. *Mol Ther* **16**, 1073–1080 (2008).
72. Schuster, D. J. *et al.* Biodistribution of adeno-associated virus serotype 9 (AAV9) vector after intrathecal and intravenous delivery in mouse. *Frontiers in Neuroanatomy* **8**, (2014).
73. Kuzmin, D. A. *et al.* The clinical landscape for AAV gene therapies. *Nature Reviews Drug Discovery* **20**, 173–174 (2021).
74. ClinicalTrials.gov. https://clinicaltrials.gov/ct2/home.
75. Duque, S. *et al.* Intravenous administration of self-complementary AAV9 enables transgene delivery to adult motor neurons. *Mol Ther* **17**, 1187–1196 (2009).
76. Dominguez, E. *et al.* Intravenous scAAV9 delivery of a codon-optimized SMN1 sequence rescues SMA mice. *Hum Mol Genet* **20**, 681–693 (2011).
77. Valori, C. F. *et al.* Systemic delivery of scAAV9 expressing SMN prolongs survival in a model of spinal muscular atrophy. *Sci Transl Med* **2**, 35ra42 (2010).
78. Foust, K. D. *et al.* Rescue of the spinal muscular atrophy phenotype in a mouse model by early postnatal delivery of SMN. *Nat Biotechnol* **28**, 271–274 (2010).
79. EMA. Zolgensma. *European Medicines Agency* https://www.ema.europa.eu/en/medicines/human/EPAR/zolgensma (2020).
80. Tukov, F. F. *et al.* Single-Dose Intrathecal Dorsal Root Ganglia Toxicity of Onasemnogene Abeparvovec in Cynomolgus Monkeys. *Hum Gene Ther* **33**, 740–756 (2022).
81. Mendell, J. R. *et al.* Single-Dose Gene-Replacement Therapy for Spinal Muscular Atrophy. *N Engl J Med* **377**, 1713–1722 (2017).

82. Nizzardo, M. *et al.* Gene therapy rescues disease phenotype in a spinal muscular atrophy with respiratory distress type 1 (SMARD1) mouse model. *Sci Adv* **1**, e1500078 (2015).

83. Shababi, M. *et al.* Rescue of a Mouse Model of Spinal Muscular Atrophy With Respiratory Distress Type 1 by AAV9-IGHMBP2 Is Dose Dependent. *Mol Ther* **24**, 855–866 (2016).

84. Shababi, M., Villalón, E., Kaifer, K. A., DeMarco, V. & Lorson, C. L. A Direct Comparison of IV and ICV Delivery Methods for Gene Replacement Therapy in a Mouse Model of SMARD1. *Mol Ther Methods Clin Dev* **10**, 348–360 (2018).

85. Shababi, M. *et al.* Development of a novel severe mouse model of spinal muscular atrophy with respiratory distress type 1: FVB-nmd. *Biochem Biophys Res Commun* **520**, 341–346 (2019).

86. Shababi, M. *et al.* Defining the optimal dose and therapeutic window in SMA with respiratory distress type I model mice, FVB/NJ-Ighmpb2 nmd-2J. *Mol Ther Methods Clin Dev* **23**, 23–32 (2021).

87. Bushby, K. *et al.* Ataluren treatment of patients with nonsense mutation dystrophinopathy. *Muscle & Nerve* **50**, 477–487 (2014).

88. Finkel, R. S. *et al.* Treatment of infantile-onset spinal muscular atrophy with nusinersen: a phase 2, open-label, dose-escalation study. *Lancet* **388**, 3017–3026 (2016).

89. Baranello, G. *et al.* Risdiplam in Type 1 Spinal Muscular Atrophy. *N Engl J Med* **384**, 915–923 (2021).

90. Sun, L., Lutz, B. M. & Tao, Y.-X. The CRISPR/Cas9 system for gene editing and its potential application in pain research. *Transl Perioper Pain Med* **1**, 22–33 (2016).

91. Wang, L. *et al.* CRISPR/Cas9-mediated targeted gene correction in amyotrophic lateral sclerosis patient iPSCs. *Protein Cell* **8**, 365–378 (2017).

92. Nelson, C. E. *et al.* In vivo genome editing improves muscle function in a mouse model of Duchenne muscular dystrophy. *Science* **351**, 403–407 (2016).

93. Firth, S. M. & Baxter, R. C. Cellular Actions of the Insulin-Like Growth Factor Binding Proteins. *Endocrine Reviews* **23**, 824–854 (2002).

94. Feldman, E. L., Sullivan, K. A., Kim, B. & Russell, J. W. Insulin-like growth factors regulate neuronal differentiation and survival. *Neurobiol Dis* **4**, 201–214 (1997).

95. Hughes, R. A., Sendtner, M. & Thoenen, H. Members of several gene families influence survival of rat motoneurons in vitro and in vivo. *J Neurosci Res* **36**, 663–671 (1993).

96. Caroni, P. & Schneider, C. Signaling by insulin-like growth factors in paralyzed skeletal muscle: rapid induction of IGF1 expression in muscle fibers and prevention of interstitial cell proliferation by IGF-BP5 and IGF-BP4. *J Neurosci* **14**, 3378–3388 (1994).

97. Martins, K. J. B. *et al.* Intramuscular administration of PEGylated IGF-I improves skeletal muscle regeneration after myotoxic injury. *Growth Horm IGF Res* **23**, 128–133 (2013).

98. Bilic, E. *et al.* Comparison of the growth hormone, IGF-1 and insulin in cerebrospinal fluid and serum between patients with motor neuron disease and healthy controls. *European Journal of Neurology* **13**, 1340–1345 (2006).

99. Jablonka, S., Holtmann, B., Sendtner, M. & Metzger, F. Therapeutic effects of PEGylated insulin-like growth factor I in the pmn mouse model of motoneuron disease. *Exp Neurol* **232**, 261–269 (2011).

100. Saenger, S. *et al.* Functional improvement in mouse models of familial amyotrophic lateral sclerosis by PEGylated insulin-like growth factor I treatment depends on disease severity. *Amyotroph Lateral Scler* **13**, 418–429 (2012).

101. Metzger, F. *et al.* Separation of fast from slow anabolism by site-specific PEGylation of insulin-like growth factor I (IGF-I). *J Biol Chem* **286**, 19501–19510 (2011).

102. Ruiz, R. *et al.* Treatment with trkC agonist antibodies delays disease progression in neuromuscular degeneration (nmd) mice. *Hum Mol Genet* **14**, 1825–1837 (2005).

103. Krieger, F. *et al.* Polyethylene glycol-coupled IGF1 delays motor function defects in a mouse model of spinal muscular atrophy with respiratory distress type 1. *Brain* **137**, 1374–1393 (2014).

104. Wichterle, H., Lieberam, I., Porter, J. A. & Jessell, T. M. Directed differentiation of embryonic stem cells into motor neurons. *Cell* **110**, 385–397 (2002).

105. Teng, Y. D. *et al.* Multimodal actions of neural stem cells in a mouse model of ALS: a meta-analysis. *Sci Transl Med* **4**, 165ra164 (2012).

106. Corti, S. *et al.* Transplanted ALDHhiSSClo neural stem cells generate motor neurons and delay disease progression of nmd mice, an animal model of SMARD1. *Human Molecular Genetics* **15**, 167–187 (2006).

107. Corti, S. *et al.* Motoneuron Transplantation Rescues the Phenotype of SMARD1 (Spinal Muscular Atrophy with Respiratory Distress Type 1). *J. Neurosci.* **29**, 11761–11771 (2009).

108. Gutierrez-Aranda, I. *et al.* Human induced pluripotent stem cells develop teratoma more efficiently and faster than human embryonic stem cells regardless the site of injection. *Stem Cells* **28**, 1568–1570 (2010).

109. Laursen, S. E. & Belknap, J. K. Intracerebroventricular injections in mice. Some methodological refinements. *J Pharmacol Methods* **16**, 355–357 (1986).

110. Abati, E., Citterio, G., Bresolin, N., Comi, G. P. & Corti, S. Glial cells involvement in spinal muscular atrophy: Could SMA be a neuroinflammatory disease? *Neurobiology of Disease* **140**, 104870 (2020).

111. Ren, J., Samson, W. K. & Sowers, J. R. Insulin-like growth factor I as a cardiac hormone: physiological and pathophysiological implications in heart disease. *J Mol Cell Cardiol* **31**, 2049–2061 (1999).

112. Van Alstyne, M. *et al.* Gain of toxic function by long-term AAV9-mediated SMN overexpression in the sensorimotor circuit. *Nat Neurosci* **24**, 930–940 (2021).

113. Poletti, A. & Fischbeck, K. H. Combinatorial treatment for spinal muscular atrophy: An Editorial for 'Combined treatment with the histone deacetylase inhibitor LBH589 and a splice-switch antisense oligonucleotide enhances SMN2 splicing and SMN expression in Spinal Muscular Atrophy cells' on page 264. *J Neurochem* **153**, 146–149 (2020).

114. Zhou, H. *et al.* Myostatin inhibition in combination with antisense oligonucleotide therapy improves outcomes in spinal muscular atrophy. *J Cachexia Sarcopenia Muscle* **11**, 768–782 (2020).

115. Dumas, S. A. *et al.* A combinatorial approach increases SMN level in SMA model mice. *Hum Mol Genet* **31**, 2989–3000 (2022).